

**Examining whether Multicopper Oxidase 4 (*Mco4*) acts as a high affinity iron importer in
*Drosophila melanogaster***

by

Qingxuan Yu

A thesis submitted in partial fulfillment of the requirements for the degree of

Master of Science

in

Molecular Biology and Genetics

Department of Biological Sciences

University of Alberta

© Qingxuan Yu, 2024

ABSTRACT

Iron is a crucial micronutrient for nearly all living organisms, playing a vital role in various biological processes. In humans, it is essential for the production of hemoglobin, which is necessary for oxygen transport in red blood cells. Beyond oxygen transport, iron is a key component of heme and iron-sulfur clusters, which are involved in numerous cellular functions, including DNA repair and hormone synthesis. The model organism *Drosophila melanogaster* has proven to be a valuable tool for studying iron metabolism due to its genetic similarities to humans and its high iron demand for steroid hormone synthesis.

Multicopper oxidase 4 (*Mco4*) was first discovered as a gene upregulated in response to genetic or dietary disruption of iron homeostasis. *Mco4* is expressed on the cell membrane and has a yeast ortholog, Fet3p, which acts as a component of a high-affinity iron import system. This thesis investigates whether *Mco4* also plays a role in high-affinity iron import in *Drosophila*, which would represent the first such system identified in animals.

In this study, I performed the phenotypic analysis of an *Mco4* knockout line, which showed that loss of *Mco4* function causes sensitivity to iron starvation. Specifically, multi-generational iron depletion showed that *Mco4* null mutant flies exhibit decreased survival rates when reared on iron-deprived food due to lower body iron content compared to wild-type flies. I also constructed a *Mco4-3xFlag* knock-in line to analyze the expression pattern of *Mco4*. Immunofluorescence experiments revealed that *Mco4* is predominantly expressed in the proventriculus. In other tissues, primarily the gut, *Mco4* is only detectable under low dietary iron level, indicating a role during iron starvation.

To further understand its function, I explored the effects of *Mco4* overexpression and found that whole-body overexpression of *Mco4* leads to increased iron content in the gut and strongly enhanced resistance to iron deprivation. Remarkably, *Mco4* overexpression allows animals to survive extreme iron deprivation, which is not seen in controls. Additionally, *Mco4* overexpression in S2 cells demonstrated ferroxidase activity comparable to that of human Hephaestin, a known ferroxidase. Using the TurboID proximity labeling technique, I identified interactions between *Mco4* and ferritin heavy and light chains. Together, these findings indicate that *Mco4* plays a critical role in the cellular response to iron deprivation and likely functions as a high-affinity iron importer, thus facilitating the import of iron when it is scarce.

ACKNOWLEDGEMENTS

I would like to express my heartfelt gratitude to my supervisor, Dr. Kirst King-Jones. Over the past three years in his lab, his guidance and support have been invaluable. He has helped me overcome numerous challenges and has been a constant source of inspiration. I am also deeply thankful to our postdocs, Dr. Wen Liu and Dr. Sattar Soltani. Their technical expertise and willingness to teach have greatly contributed to my learning and research. I have learned so much from them and their patience and generosity.

Special thanks to my lab mate and friend, Minyi Yan. Her support and friendship have made my time in the lab more enjoyable and productive. I could not have asked for a better colleague and friend.

I would like to thank the Department of Biological Sciences for providing the teaching assistantships that made my research possible. Their support has been essential for my studies. I am also grateful to my committee member, Dr. Anna Phan, for her valuable advice and suggestions. Her input has greatly improved my research and provided new perspectives.

To my partner, ZiFu Chen, thank you for your unwavering support and encouragement throughout this journey. Your belief in me has kept me motivated and confident.

Finally, I would like to acknowledge all the people and facilities that have supported my research, including the Molecular Biology Service Unit (MBSU) team for their assistance and access to resources. Thank you all for your support and contributions. I will forever be grateful.

Table of Contents

CHAPTER 1 Introduction.....	1
1.1 The importance of iron.....	2
1.2 <i>Drosophila melanogaster</i> as a model to study iron metabolism.....	2
1.2.1 The heme synthesis pathway	3
1.2.2 The ecdysone synthesis pathway	6
1.3 Iron homeostasis in mammals.....	8
1.3.1 Iron uptake from diet	8
1.3.2 Iron regulation by mammalian IRPs	10
1.4 Iron homeostasis in <i>Drosophila melanogaster</i>	10
1.4.1 Iron uptake from diet in flies	10
1.4.2 Iron regulation by IPRs in flies.....	13
1.5 <i>Mco4</i> is induced under iron-deprived conditions.....	15
1.5.1 <i>Mco4</i> upregulation in iron-chelating diet.....	15
1.5.2 <i>Mco4</i> upregulation in genetic disruption of iron.....	16
1.6 Multicopper oxidases	18
1.6.1 Multicopper oxidases in mammals	19
1.6.2 Multicopper oxidases in <i>Drosophila</i>	19
1.7 Iron uptake in yeast.....	22
1.8 Iron import systems in plants.....	24
1.9 Research objectives.....	25
1.8.1 Identifying <i>Mco4</i> 's expression pattern.....	25
1.8.2 Characterization of <i>Mco4</i> null mutant phenotype.....	25
1.8.3 Investigating the molecular function of <i>Mco4</i>	25
CHAPTER 2 Material and methods	27
2.1 <i>Drosophila</i> husbandry and maintenance.....	28
2.2 Iron-supplemented medium	28

2.3 Iron-chelated medium	28
2.4 Survival Study.....	29
2.4.1 Preparing embryo collection plates.....	29
2.4.2 Embryo collection and survival count	29
2.5 <i>Drosophila</i> staging and dissection	29
2.6 <i>Drosophila</i> tissue immunostaining and imaging	29
2.7 <i>Drosophila</i> whole larvae co-IP	30
2.8 TurboID using <i>Drosophila</i> whole larvae samples	31
2.9 Single fly DNA extraction	33
2.10 <i>Drosophila</i> Genomic DNA extraction	33
2.11 <i>Drosophila</i> RNA extraction.....	34
2.12 cDNA synthesis	35
2.13 Preparation of ultra-competent cells	35
2.14 Gibson Assembly	36
2.15 Bacteria transformation.....	36
2.16 Colony PCR	37
2.17 Plasmid extraction.....	37
2.18 Quantitative real time PCR (qPCR).....	37
2.19 Ferroxidase activity assay	38
2.20 Ferrozine-based iron content assay	39
2.21 Gel extraction of PCR products	39
2.22 Schneider 2 cell culturing	40
2.23 Generation of constructs of S2 cell transfection	41
2.24 S2 cell transfection.....	41
2.25 S2 cell immunostaining and imaging.....	42

2.26 Western blot analysis	43
2.27 Coomassie blue staining	44
2.28 Generation of <i>Mco4</i> knock-in CRISPR line	44
2.28.1 gRNA plasmids construction	44
2.28.2 Donor plasmids construction	45
2.28.3 Injection and generation of homozygous line	45
2.29 Generation of <i>UAS-Mco4-V5-Tb</i> line	46
CHAPTER 3 Characterization of <i>Mco4</i> expression	63
3.1 Introduction.....	64
3.2 Results.....	65
3.2.1 Validation of <i>Mco4</i> localization using S2 cells	65
3.2.2 Analysis of <i>Mco4</i> localization in a transgenic line	66
3.2.3 Generation of <i>Mco4</i> CRISPR/Cas9 knock-in line	67
3.2.4 <i>Mco4</i> is strongly expressed in the proventriculus regardless of dietary iron concentrations	69
3.2.5 <i>Mco4</i> is strongly upregulated in the gut under iron-deprived conditions	72
3.3 Discussion and future directions.....	74
3.3.1 <i>Mco4</i> have separate functions in the PV and gut.....	74
3.3.2 <i>Mco4</i> as an indicator of dietary iron deprivation in flies.....	74
3.3.3 PV-specific and gut-specific <i>Mco4</i> knockdown	74
3.3.4 Investigating the PV's role in dietary sensing	75
3.3.5 Investigating <i>Mco4</i> expression in the gut membrane using high resolution IF	76
CHAPTER 4 Characterization of <i>Mco4</i> null mutant phenotype	77
4.1 Introduction.....	78
4.1.1 <i>Mco4</i> ^{-/-} flies shows no phenotypes under a normal iron diet	78
4.1.2 Dietary iron deprivation is achieved by adding BPS to Nutri-fly food	78
4.2 Results.....	80
4.2.1 Validation of <i>Mco4</i> ^{-/-} line.....	80

4.2.2 <i>Mco4</i> ^{-/-} flies displayed reduced survival under multi-generational iron-deprivation .	81
4.2.3 <i>Mco4</i> ^{-/-} flies displayed reduced iron content.....	84
4.2.4 <i>Mco4</i> knockout combined with AGBE-RNAi resulted in more severe iron deficiency phenotype.....	86
4.3 Discussion and future directions.....	87
4.3.1 <i>Mco4</i> imports iron under iron-deprived conditions.....	87
4.3.2 Upregulation of <i>Mco4</i> as a compensatory mechanism to import iron into the PG.....	87
4.3.3 Examine <i>Mco4</i> and <i>Mvl</i> double knockout mutant phenotypes.....	88
CHAPTER 5 Characterization of <i>Mco4</i> function.....	89
5.1 Introduction.....	90
5.1.1 <i>Mco4</i> is a potential ferroxidase and may require a partner to function.....	90
5.1.2 The effect of <i>Mco4</i> overexpression on iron homeostasis.....	90
5.2 Results.....	91
5.2.1 <i>Mco4</i> has ferroxidase activity.....	91
5.2.2 <i>Mco4</i> overexpression increased iron content.....	93
5.2.3 <i>Mco4</i> overexpression increased resistance to iron deficiency.....	94
5.2.4 TurboID as a tool to investigate protein-to-protein interactions.....	96
5.2.5 Construction and validation of TurboID- <i>Mco4</i> lines.....	97
5.2.6 <i>Mco4</i> interacts with iron-related proteins.....	100
5.2 Discussion and future directions.....	108
5.2.1 <i>Mco4</i> interaction necessity and independence.....	108
5.2.2 The possible regulatory role between <i>Mco4</i> and ferritin.....	108
5.2.3 Tissue-specific interactions of <i>Mco4</i>	109
5.3 Conclusion and outlook.....	109
References:.....	110
Appendices.....	120
A 1. Gibson Assembly Mastermix Recipe.....	121
A 2. <i>Drosophila</i> whole body Co-IP reagent recipe.....	122

A 3. SOC medium recipe:	125
A 4. SDS-PAGE gels recipe	126

LIST OF FIGURES

Figure 1.1 The heme biosynthesis pathway	5
Figure 1.2 The ecdysone synthesis pathway	7
Figure 1.3 Iron uptake and transport in mammals	9
Figure 1.4 Iron uptake and transport in flies	12
Figure 1.5 Two IRP1A mutants.	14
Figure 1.6 <i>Mco4</i> is upregulated in iron-deprived conditions	17
Figure 1.7 The protein structure of Ceruloplasmin	18
Figure 1.8 Whole-body overexpression of <i>Mco4</i> shows a membrane-bound localization in three different tissues.	21
Figure 1.9 Two iron import system in yeast	23
Figure 4.1 The validation of <i>Mco4</i> null mutants with RT-qPCR	80
Figure 4.2 <i>Mco4</i> ^{-/-} showed gradually decreased survival over generations on an iron deprived diet	82
Figure 4.3 <i>Mco4</i> ^{-/-} showed gradually decreased survival over generations on an iron deprived diet using a higher concentration of BPS	83
Figure 4.4 <i>Mco4</i> ^{-/-} flies showed less iron content when reared on BPS-supplemented food.	85
Figure 4.5 <i>Mco4</i> ^{KO} in PG>AGBE-RNAi background results in more severe iron deficiency phenotype in the PG	86
Figure 5.1 Ferroxidase activity assay of <i>Mco4</i> and HEPH	92
Figure 5.2 <i>Mco4</i> whole body overexpression increased iron content in larvae	93
Figure 5.3 <i>Mco4</i> overexpression increased resistance to iron deficiency	95
Figure 5.4 The TurboID technique.	97
Figure 5.5 Construction and verification of UAS-TurboID-V5- <i>Mco4</i>	99
Figure 5.6 Overlaps of <i>Mco4</i> interacting proteins	103

LIST OF TABLES

Table 2.1 List of <i>Drosophila</i> stocks used in this study.....	47
Table 2.2 List of plasmids used in this study.....	49
Table 2.3 List of antibodies used in this study.....	52
Table 2.4 List of qPCR primers	54
Table 5.1 16 interacting candidates of Mco4 on both Nutri-fly food and BPS food.....	104
Table 5.2 64 interacting candidates of Mco4 identified only on BPS food.....	105

LIST OF ABBREVIATIONS

20E	20-hydroxyecdysone
7DC	7-dehydrocholesterol
AGBE	1,4-Alpha-Glucan Branching Enzyme
ALA	aminolevulinic acid
ALAD	aminolevulinic acid dehydratase
ALAS	aminolevulinic acid synthase
attB	bacteria attachment site
attP	bacteria attachment site
BDSC	Bloomington <i>Drosophila</i> Stock Center
BPS	bathophenanthroline sulfate
BRGC	brain-ring gland complex
CNS	central nervous system
co-IP	co-immunoprecipitation
CPgenIII	coproporphyrinogen III
CPOX/CPO	coproporphyrinogen oxidase
CRISPR	clustered regularly interspaced short palindromic repeats
DAPI	4',6-diamidino-2-phenylindole
DCytb	duodenal cytochrome b
DMSO	dimethyl sulfoxide
DMT1	Divalent Metal Transporter 1
<i>E. coli</i>	<i>Escherichia coli</i>
EGFP	Enhanced Green Fluorescent Protein
Evi5	Ecotropic Viral Integration Site
FAC	ferric ammonium citrate
FBS	fetal bovine serum
Fe-S	iron-sulfur cluster
Fe²⁺	ferrous iron

Fe³⁺	ferric iron
FECH	ferrochelatase
Fer1HCH	Ferritin 1 Heavy Chain Homologue
Fer2LCH	Ferritin 2 Light Chain Homologue
Fer3HCH	Ferritin 3 Heavy Chain Homologue
g	gram
G	generation
Gdh	glutamate dehydrogenase
GlyP	glycogen phosphorylase
Gp	glycoprotein
gRNA	guide RNA
hr	hour
H₂O₂	hydrogen peroxide
HDR	Homology Directed Repair
ICP-MS	Inductively Coupled Plasma Mass Spectrometry
Idh3b	Isocitrate Dehydrogenase 3b
IF	immunofluorescence
IRP	Iron Regulatory Protein
IRE	Iron Responsive Element
kDa	kilodalton
L	liter
L3	third instar larvae
LB	Luria-Bertani
LIP	labile iron pool
M	molar
MCO	multicopper oxidase
min	minute
mL	milliliter
mM	millimolar
mU	milli-unit

Mvl	Malvolio
N	Nutri-fly food
nemy	no extended memory
NES	nuclear export signal
nm	nanometer
ns	not significant
Nvd	Neverland
OD	optical density
PBG	porphobilinogen
PBGD	PBG deaminase
PBS	phosphate-buffered saline
PCR	polymerase chain reaction
PG	prothoracic gland
Pgd	phosphogluconate dehydrogenase
pmol	picomole
PPOX	protoporphyrinogen oxidase
PV	proventriculus
PVDF	polyvinylidene fluoride
qPCR	quantitative real time PCR
RG	ring gland
RNAi	RNA interference
ROS	reactive oxygen species
rp49	ribosomal protein 49
Rpm	revolutions per minute
RT	room temperature
s	second
S2	Schneider 2
SD	standard deviation
SDS-PAGE	sodium dodecyl sulfate–polyacrylamide gel electrophoresis
Sk	slope of the samples

SOC	Super Optimal broth with Catabolite repression
Ss	slope of the standard curve
Tb	TurboID
TCA	tricarboxylic acid
TfR	transferrin receptor
UAS	Upstream Activation Sequence
UROD	uroporphyrinogen decarboxylase
UROS	uroporphyrinogen synthase
UTR	untranslated region
V	volt
vol	volume
WB	Western blot
wt	weight
μL	microliter

CHAPTER 1 Introduction

1.1 The importance of iron

Iron is an essential micronutrient for the survival of almost all living organisms due to its critical roles in many biological processes. In humans, iron is required for the daily production of approximately 200 billion red blood cells, which uses about 20 mg of iron to synthesize the hemoglobin necessary for oxygen transport[1][2]. Humans can take up both inorganic iron and heme through enterocytes, but only about 2 mg of dietary iron is absorbed per day. The remaining 18 mg mostly comes from the recycling of iron through the breakdown of old or damaged red blood cells in the spleen, where iron is salvaged and transported back to the bone marrow for reuse[2].

Beyond oxygen transport, iron is the fundamental component of heme and iron-sulfur clusters (Fe-S), which are crucial protein cofactors involved in many cellular functions including steroid hormone synthesis and DNA repair[3]. For example, members of the cytochrome P450 enzyme superfamily contain a heme group with an iron atom at its center, allowing them to bind oxygen and transfer electrons[15]. The human iron regulatory protein 1 (IRP1) can switch between two structures depending on the presence or absence of the 4Fe-4S cluster[3].

Although the ability of iron in facilitating electron transfer allows it to participate in many biochemical reactions, it also predisposes cells to the risk of oxidative stress through the production of reactive oxygen species (ROS) such as hydroxyl radicals which damage membrane integrity through lipid peroxidation[4]. Disruption of iron homeostasis is also associated with severe disorders, including neurodegenerative diseases like Alzheimer's and Parkinson's, hemochromatosis, and various forms of anemia[5]. Iron deficiency is affecting over two billion people worldwide, making it one of the most prevalent nutritional deficiencies[6]. Conversely, iron overload, resulting from genetic conditions or excessive iron intake, has significant health risks, including liver disease, cardiomyopathy, and diabetes[7].

1.2 *Drosophila melanogaster* as a model to study iron metabolism

Given the importance of iron in biological systems and its complex role in health and disease, understanding iron metabolism is crucial. Many aspects of the cellular pathways needed to absorb, transport and store iron are still poorly understood. The fruit fly *Drosophila*

melanogaster shares significant genetic similarities with humans and represents a useful and important model for studying iron-related processes and disorders[9][8]. As I will outline below, a key advantage of using *Drosophila* for studying iron biology is the synthesis of the steroid hormone ecdysone, which requires mass production of heme cofactors. As such, ecdysone biosynthesis requires high levels of iron [10][11], which can be experimentally exploited to study cellular iron biology. Another advantage is that flies can be subjected to extreme iron depletion, which is considered unethical in mammalian model systems as this would result in asphyxiation (red blood cells require heme). Understanding the mechanisms underlying iron acquisition and regulation in *Drosophila* facilitates the study of iron-related disorders and potentially the development of new treatments in humans.

1.2.1 The heme synthesis pathway

Although heme is a critical iron cofactor, free heme is potentially cytotoxic and needs to be tightly regulated. Heme synthesis is a critical biochemical pathway that is highly conserved in all animals, including humans and *Drosophila*[14]. Consequently, there is no cellular capacity to store heme, and newly produced heme is directly incorporated into client proteins. The heme biosynthesis pathway begins from the mitochondria-mediated synthesis of aminolevulinic acid (ALA) by aminolevulinic acid synthase (ALAS). Two ALA molecules form porphobilinogen (PBG) catalyzed by aminolevulinic acid dehydratase (ALAD)[16]. Four PBG molecules then form tetrapyrrole hydroxymethylbilane by the enzyme PBG deaminase (PBGD)[17]. The hydroxymethylbilane molecules are subsequently converted to uroporphyrinogen III by uroporphyrinogen synthase (UROS), which then forms coproporphyrinogen III (CPgenIII), catalyzed by uroporphyrinogen decarboxylase (UROD)[18]. Subsequent modifications by coproporphyrinogen oxidase (CPOX/CPO) forms protoporphyrinogen IX, which is then converted into protoporphyrin IX by protoporphyrinogen oxidase (PPOX) and eventually heme[19]. This final step of heme synthesis requires the incorporation of ferrous iron into the porphyrin ring, and the process is catalyzed by ferrochelatase (FECH)[20] (Figure 1.1).

In humans, accumulation or overproduction of heme precursors has been shown to cause porphyria [21]. There are so far nine types of porphyria identified in humans, resulting from the

accumulation of different heme precursors. For example, pathogenic porphyrins (uroporphyrin I and coproporphyrin I) accumulate when URO3S dysfunctions, and these porphyrins isomerize and become fluorescent porphyrins under the UV light. Congenital Erythropoietic Porphyria (CEP) is caused by mutations in the UROS gene, and its symptoms usually include red or pink fluorescence teeth and urine when exposed in the sun. It also leads to a decrease in heme levels within erythroid cells, contributing to anemia. Interestingly, disruption in the *Drosophila* heme synthesis pathway leads to similar “porphyria-like” phenotypes. Prothoracic gland (PG) specific RNA interference (RNAi) targeted at PPOX causes the accumulation of protoporphyrin IX, and the flies show enlarged, red auto-fluorescence PG[22]. Interestingly, this red autofluorescence is also observed in mutants where genes that are not part of the core heme biosynthetic pathway are affected. For example, PG-specific disruption of *Drosophila* iron regulatory protein 1A (IRP1A), a key regulator of cellular iron levels, also leads to red auto-fluorescence in the PG[23], indicating that mutations affecting iron homeostasis can also disrupt heme production.

Heme Biosynthesis in *Drosophila*/humans

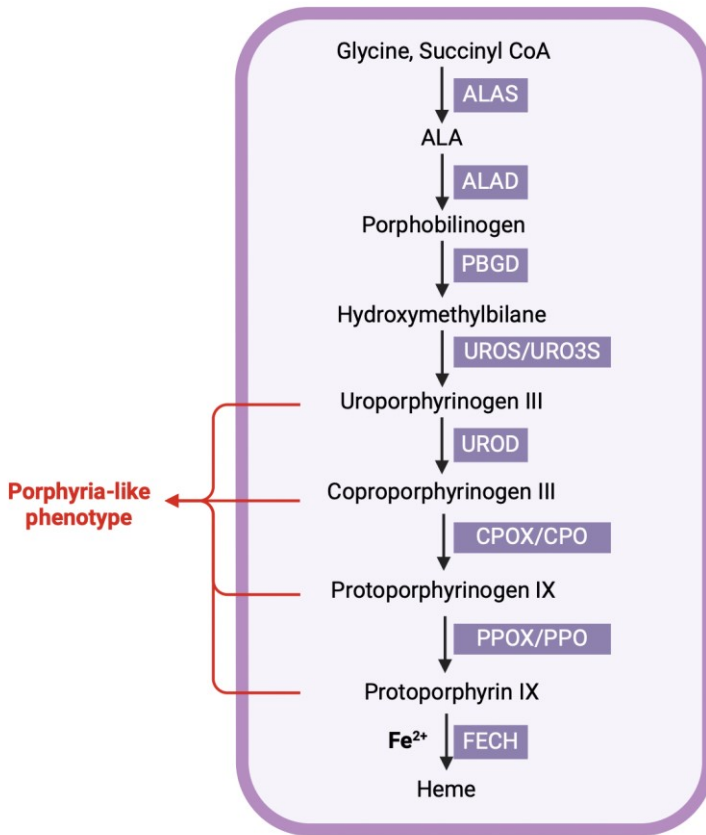


Figure 1.1 The heme biosynthesis pathway

Heme production involves eight enzymatic reactions. Disrupting genes downstream of UROS leads to the accumulation of protoporphyrinogens and a porphyria-like phenotype. Such larvae typically show an enlarged PGs that auto-fluorescence red, which is reminiscent of the human porphyrias. ALA: aminolevulinic acid; ALAS: aminolevulinic acid synthase; ALAD: aminolevulinic acid dehydratase; PBGD: porphobilinogen deaminase; UROS/URO3S: uroporphyrinogen III synthase; UROD: uroporphyrinogen decarboxylase; CPOX/CPO: coproporphyrinogen oxidase; PPOX/PPO: protoporphyrinogen oxidase; FECH: ferrochelatase.

1.2.2 The ecdysone synthesis pathway

The prothoracic gland (PG) is part of the larval ring gland in *Drosophila*. The PG comprises large, polyploid cells rich in organelles such as mitochondria and endoplasmic reticulum. The gland is also interconnected with the central nervous system, allowing it to receive regulatory signals that modulate ecdysone synthesis and release. Ecdysone is a crucial hormone for the metamorphosis of larval to pupal development of flies[25]. It is produced in the PG and controls developmental transitions such as molting and metamorphosis.[26]. The biosynthesis of ecdysone starts by converting cholesterol to 7-dehydrocholesterol (7DC) by the enzyme Neverland (Nvd), which harbours a Fe-S cluster cofactor[30]. 7DC then undergoes a series of enzymatic reactions and eventually forms 20-hydroxyecdysone (20E)[31]. These reactions are catalyzed by a set of enzymes known as the “Halloween enzymes” (Nvd, Shroud, Cyp6t3, Spookier, Phantom, Disembodied, Shadow and Shade)[26]. Except for Shroud, all the Halloween enzymes require heme or Fe-S cluster cofactors (Figure 1.2)[26]. The high demand of such iron cofactors in the ecdysone synthesis pathway makes the PG an iron-rich tissue that is sensitive to iron concentration changes[36]. It’s also worth noting that Shade is in the peripheral tissues, converting E to 20E, and spook expression is in follicle cells and embryo prior to the development of the ring gland. This is different in other insects, because they only have one of the two (spook), whereas *Drosophila* has two (spook and spookier).[130]

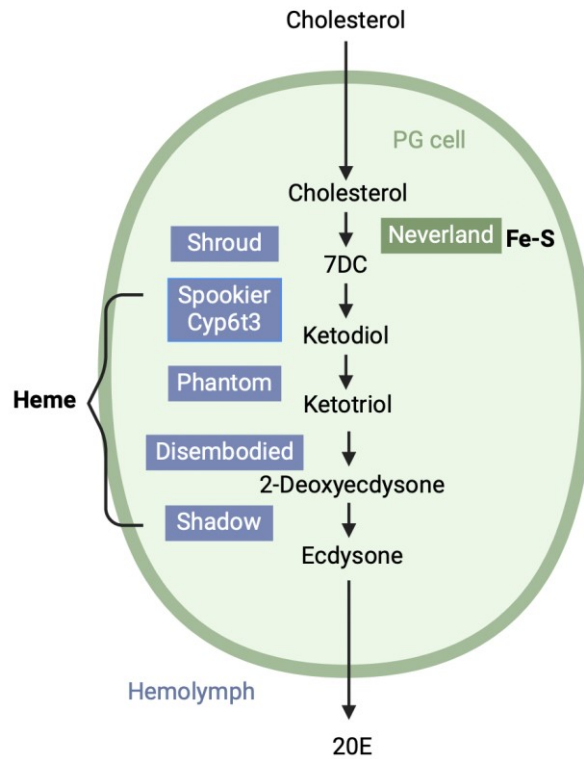


Figure 1.2 The ecdysone synthesis pathway

Production of ecdysone in the PG involves a series of enzymatic reactions. Such enzymes are known as the Halloween enzymes. Neverland requires the Fe-S cluster as a co-factor. The rest of the Halloween enzymes, except for Shroud, need heme as co-factors. 7DC: 7-dehydrocholesterol; 20E: 20-hydroxyecdysone, which is ecdysone's biologically active form.

1.3 Iron homeostasis in mammals

1.3.1 Iron uptake from diet

Iron is derived from the diet in two primary forms: heme and non-heme iron. Heme iron is associated with animal proteins, particularly hemoglobin and myoglobin, and is more efficiently absorbed by the body[32]. Non-heme iron, found in both plant and animal sources, primarily exists in the oxidized ferric iron (Fe^{3+}) state. This form of iron is generally less readily absorbed and requires enzymatic reduction before it can be taken up by intestinal cells[32].

The absorption of dietary iron begins in the duodenum, where ferric iron is first reduced to ferrous iron (Fe^{2+}) by the action of the enzyme duodenal cytochrome b (DCytb)[24]. This reduction is a crucial step as only ferrous iron can be transported across the intestinal epithelium[29]. Once reduced, iron is transported into duodenal enterocytes via the divalent metal transporter 1 (DMT1), which is a metal transporter that is not specific to iron, as it also transports copper, zinc, and cadmium[29]. Inside enterocytes, iron is transiently stored in the labile iron pool (LIP), which acts as a buffer to manage the iron supply for cellular processes, storage, or export[27]. Excess iron is sequestered within ferritin, a spherical protein complex capable of storing up to 4,500 ferric ions[33]. This storage is crucial for preventing free iron-induced formation of reactive oxygen species, which can lead to cell membrane damage[33].

Iron export from enterocytes is mediated by Ferroportin, the sole known iron exporter in mammals[35]. Exported iron is then oxidized back to its ferric form by a multicopper oxidase known as Hephaestin[35], which allows transport by Transferrin, the main iron transport protein in blood that delivers iron to target cells throughout the body. Cells internalize transferrin-bound iron through transferrin receptor 1 (TfR1)-mediated endocytosis, which leads to the release of iron within the acidic environment of endosomes[24].

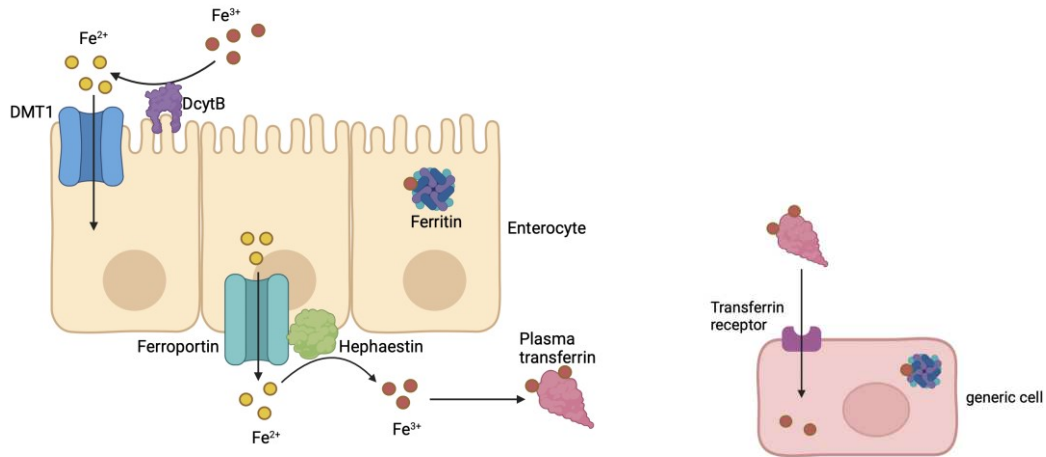


Figure 1.3 Iron uptake and transport in mammals

Dietary ferric iron is reduced to ferrous iron by the ferrireductase Dcytb and transported into the enterocyte by DMT1. Excess intracellular ferrous iron is oxidized to Fe^{3+} and stored in ferritin nanocages. Ferroportin transports ferrous iron out of the cell, and this process is coupled with a multicopper oxidase. Ferric iron binds to transferrin and is delivered to other cells. Dcytb: duodenal cytochrome b; DMT1: divalent metal transporter 1.

1.3.2 Iron regulation by mammalian IRPs

At the cellular level, regulation of iron homeostasis is achieved through the Iron Regulatory Protein/Iron Responsive Element (IRP/IRE) system. Under low dietary iron level, IRP1 and IRP2 bind to IREs found in the untranslated regions (UTRs) of iron-related genes' mRNAs. This interaction can either stabilize the mRNA to enhance translation or inhibit translation, thus increasing or decreasing the synthesis of proteins involved in iron uptake, storage, and export[37]. When iron level is low, the binding of IRPs to IREs on ferritin and ferroportin mRNAs inhibits their translation, reducing iron storage and export, while binding to DMT1 and TfR1 mRNAs enhances their translation, facilitating iron uptake[38]. When iron is abundant, IRP1 adopts the holo-form by undergoing a conformational change upon binding an iron-sulfur cluster (apo-IRP1 binds mRNAs in the absence of Fe-S clusters). IRP1 holo-form is a cytosolic aconitase that converts between citrate and isocitrate. Meanwhile, IRP2 is targeted for degradation via the ubiquitin-proteasome pathway, mediated by the F-box protein FBXL5 (F-box and leucine-rich repeat protein 5), which serves as an iron and oxygen sensor[39].

1.4 Iron homeostasis in *Drosophila melanogaster*

1.4.1 Iron uptake from diet in flies

Iron homeostasis in flies is a complex and less understood system compared to mammals, yet it remains critical for the fly's physiological and developmental processes[40]. Under iron-replete conditions, ferrous iron is taken through Malvolio (Mvl), which is divalent metal transport and is the homolog of mammalian DMT1 (Figure 1.4). Ferrous iron is either already present in the diet or produced by an unknown gut ferric reductase from ferric iron likely to be similar to mammalian Dcytb[41]. Candidates for this reductase activity include CG1275, CG8399, and no extended memory (nemy), though their exact roles in iron reduction are yet to be fully determined. Noticeably, both null DMT1 mice and null Malvolio flies are viable, suggesting the existence of other iron uptake systems in flies[40].

Ferritin, typically a storage protein, is suggested to have a dual function in flies, both as an iron storage unit and a transporter. Unlike in mammals, where ferritin is primarily

intracellular, in *Drosophila*, ferritin is predominantly found in the hemolymph and the secretory pathway (ER and Golgi), suggesting its involvement in systemic iron transport[42]. The transport of iron to these secretory pathways could involve the zinc transporter ZIP13, which plays a role in moving iron from the cytosol into these compartments[43]. Fly cytosolic ferritin is a heteropolymer consisting of 12 Fer1HCH (Ferritin 1 Heavy Chain Homologue) and 12 Fer2LCH (Ferritin 2 Light Chain Homologue) molecules. Fer1HCH is predicted to have ferroxidase activity, and Fer2LCH is associated with stabilizing the iron core[44]. Flies also have mitochondrial ferritin Fer3HCH (Ferritin 3 Heavy Chain Homologue), which contains a ferroxidase domain and is presumed to protect the mitochondria from oxidative stress[44].

There are three genes encoding Transferrins (Tsf1, Tsf2, and Tsf3) in *Drosophila*. Tsf1 is thought to function similarly to mammalian transferrin[45]. Dr. Soltani from our lab found out that Tsf1 binds iron in the hemolymph and delivers them to the PG, and this process is dependent on another protein named Evi5. A putative transferrin receptor on the PG surface mediates the uptake of iron-bound Tsf1 into the cells through receptor-mediated endocytosis[120]. The roles of Tsf2 and Tsf3 remain less clear, with Tsf2 involved in non-iron related cellular functions and Tsf3 potentially linked to circadian rhythm regulation[46]. However, transferrin receptors are still yet to be identified. Additionally, the absence of orthologs to mammalian Ferroportin in *Drosophila* makes it unclear how iron is exported from enterocytes[40].

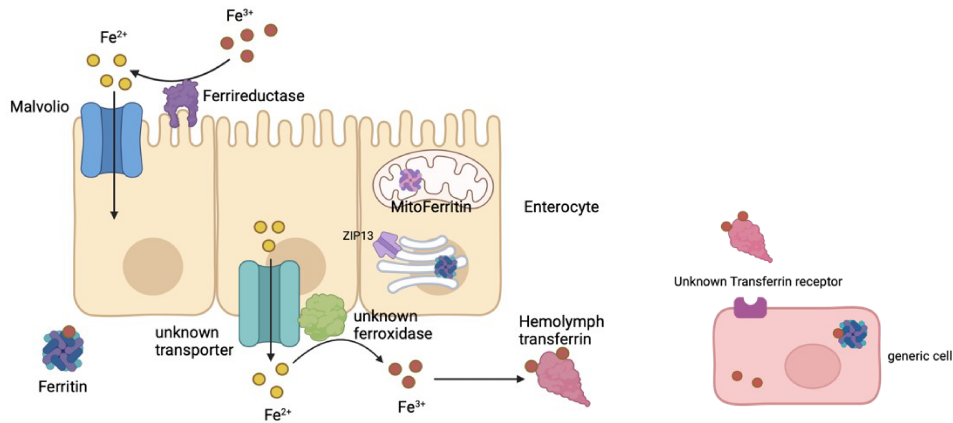


Figure 1.4 Iron uptake and transport in flies

Dietary ferric iron is presumably reduced to ferrous iron by a ferric reductase and transported into the enterocyte through Malvolio. Excess ferrous iron is converted to ferric iron and then stored inside ferritin. ZIP13 exports iron from the cytosol into the ER/Golgi for incorporation into ferritin. How iron is exported out of the enterocyte is unclear, since no *Drosophila* protein with ferroportin-like function has been identified so far. High concentrations of ferritin are found in the hemolymph, suggesting a potential iron transport function. Hemolymph transferrin takes up ferrous iron and circulates through the body, but no transferrin receptors have been identified so far.

1.4.2 Iron regulation by IPRs in flies

The regulation of iron at the cellular level in *Drosophila* is also mediated by the IRP/IRE system, but with notable differences from the mammalian system. *Drosophila* expresses two IRP1 orthologs, IRP1A and IRP1B, of which IRP1A functions similarly to mammalian IRP1 [53]. Like vertebrate IRP1, *Drosophila* IRP1A can switch between apo-form and holo-form (Figure 1.5). Under conditions of iron deficiency, apo-IRP1A binds to IREs located in the mRNAs of critical iron management genes, such as those encoding the heavy chain of ferritin (Fer1HCH) and succinate dehydrogenase subunit B (SdhB)[44]. This binding activity regulates the translation of these gene transcripts, thereby managing iron storage and utilization in response to cellular iron levels[53].

When iron levels are sufficient, IRP1A undergoes a conformational change by incorporating an iron-sulfur (Fe-S) cluster, which shifts its functionality from an RNA-binding protein to a cytosolic aconitase. This transformation effectively ceases its role in iron metabolism regulation, shifting to help manage metabolic processes that require aconitase activity. Unlike IRP1A, IRP1B appears to exist predominantly in its holo-form, acting solely as an aconitase and not participating in RNA binding or in canonical iron regulation directly[53]. However, nuclear localization has been observed for both IRP1A and IRP1B, and it implies IRP1A having potential regulatory functions in gene expression beyond its cytosolic activities. Its nuclear role might involve interactions with chromatin or transcription factors, thereby influencing gene expression related to iron homeostasis and other cellular processes. Similarly, IRP1B's presence in the nucleus suggests it might also play a role in iron regulation, although the mechanisms are yet to be fully understood, and nuclear IRP1 has been observed in human hepatocytes[53].

The IRP1A null mutant exhibits a severe phenotype characterized by L2 arrest under normal dietary conditions. Moreover, two mutants of IRP1A have been previously generated and studied in my lab. IRP1A^{C450S} locks the protein into its apo-form, abolishing iron-sulfur binding ability. As such, this protein variant remains locked in the RNA-binding state, even under iron-rich conditions[44]. This can lead to iron imbalances, such as increased iron storage or altered iron utilization. Conversely, the other described mutant IRP1A^{3R3Q} disrupts the RNA binding

capability of IRP1A entirely. This variant has the holo-form behavior, reducing the protein's ability to regulate iron metabolism under iron-deficient conditions[44][52].

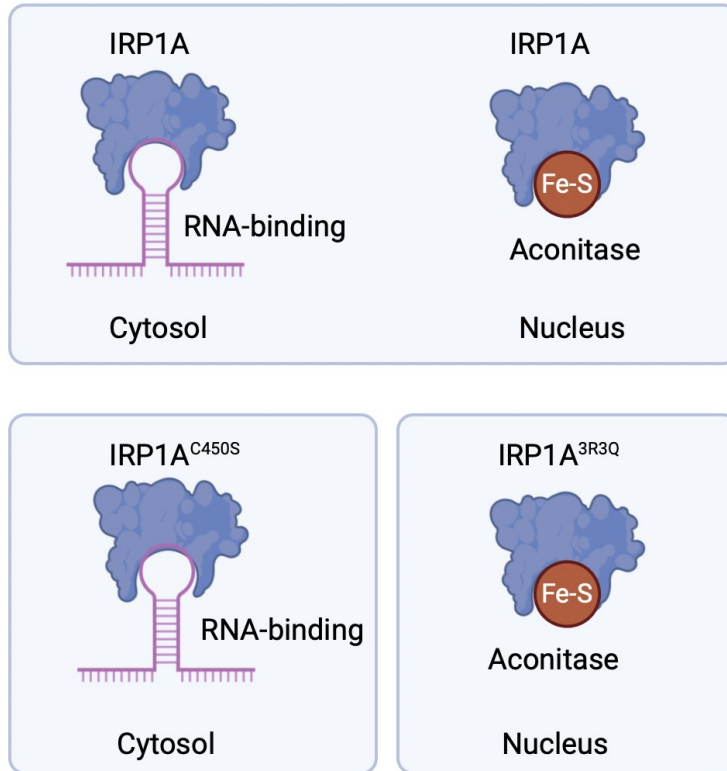


Figure 1.5 Two IRP1A mutants.

IRP1A apo-form has RNA-binding ability and resides in the cytoplasm. It can undergo a conformational change and become the holo-form by incorporating a single iron sulfur cluster. The holo-form is in the nucleus and functions as an aconitase. The mutant IRP1A^{C450S} is locked into its apo-form and no longer enters the nucleus. The mutant IRP1A^{3R3Q} has impaired RNA-binding ability and functions as an aconitase in the nucleus. IRP: Iron Regulatory Protein.

1.5 *Mco4* is induced under iron-deprived conditions

1.5.1 *Mco4* upregulation in iron-chelating diet

Iron-chelating diet was made by adding Bathophenanthroline Sulfate (BPS) to Nutri-fly food. The BPS molecule consists of phenanthroline, a heterocyclic compound that forms a planar, tridentate ligand capable of coordinating with metal ions. The sulfonic acid groups on BPS increase its solubility in aqueous solutions, facilitating its interaction with iron in biological systems. When BPS encounters Fe^{2+} ions, it forms a hexadentate complex by binding through nitrogen atoms in its aromatic rings[127][126]. This strong coordination creates a highly stable and inert complex, effectively sequestering Fe^{2+} and preventing it from engaging in redox reactions or being utilized in biological processes. Three BPS molecules bind to one ferrous iron to form one 3BPS- Fe^{2+} complex that has a pink or light red color[127].

In our lab, we used BPS as the ferrous iron chelator due to its stability and colorimetric properties. 3BPS- Fe^{2+} complexes can be detected and quantified using spectrophotometric assays. However, disadvantages comes with using BPS as well. At higher concentrations, BPS may begin to chelate other divalent metal ions and cause non-specific effect. Additionally, flies generally exhibit an aversion to food containing BPS, which can lead to reduced food intake. During the food making process, BPS is added to Nutri-fly food and mixed by hand. If the food is not thoroughly mixed, flies may selectively eat areas of the food that contain less BPS.

Iron deprivation has different effect on the flies' survival depending on the BPS concentration used. Previously it was found in my lab that when w^{1118} animals were raised on a moderately iron-limited diet (120 μM BPS), their survival rate would gradually decline and reach around 50% in the fifth generation. At this concentration, iron availability is reduced, but some iron may still be accessible, allowing the organism to survive over several generations. At higher concentrations, such as 500 μM , BPS chelates most of the available ferrous iron from the diet and creates a rapid depletion of iron, resulting in lethality at the first or the second generation.

Dr. Sattar Soltani from my lab carried out an RNA-Seq experiment following raising these iron-deprived w^{1118} flies. After the five generations of rearing animals on 120 μM BPS

media, the flies were either transferred to an iron-enriched medium (1 mM Ferric Ammonium Citrate; FAC) or transferred to a fresh iron-chelating diet (i.e., no change in BPS). Brain ring gland complex, gut and whole-body samples from 16 hr post-L3 instar molt were collected, and the analysis of RNA-Seq revealed 88 genes that responded to a change in dietary iron concentrations in the BRGC. Among them, the gene multicopper oxidase 4 (*Mco4*) showed a ~2,000-fold increase compared to the same time point under normal dietary iron levels. Following this, Dr. Sattar Soltani performed an RT-qPCR experiment using the ring gland tissue of *w¹¹¹⁸* raised on BPS- or FAC-containing media separately for one generation. *Mco4* expression was measured at 12 hr, 16 hr, and 44 hr after the L2/L3 molt. Compared to iron-rich conditions (FAC diet), *Mco4* expression increased 2-, 5-, and 13-fold respectively (Figure 1.6 A), further supporting the idea that *Mco4* is transcriptionally induced in response to dietary iron deprivation.

1.5.2 *Mco4* upregulation in genetic disruption of iron

Mco4 not only responds to dietary deprivation of iron, but genetic disruption of cellular iron homeostasis or iron transport as well. The gene 1,4-Alpha-Glucan Branching Enzyme (*AGBE*) is involved in iron homeostasis by physically interacting with the IRP1A holo-form, likely to repair oxidatively damaged Fe-S clusters (i.e., clusters that lost an iron atom). A disruption in *AGBE* through RNAi impairs iron metabolism and phenocopies iron deprivation, resulting in L3 arrest and red ring gland phenotype. It is worth mentioning that the red ring gland phenotype in flies is a result of heme biosynthesis pathway disruption, and it is not always equal to iron deficiency. In wild type flies, dietary iron deficiency ultimately leads to death, but they do not exhibit the red ring gland phenotype even at the time of death. The gene Ecotropic Viral Integration Site (*Evi5*) is a GTPase-activating protein and is involved in iron transport especially during ecdysone synthesis. Disruption of *Evi5* by PG-specific RNAi also leads to red autofluorescence ring glands. Dr. Sattar Soltani tested *Mco4* expression in PG-specific RNAi of *AGBE* and *Evi5* and found a 114-fold and 52-fold induction of *Mco4* in the PG respectively (Figure 1.6 B). Together, these data suggest that *Mco4* is strongly induced by genetic disruption of iron homeostasis or transport.

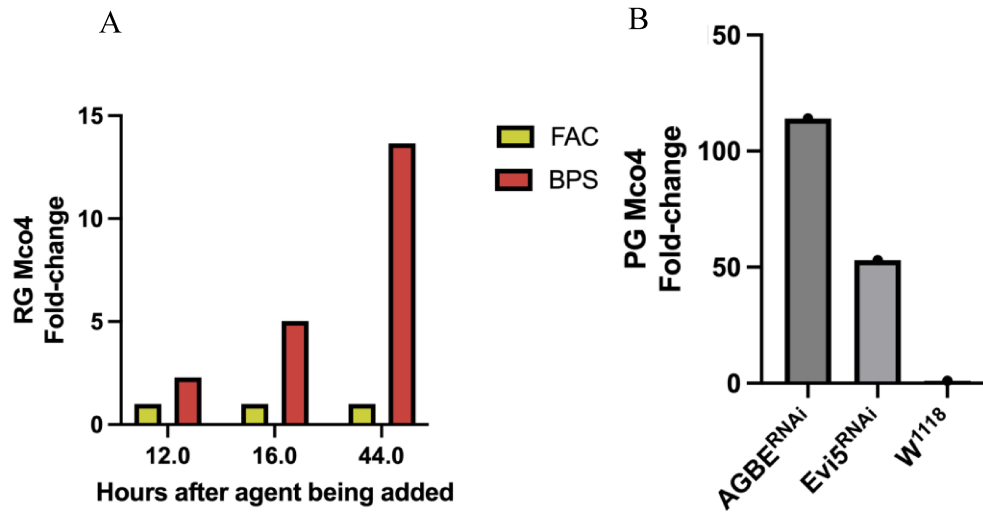


Figure 1.6 *Mco4* is upregulated in iron-deprived conditions

(A) *Mco4* is upregulated when flies were transferred to the iron-chelating diet. The experiment was based on ring gland samples isolated from *w¹¹¹⁸* larvae reared on BPS or FAC for one generation. *Mco4* increased 2-, 5-, and 13-fold at 12 h, 16 h and 44 h post L3 molt respectively. (B) *Mco4* upregulation in response to genetic disruption of iron homeostasis. AGBE and Evi5 are involved in iron homeostasis, and mutations in either of them mimic iron deprivation. *Mco4* expression increased 114- and 52- fold in PG-specific RNAi. *AGBE*: 1,4-Alpha-Glucan Branching Enzyme; *Evi5*: Ecotropic Viral Integration Site; RG: ring gland; PG: prothoracic gland; BPS: Bathophenanthrolinedisulfonic acid; FAC: Ferric ammonium citrate.

1.6 Multicopper oxidases

Mco4 is a member of the multicopper oxidase family. *Drosophila* has four genes encoding MCOs, and three out of them are ferroxidase, laccases and ascorbate oxidases. This protein family comprises enzymes characterized by their ability to oxidize substrates by accepting electrons that are then transferred to molecular oxygen[62]. These enzymes are characterized by their multicopper centers and copper-binding sites, which are essential for their catalytic activity[62]. A generic multicopper oxidase has three types of copper-binding sites. The Type 1 Copper site is located in the center and responsible for the electron transfer process. The Type 2 and Type 3 copper sites are involved in the reduction of molecular oxygen to water[60]. Taking a human MCO ceruloplasmin as an example, it has a complex structure comprising six domains arranged in ternary symmetry[129]. Type I copper atoms are located in domain 2, 4, and 6, and are approximately 18 angstroms apart away from each other, facilitating electron flow. The trinuclear copper cluster consists of Type II and Type III copper sites. It is positioned at the interface between domains 1 and 6[129].

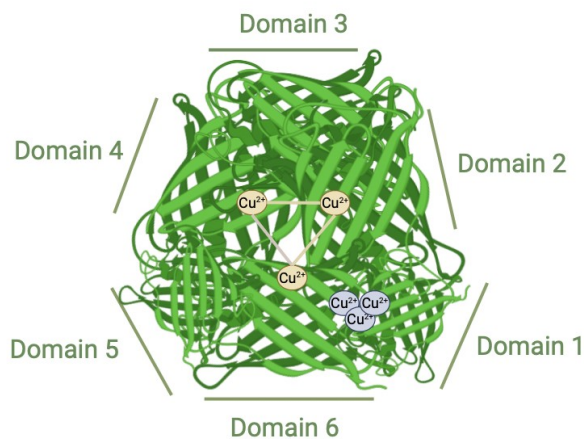


Figure 1.7 The protein structure of Ceruloplasmin

Ceruloplasmin metalloprotein has six copper atoms and six domains. The six domains are shown with lines that exhibit ternary symmetry. Domains 2, 4, and 6 house the mononuclear type I blue copper sites (indicated by yellow circles) The trinuclear copper cluster (type II and type III copper ions) is located at the interface between domains 1 and 6 (grey circles)[129].

1.6.1 Multicopper oxidases in mammals

Mammals have three multicopper oxidases: ceruloplasmin, Hephaestin, and zyklopen. Ceruloplasmin is a 130-kDa plasma glycoprotein predominantly synthesized in the liver[58]. It is actively involved in copper transport, ferroxidase activity, blood coagulation, and defense against oxidative stress. Ceruloplasmin is essential for the oxidation of Fe^{2+} to Fe^{3+} , facilitating iron binding to transferrin for systemic transport. This process not only aids in iron homeostasis but also serves as an antioxidant function by limiting iron's potential to catalyze the production of reactive oxygen species[58]. Disruption of ceruloplasmin gene expression in mice leads to abnormal iron accumulation in the liver, spleen, and brain[61].

Hephaestin is a membrane-bound homolog of ceruloplasmin with around 50% sequence identity, and it is predominantly expressed in the intestinal epithelium[35]. Hephaestin is a ferroxidase, and it works with the iron transporter ferroportin to oxidize and export iron from enterocytes into the bloodstream. Hephaestin's expression is not limited to the intestine; it is also found in other organs like the brain, heart, and pancreas, suggesting additional roles in protecting these tissues from iron-induced oxidative stress[56].

Zyklopen is a more recently discovered MCO with a putative transmembrane domain and shares structural similarities with Hephaestin[54]. Its expression is high in the placenta, suggesting a specialized role in placental iron transport from mother to fetus. The functional dynamics of Zyklopen are still being explored, particularly its involvement in maintaining fetal iron levels during conditions of maternal anemia or copper deficiency[54].

1.6.2 Multicopper oxidases in *Drosophila*

There are four genes encoding the multicopper oxidase family in *Drosophila*: *Mco1*, *Mco2*, *Mco3*, and *Mco4*.

Mco1: *Mco1* is prominently expressed on the basal surface of the intestine and the Malpighian tubules. Strong knockdown of *Mco1* is lethal, while weak knockdown shows reduced iron content. It is a potent ascorbate oxidase and affects iron homeostasis through an unknown mechanism[44].

Mco2: *Mco2* is also known as *Straw*. It is a laccase primarily involved in the pigmentation processes of the newly synthesized cuticle. It participates in the sclerotization of the cuticle by oxidizing ectodermal cell-derived phenols to melanin. Knockdown of *Straw* in flies results in unpigmented cuticles[59].

Mco3: *Mco3* encodes a protein with a putative iron-binding region and a transmembrane domain. *MCO3* has potent ferroxidase activity and is also linked to copper homeostasis. Knockout of *Mco3* in flies shows increased iron accumulation and reduced *Mvl* expression, suggesting an iron reflux function similar to that of mammalian ferroportin/ferroxidase[57].

Mco4: *Mco4* is a ~2k bp gene located on the X-chromosome. The *Mco4* sequence is predicted to contain an iron-binding region, a transmembrane domain and a signal peptide. Interestingly, *Mco4* shares homology with yeast's Fet3p, which is part of the high affinity iron import system of yeast cells. As previously mentioned, expression studies in our lab indicated that *Mco4* is strongly upregulated under iron-deprived conditions or genetic disruption of cellular iron homeostasis, pointing to its potential involvement in response to iron deficiency through iron import.

Our former lab member Areeg Abd Elhafiz generated a CRISPR/Cas9-mediated *Mco4* null mutant line and an *UAS-Mco4* transgenic line. Overexpression of *Mco4* (*tubulin>UAS-Mco4-3Myc*) revealed that *Mco4* localized to the plasma membrane in the gut, the PG, and salivary glands, in line with its putative function in iron import (Figure 1.7)[121].

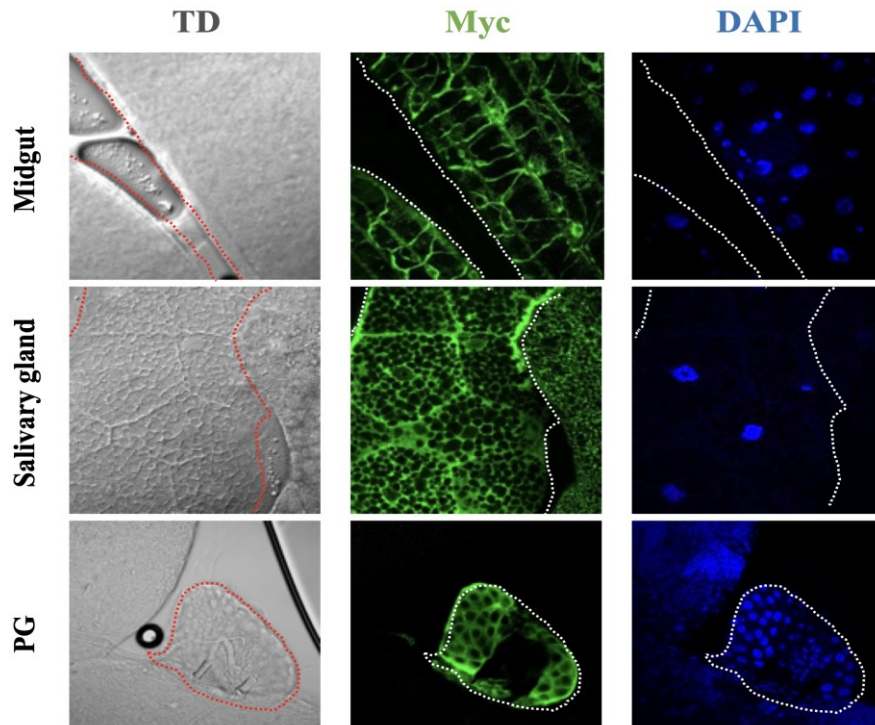


Figure 1.8 Whole-body overexpression of *Mco4* shows a membrane-bound localization in three different tissues.

Midgut, PG, and salivary gland were dissected using *tubulin>UAS-Mco4-3xMyc* L3 larvae, and tissues were stained with anti-Myc antibody (green) and DAPI (blue). Pictures were taken under a 60X confocal microscope lens. The green signals indicate the subcellular localization of Mco4, and DAPI/blue signal is used to visualize the nuclear. PG: Prothoracic gland. TD: brightfield of the transmitted detector.

Mco4 null mutants (*Mco4^{KO}*) are viable and phenotypically normal under iron-replete conditions. *Mco4^{KO}* mutants do not show red ring glands nor reduced survival on standard fly media, suggesting that *Mco4* has little involvement in iron import under normal dietary iron levels. However, *Mco4* was only upregulated when iron is depleted (Figure 1.6 A), and its yeast counterpart Fet3p is mainly expressed under iron-deficient conditions as well. The investigation of *Mco4* null mutant's phenotype remains to be continued in an iron-deficient background.

1.7 Iron uptake in yeast

In yeast, iron import is governed by two main uptake systems: the high-affinity Fet3p/Ftr1p complex and the low-affinity Fet4p transporter. Fet3p is a ferroxidase with a single transmembrane domain, and it oxidizes ferrous iron (produced by the ferric reductase FREp) to ferric iron, which is then transported across the plasma membrane via Ftr1p. Ftr1p is an integral membrane protein with 6 transmembrane domains, forming a channel through which Fe^{3+} can be translocated. The expression of FET3 and FTR1 is tightly regulated at the transcriptional level by the Aft1p and Aft2p transcription factors. Under iron-limited conditions, Aft1p and Aft2p activate the expression of genes involved in iron uptake, including FET3 and FTR1. Together, the Fet3p/Ftr1p complex forms a high-affinity iron transport system essential for iron uptake when yeast cells face low iron availability[63][70][71]. In contrast, the Fet4p system is a non-specific divalent metal ion transporter that imports transition metals, including zinc, copper, and cadmium, alongside iron. Although it has a similar function to mammalian DMT1, they are not homologous proteins. Fet4p belongs to the major facilitator superfamily (MFS), which transports small solutes in response to chemiosmotic gradients., whereas DMT1 is a member of the solute carrier 11 (SLC11) family. The low-affinity Fet4p system is predominantly utilized under iron-replete conditions. In addition to Fet3p, yeast encodes another ferroxidase, Fet5p, which works with the Fth1p protein to mobilize iron from vacuolar stores[69]. This internal iron trafficking mechanism ensures that cellular compartments receive adequate iron during fluctuating external conditions[66].

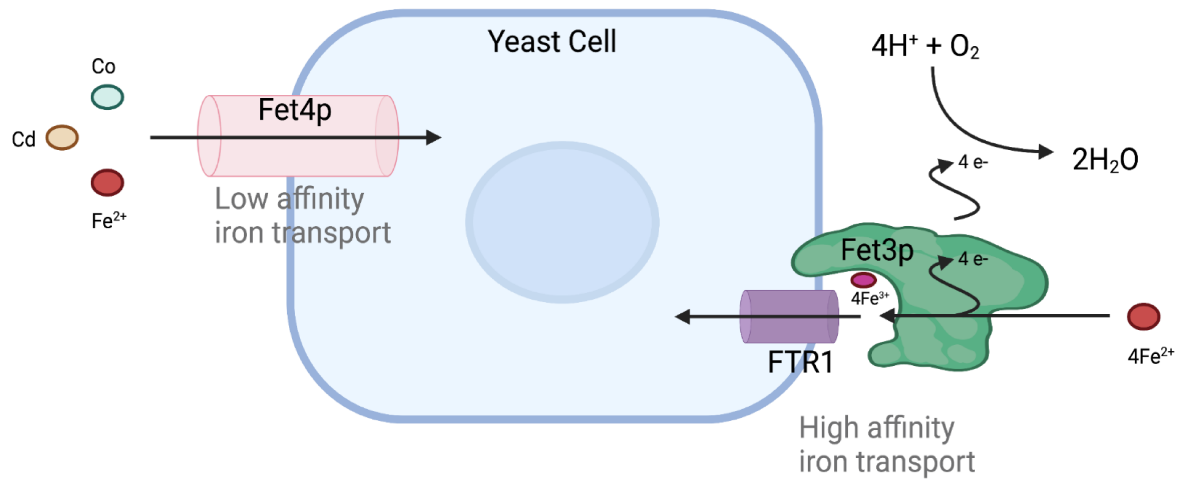


Figure 1.9 Two iron import system in yeast

The low-affinity iron transport system (Fet4p) is a non-specific divalent metal ion transporter responsible for the uptake of several transition metals, including zinc, copper, cadmium, and iron. This system is expressed primarily under iron-replete conditions. The high-affinity iron import system (Fet3p/Ftr1p complex) is activated under low iron condition to ensure efficient iron uptake. Ferrous iron is produced by the ferric reductase FREp. Fet3p is a multicopper oxidase that changes ferrous iron into ferric iron, and Ftr1p is a ferric iron transporter.

1.8 Iron import systems in plants

Given the poor solubility of iron in aerobic and neutral to alkaline soil conditions, plants also have evolved high-affinity iron transport systems, known as Strategy I (non-grass species) and Strategy II (grass species)[125][126]. Strategy I involves the reduction of ferric iron (Fe^{3+}) to ferrous iron (Fe^{2+}) at the root surface before uptake. The enzyme Ferric Chelate Reductase (FRO2) is located in the plasma membrane of root epidermal cells and is responsible for reducing Fe^{3+} to Fe^{2+} . The high-affinity ferrous iron importer Iron-Regulated Transporter 1 (IRT1) facilitates the uptake of Fe^{2+} into root cells[126]. Together, the expression of FRO2 and IRT1 is upregulated under iron-deficient conditions. Strategy II involves the secretion of phytosiderophores (PS), which are organic compounds that chelate Fe^{3+} in the soil, forming soluble Fe^{3+} -PS complexes that can be taken up by the Yellow Stripe1 (YS1) Transporters. The secretion of phytosiderophores and the expression of YS1 transporters are also upregulated under iron deficiency.

Interestingly, plants also have an Iron-Regulated Transporter 2 (IRT2), which is a member of the ZIP family. IRT2 is expressed in root cell and the protein transports a range of divalent metal ions, including Fe^{2+} , Zn^{2+} , Mn^{2+} , and Cd^{2+} , similar to the low affinity iron transport system in mammals or yeast[126]. The presence of both high and low affinity iron import systems in yeast and plants reflects the evolutionary adaptation of these organisms to fluctuating environmental iron levels, and such mechanisms could also be present in animals.

1.9 Research objectives

The evidence suggests that *Mco4* responds to iron deprivation and functions as an iron importer, but understanding of its exact role remains limited due to a lack of comprehensive *in vivo* characterization. This study aims to investigate the function of *Mco4* in *Drosophila* as a high affinity iron importer through three primary objectives:

1.8.1 Identifying *Mco4*'s expression pattern

Although transgenically produced Mco4 localized to the plasma membrane, its endogenous expression in different tissues is still to be investigated. A high affinity iron import system is expected to be found in the plasma membrane of enterocytes, facing the gut lumen, and expression may increase in response to iron deprivation. To address this aim, I generated a tagged *Mco4* knock-in line via CRISPR/Cas9, which allowed me to study its endogenous expression *in vivo*. In addition, I also performed expression studies of *Mco4* using RT-qPCR in high and low dietary iron levels.

1.8.2 Characterization of *Mco4* null mutant phenotype

In an iron-deprived diet, ferrous iron is bound to BPS and becomes inaccessible to Mvl, causing *Mco4* to be upregulated to facilitate ferric iron import. *Mco4* loss-of-function is expected to trigger a stronger phenotype in iron-deprived conditions. By analyzing the iron-related phenotypic consequences of *Mco4* disruption, such as developmental defects and decreased iron content, I aimed to establish a direct relationship between *Mco4* and iron under iron-deprived conditions.

1.8.3 Investigating the molecular function of Mco4

This objective examined the biochemical activity of Mco4, including its ferroxidase activity, which is an essential function of a ferric iron importer. The effect of *Mco4* overexpression in flies was also investigated to further investigate its role in iron import. Finally,

to identify potential interactors of Mco4, I characterized the protein-protein interaction profile of Mco4 in normal and deprived iron conditions.

CHAPTER 2 Material and methods

2.1 *Drosophila* husbandry and maintenance

All *Drosophila* lines utilized in this study are listed in Table 2.1. Stocks were maintained at 18°C on a standard cornmeal diet. Each line had at least one backup vial and was transferred to new food every four weeks.

Active experimental flies were kept at 25°C with 50-60% humidity on Nutri-Fly food (Genesee Scientific, Catalog # 66113). The Nutri-Fly food recipe was modified from the Bloomington *Drosophila* Stock Center (BDSC) as follows: 4.25 liters (L) of Nutri-Fly food includes 67.5 grams (g) of yeast, 39 g of soy flour, 285 g of yellow cornmeal, 22.5 g of agar, 300 milliliters (mL) light corn syrup, and 18.8 mL of propionic acid. To prepare a 100 mL of Nutri-Fly media, 17.8 g of the Nutri-Fly powder was boiled in 100 mL of sterile Mili-Q water for 5-10 minutes (min). Once the temperature dropped to 50-60°C, 450 microliters (µL) of propionic acid (Sigma, Catalog # P1368) was added for every 100 mL of the media and thoroughly mixed. Media were prepared into vials, bottles, or petri dishes one day prior to use and stored at 4°C for up to five weeks. For crossing experiments, around 20 flies were put into one Nutri-Fly food vial with a male to female ratio of 1:3.

2.2 Iron-supplemented medium

Ferric Ammonium Citrate (FAC, Sigma Aldrich, #F5879) was used as the dietary iron supplement. The 100X stock was prepared by adding 0.265 g of FAC in 10 mL sterile milliQ water. 1 mM FAC food was made by adding 1 mL of the stock into 100 mL of newly prepared Nutri-Fly food before the food cooled down.

2.3 Iron-chelated medium

Bathophenanthrolinedisulfonic acid disodium salt hydrate (BPS, Sigma Aldrich, #146617) was used to chelate ferrous iron from the food. The 100X stock was prepared by adding 0.059 g of BPS in 10 mL sterile milliQ water. To make iron-chelated medium, the stock was added to newly prepared Nutri-Fly food before the food solidified. After mixing, the food presents a light red color due to the presence of propionic acid that reduces ferric iron to ferrous iron.

2.4 Survival Study

2.4.1 Preparing embryo collection plates

Petri dishes containing grape juice were prepared one day prior to embryo collection. 3 g of Bacto agar was dissolved in 100 mL milliQ water and autoclaved for at least 30 min. When cooling down, 25 mL grape juice concentrate was added and mixed thoroughly. After the mixture cooled down to room temperature (RT), 0.125 g of methylparaben and 2.5 mL of ethanol were added and mixed. The mixture was prepared into petri dishes and stored at 4°C.

2.4.2 Embryo collection and survival count

50-100 newly hatched flies were isolated in a cage containing Nutri-Fly food and allowed to age 1-3 days under 25°C. Before collection, grape juice medium was placed into the cage instead of Nutri-Fly food. To collect freshly fertilized eggs, the medium was changed three times per hour. For each of the three experimental replicates, fifty embryos were collected from grape juice medium and placed in petri dishes containing appropriate medium. The number of L1 larvae hatched was recorded the next day, and the number of L2 and L3 larvae were scored and transferred to vials on the third day. In the following 4-7 days, the number of pupae and enclosed adults were monitored and counted. Throughout the study, all flies, embryos and larvae were allowed to develop at 25°C.

2.5 *Drosophila* staging and dissection

Embryos were collected on Nutri-Fly medium and allowed to grow until 68–70 hours later. L3 larvae were counted and removed, leaving behind only those in the L2 stage. These L2 larvae were then monitored closely. As they progressed to the L3 stage, they were transferred to a petri dish containing Nutri-Fly medium every 2 hours. After 44-48 hours, all L3 larvae were washed in water or 1X PBS to detach any residual food medium before being dissected.

2.6 *Drosophila* tissue immunostaining and imaging

Larvae were collected and washed in chilled 1X PBS. Tissues were dissected in sterile 1X PBS and then fixed in 4% formaldehyde for 15 min at RT. The fixative was then removed,

and the samples were washed thrice with 1X PBST (1X PBS with 0.3% Triton X-100) for 10 min each time. A blocking buffer (5% normal goat serum and 0.3% TritonTM X-100 in 1X PBS) was added, and the tissue was incubated for 60 min at RT. After that, the primary antibody (Table 2.3) was diluted 1:1000 or 1:2000 in an antibody dilution buffer (0.3% TritonTM X-100 and 1% BSA in 1X PBS). After removing the blocking buffer, the specimen was added with the diluted primary antibody and incubated overnight at 4°C on a shaker. On the following day, the sample was washed three times in 1X PBST for 10 min each. A fluorochrome-linked secondary antibody (see Table 2.3) was diluted in the same antibody dilution buffer and added to the tissue. The tissue was then incubated for 1-2 hours at RT in a light-protected environment. Following this, the tissue was washed three times with 1X PBST for 10 min each. Nuclear staining was done by incubating with DAPI (Cell Signaling, #4083) for 20 min at RT, followed by three 10-min washes in 1X PBST. The samples were then prepared on slides with a drop of mounting buffer (50% PBS, 50% glycerol). Slides were stored at -20°C protected from light. Imaging was done using a Nikon Eclipse 80i Confocal C2+ microscope and camera.

2.7 *Drosophila* whole larvae co-IP

Whole body Mco4-3Myc overexpression larvae were collected by crossing *UAS-Mco4-3Myc* with *Act5C-Gal4* (hereafter: *Actin-Gal4*), and 50 of such late L3 (40 h) larvae were collected for each biological replicate. The same amount of *w¹¹¹⁸* larvae was collected as the controls. Larvae were collected in 1X PBS, allowed to remain in the buffer for 2-5 min to expel gut contents, then washed twice with fresh 1X PBS for further cleaning. After that, larvae were transferred into 1.5 mL tubes filled with ice-cold PBST (1X PBS, pH 7.4, with 0.1% Tween⁻²⁰). After removing as much PBST as possible from the samples, the dissected tissues were fixed in freshly prepared 1X PBS with 0.2% formaldehyde at RT on a rotary shaker for at least 10 min. After removing the fixative solution, 0.25 M glycine solution in PBST was added to quench the crosslinking, shaken for 5 min, and subsequently removed. The samples were then washed three times in PBST with gentle inversion. After washing, PBST was removed, and the samples were snap-frozen in liquid nitrogen, stored at -80°C until use.

For further processing, samples were thawed on ice and lysed using a Dounce homogenizer pre-rinsed with the lysis buffer (recipe in Appendix A2). Samples were transferred

to 1 mL of lysis buffer and repeatedly homogenized every 15 min for 1 hour on ice. The lysate was incubated in the lysis buffer for another 15 min on ice for complete lysis and then centrifuged at 16,000 rpm for 30 min at 4°C. In the meantime, 50 µL of anti-Flag M2 affinity gel was prepared in a spin column (Sigma, #A2220), washed five times with 300 µL lysis buffer without proteinase inhibitors by quick spin down. For the sixth wash, the spin column was plugged tightly and washed with 300 µL of lysis buffer containing proteinase inhibitors (Sigma, #P2714). The spin column was kept on ice until use. When lysate centrifugation is ready to collect, the spin column was unplugged, and the supernatant was discarded by spin down.

The clear lysate supernatant was transferred to a spin column. 50 µL of the lysate was reserved for protein concentration analysis. The samples were incubated with anti-Flag M2 affinity gel for 3 hours at 4°C on rotation, then centrifuged at 12,000 rpm for 10s to discard the flow-through. Samples were washed three times with 300 µL of wash buffer 1 (1X buffer G, 0.1% Triton X⁻¹⁰⁰, 5% glycerol) and then three times with 300 µL of wash buffer 2 (1X bugger G, 5% glycerol). Each wash was done by centrifuge at 12,000 rpm for 30 s.

For protein elution, 30 µL of the elution buffer (1X SDS loading buffer with 2-mercaptoethanol) was applied to the column. The column was heated at 95-100°C for 5 min. The eluate was collected by centrifugation at 10,000 g for 10s and stored at -80°C until use. Prior to electrophoresis, a fresh 12.5% SDS-PAGE gel was prepared, and samples were allowed to run on the gel for around 20 min at 100 V. The gel was stained by Coomassie Blue to visualize protein bands. The gel was then sent for mass spectrometry at the Alberta Proteomic and Mass Spectrometry Facility (4096, Katz Group Centre for Pharmacy and Health Research, Edmonton, Alberta, Canada).

2.8 TurboID using *Drosophila* whole larvae samples

Whole body *Mco4-Tb* overexpression larvae were generated by crossing *UAS-Mco4-V5-Tb* with *Actin-Gal4*, and 50 of such larvae were collected for each biological replicate. Controls were the offspring from *w¹¹¹⁸* crossed with *Actin-Gal4*. Three biological replicates were collected for both experimental and control groups, and samples were stored at -80°C until use. Samples were lysed by homogenization with a pestle in 1-2 mL of RIPA lysis buffer (50 mM Tris, 150

mM NaCl, 0.1% (wt/vol) SDS, 0.5% (wt/vol) sodium deoxycholate, 1% (wt/vol) Triton X⁻¹⁰⁰, pH7.5), repeated every 10 min for a total duration of 1 hour. The cell lysate was then centrifuged at 4°C, 13,000 rpm for 30-45 min. The upper clear supernatant was then transferred to a new 1.5 mL Eppendorf tube. Protein concentration was measured using the BCA protein assay.

For protein collection, 25 µL of streptavidin magnetic beads (Thermo Fisher Scientific, Catalog # 88816), were rinsed twice with 1 mL of RIPA lysis buffer. Beads were then incubated with 300 µg of protein sample and an additional 500 µL of RIPA lysis buffer at 4°C for 2-3 hours with rotation. The rest of the cell lysates was reserved as the input sample for Western Blot (WB) analysis and stored at -20°C. After incubation, beads were collected with a magnetic rack, and the supernatant was saved as the flow-through sample for WB analysis. The beads were first washed with 1 mL RIPA lysis buffer at RT for 2 min each, and then washed with 1 mL of 1M KCl for 2 min. 1 mL of 0.1M Na₂CO₃ was added to the bead for 10s and then removed immediately. After that, 1 mL of 2 M urea in 10 mM Tris-HCl (pH 8.0) was added to the beads for another 10s and removed immediately. The beads were then washed with 1 mL RIPA lysis buffer for 2 min each and transferred to new tubes with 1 mL RIPA lysis buffer. Before use, the buffer was removed, and the beads were pelleted by the magnetic rack.

For protein elution, beads were boiled in 60 µL of 3X protein loading buffer with 2 mM biotin and 0.6 µL of 2-mercaptoethanol at 95°C for 10 min. After that, beads were transferred back to the magnetic rack, and the eluate was collected. For western blot analysis, input and flow-through samples were prepared in the 6X protein loading buffer and boiled at 95°C for 10 min. The input, flow-through and the eluate were loaded onto 12.5% (vol/vol) SDS-PAGE gel and allowed to run under 100 V for 2 h. Samples in the gel were then transferred to a PVDF membrane and blocked with 5% non-fat dry milk in 1X TBST and rocked gently at RT for 1 h. After blocking, the membrane was washed three times 1X TBST with 5 min each.

For protein detection, membranes were incubated with 0.3 µg/mL streptavidin-HRP in 3% (wt/vol) BSA in 1X TBST at RT for 30 min. Fusion protein expression was detected with mouse anti-V5 (1:10,000) in 3% BSA in 1X TBST at RT overnight at 4°C. On the following day, membranes were washed three times in 1X TBST and incubated with the appropriate secondary antibody in 3% BSA in 1× TBST at RT for 30 min. After successful detection of

fusion protein expression, the remaining elution samples were loaded on another 12.5% (vol/vol) SDS-PAGE gel, stained with Coomassie blue and analyzed for mass spectrometry at the Alberta Proteomic and Mass Spectrometry Facility (4096, Katz Group Centre for Pharmacy and Health Research, Edmonton, Alberta, Canada).

2.9 Single fly DNA extraction

A squishing buffer was freshly prepared with 20 µl of 200 g/mL Proteinase K (Sigma AM2546), 10 mM Tris-HCl pH 8.0, 1 mM EDTA and 25 mM NaCl. One fly was collected in an Eppendorf tube and homogenized with a pipette tip. Subsequently, 50 µl of the squishing buffer was added to the fly and the mixture was incubated at 37°C for 30 min. To deactivate the Proteinase K, the mixture was heated to 95°C for 3 min and then centrifuged at the maximal speed for 30 s. The clear supernatant was transferred to a fresh Eppendorf tube, from which 2.5 µl was used for a 25 µl PCR reaction.

2.10 *Drosophila* Genomic DNA extraction

A sample of 50 flies were transferred to a 1.5 mL microtube, and quickly frozen in liquid nitrogen. Flies were then pulverized into powder using pre-cooled pestles. 200 µL of DNAzol (Thermo Fisher Scientific, Catalog # 10503027) was added to each sample, followed by 15 s of homogenization with a pestle. An additional 400 µL of DNAzol was added to each sample, bringing the total volume to 1 mL. The mix was vortexed for 15 s and incubated at RT for 5 min. After that, samples were centrifuged at 13,000 rpm for 15 min at 4°C. Around 700 µL of the viscous supernatant was recovered and carefully moved to a new microtube.

Genomic DNA was then extracted by adding 700 µL of 2X PCI (Phenol: Chloroform: Isoamyl Alcohol, 25:24:1; v/v; Invitrogen, Catalog # 15593031) to each sample. After vigorous vortexing for around 20 s, the samples were centrifuged at RT for 5 min at 13,000 rpm, producing three distinct layers. The top layer, which is the aqueous phase that contains genomic DNA, was transferred to a new tube. This step was repeated until the aqueous layer was clear. Next, 200 µL of chloroform was added to each sample, the tubes were inverted 10 times to mix,

and then centrifuged for 5 min at 13,000 rpm and 4°C. The aqueous layer was again carefully transferred to a clean tube.

Genomic DNA was precipitated by adding 20 µL of 3 M sodium acetate (pH 5.5) to each sample at a 1:10 ratio. After vortexing, 500 µL of ice-cold 100% ethanol was added to each sample at a 2.5:1 ratio. Samples were then incubated on ice for 5 min and centrifuged at 13,000 rpm for 10 min at 4°C. The supernatant was discarded, and the DNA pellet was washed with 0.8-1.0 mL of 75% ethanol and then centrifuged for 2 min at 13,000 rpm and 4°C. The pellet was then air-dried for 5 min at RT. Final DNA was dissolved in 200 µL of TE buffer or nuclease-free water.

2.11 *Drosophila* RNA extraction

Around six whole larvae or equivalent amount of tissue were added into 120 µL of ice-cold TRIzol reagent (Thermo Fisher Scientific, #15596026) after dissection. Samples that were not analyzed immediately were rapidly frozen in liquid nitrogen and kept at -80°C for preservation. Before use, samples were homogenized on ice and mixed with an additional 880 µL of cold TRIzol to achieve a total volume of 1 mL, and vortexed for 15 s. 200 µL chloroform was added, and the mixture was vortexed again for 15 s, incubated on ice for 1 minute, and centrifuged at 14,000 rpm for 15 min at 4°C. The upper, clear aqueous layer (approximately 500 µL) was transferred to an RNase-free Eppendorf tube. An equal volume of 70% ethanol was added and mixed by pipetting.

The rest of the steps uses reagents from QIAGEN RNeasy® Mini Kit (#15596026). 700 µL of the mixture was then applied to a RNeasy Mini spin column and centrifuged at 12,000 rpm for 15 s, and the eluate was discarded. This step was repeated until all the mixture had been processed. The column was then washed with 700 µL of RW1 buffer, centrifuged for 15 s at 12,000 rpm, and the flow through was discarded.

Next, 500 µL of RPE buffer was added to the column, followed by a 15-s centrifugation at 12,000 rpm. The column was then placed in a fresh 2 mL collection tube, centrifuged for 1 minute at 13,000 rpm to dry the membrane, and transferred to a new 1.5 mL tube. 30 µL of

RNase-free water was added directly to the membrane. After a final centrifugation for 1 minute at 12,000 rpm, the RNA was eluted into the tube. The RNA concentration was measured with a Nanodrop (Thermo Scientific, Nanodrop 1000 Spectrophotometer) and kept at -20°C.

2.12 cDNA synthesis

ABI High-Capacity cDNA Synthesis Kit (Thermo Fisher Scientific, #4368814) was used to reverse transcribed 200 ng of RNA into cDNA. The reaction setup in a PCR tube included the following components: X μ l of RNA (equivalent to 200 ng), X - 10 μ l of RNase-free water, 2.0 μ l of RT Buffer, 0.8 μ l of 25x dNTP Mix, 2.0 μ l of 10X random primers, 4.2 μ l of RNase-free water, and 1 μ l of reverse transcriptase, making a total reaction volume of 20 μ l. The PCR cycle was set at 25°C for 10 min, 37°C for 120 min, 85°C for 5 s, and then held at 4°C. The cDNA was then diluted in a 1:10 ratio with nuclease-free water and stored at -20°C.

2.13 Preparation of ultra-competent cells

The protocol for ultra-competent cells was adapted from Cold Spring Harbor Laboratory and Princeton University. The preparation of 1 liter (L) of competent cells takes three days. On the first day, a vial of *DH5 α Escherichia coli* (*E. coli*) competent cells was spread on a Luria-Bertani (LB) agar plate without antibiotics and incubated at 37°C for 16-20 hours. On the second day, a single colony from the agar plate was used to inoculate 5 mL of SOB medium without antibiotics to create a starter culture. This culture was then incubated at 37°C on a shaker at 250-300 revolutions per minute (rpm) for 8 hours. After that, 2.5 mL of the starter culture was transferred into 1 L of SOB medium and incubated at 18-22°C with moderate shaking at 180-200 rpm for about 14 h. On the last day, the culture's optical density at 600 nanometers (OD600) was monitored until it reached 0.54-0.55. The culture was then cooled in an ice-water bath for 10 min. Cells were collected by centrifugation at 3900 rpm for 10 min at 2°C, resuspended in 80 mL of ice-cold Inoue transformation buffer, and centrifuged again. The supernatant was then discarded, and cells were resuspended in 20 mL of the same Inoue transformation buffer before transferred to a chilled 50 mL conical tube. After that, 1.5 mL of DMSO was added. After gentle mixing, the cells were placed on ice for another 10 min before transferred into pre-chilled, sterile

1.5 mL tubes (50-100 μ L per tube). Tubes were snap-frozen in liquid nitrogen and stored at -80°C.

2.14 Gibson Assembly

DNA fragments were generated via PCR using Q5 High-Fidelity DNA Polymerase (NEB, Catalog # M0491) or by enzymatic digestion of plasmids. Amplified PCR fragments were purified with the QIAquick Gel Extraction Kit (QIAGEN, Catalog # 28704). The concentration of DNA fragments was determined using a Nanodrop Spectrophotometer (NanoDrop ND-1000). For assembly, 200 ng of vector DNA was used for plasmids under 10 kb, with the insert DNA amount calculated at a 3:1 ratio using the NEB calculator (<https://nebiocalculator.neb.com/#!/ligation>). For larger plasmids (over 10 kb), 300-400 ng of vector DNA was used. Plasmid and inserts were added to the in-house Gibson Assembly Master Mix (recipe attached in Appendix A1) by a 1:3 ratio with a total volume not exceeding 20 μ L. The reaction was incubated at 50°C for 2-4 hours in a PCR thermocycler.

2.15 Bacteria transformation

Ultra-competent cells were thawed on ice for 20-30 min after being taken from the -80°C freezer. 2 μ L of the Gibson assembly mix or around 100 ng of plasmid was added into 50-100 μ L of competent cells. The tube was mixed gently by tapping several times. Competent cells and DNA were then kept on ice for 20-30 min, allowing DNA to enter the cells. The tube was then heat shocked by incubating in a 42°C water bath for 30-60 s.

After heat shock, the tubes were immediately transferred on ice for 2 min. 950 μ L of SOC media was freshly prepared (see Appendix A3 for recipe) and added to the tube. The tube was then incubated at 37°C with shaking for 1 hour, allowing cells to grow. Following incubation, the cells were centrifuged at 4,000 rpm for 2 min, and 900 μ L of the supernatant was discarded. The pellet was resuspended in the remaining supernatant (around 100 μ L), and the entire solution was spread onto a 10 cm LB agar plate containing the appropriate antibiotic. Plates were incubated at 37°C overnight.

2.16 Colony PCR

The day following bacteria transformation, single colonies were picked from LB agar plate and suspended in 5 μ L of nuclease-free water and mixed by gentle pipetting. For each PCR reaction, 1 μ L of such solution was used as the template. PCR reaction was done with the appropriate primers to screen for positive transformants. After screening, the remaining 9 μ L of the suspension was added to 5 mL LB medium with the appropriate antibiotics for future growth.

2.17 Plasmid extraction

Two different extraction kits were used based on the quantity and quality of plasmids required. For extracting a smaller volume of plasmids, a singular bacterial colony was cultured in 5 mL of LB medium supplemented with the appropriate antibiotics and incubated overnight at 37°C the day before plasmid extraction. For extracting a large number of plasmids, an appropriate amount of bacterial culture was grown in 100 mL of LB medium with antibiotics the day before extraction. The GeneJET Plasmid Miniprep Kit by ThermoFisher Scientific (# K0503) was then used to purify up to 20 μ g of plasmid DNA from 5 mL culture. The QIAGEN Plasmid Midiprep kit (QIAGEN, # 10043) was used to extract plasmid from 100 mL bacterial culture. The extraction procedures adhered strictly to the protocols specified by the kit manufacturers.

2.18 Quantitative real time PCR (qPCR)

For each qPCR assay conducted, three biological replicates were tested in triplicate. A reaction mix for each set of primers was prepared using the Luna® universal qPCR Master Mix as follows: 5 μ L of SYBR Luna Master Mix combined with 2.5 μ L of 3.2 μ M primers. For each biological replicate, 7.5 μ L of this master mix was added to the 96-well qPCR plate in triplicate. Additionally, 2.5 μ L of cDNA template, diluted 1:10, was added to each well. The qPCR cycling conditions were set as follows: 95°C for 2 min for 1 cycle, 40 cycles at 95°C for 20 s each, and 40 cycles at 60°C for 30 s. qPCR reactions were run in QuantStudio™ 6 Flex real-time PCR system (Applied Biosystems). Sample data were normalized against *ribosomal protein 49 (rp49)* and analyzed using the $\Delta\Delta$ Ct approach. The primers used are listed in Table 2.4.

2.19 Ferroxidase activity assay

The Ceruloplasmin Activity Assay (Abcam, #273296) was used for the detection of ferroxidase activity in S2 cells. S2 cells overexpressing HEPH, Mco4, Mvl or empty vectors were collected and washed five times with MilliQ water. 120 μL of NP 40 lysis buffer (with protease inhibitor) was added to the sample. Samples were vortexed and incubated on ice for 30 mins, followed by a centrifuge at 10,000 rpm under 4°C for 10 mins. After that, 100 μL of the supernatant was recovered and added with 100 μL of saturated ammonium sulfate provided by the assay kit. An additional 20 μL of the supernatant was kept and tested for concentration using the bicinchoninic acid assay (BCA) protein assay. The samples were vortexed briefly to mix and incubated on ice for 5 min. The samples were then centrifuged at 10,000 rpm under 4°C for 5 min. All supernatants were then removed. The pellet was added with 160 μL of MilliQ water and allowed to dissolve. 10-20 μL of the samples was added into a 96-well plate and the final volume was brought to 100 μL with the ceruloplasmin assay buffer provided in the kit. The buffer was placed into a water bath set at 25°C for 30 min prior to use.

All the reagents for generating the standard curve were provided by the kit. The standard curve was prepared by diluting the Oxidizer to 5 mM by adding 10 μL of 100 mM Oxidizer to 180 μL of ceruloplasmin assay buffer. 10 μL of H_2O_2 standard was added and mixed well. After that, 0, 2, 4, 6, 8, 10 μL of 5 mM Oxidizer were added in a series of wells in the same 96-well plate to generate 0, 10, 20, 30, 40, 50 nmol standard. The final volume of each well was brought to 100 μL with the ceruloplasmin assay buffer. The standard curve was read within the first 15 min.

The plate reader was set to 25°C. For each sample and standard well, 100 μL of the reaction mix was prepared by adding 10 μL of ceruloplasmin substrate provided by the kit into 90 μL of ceruloplasmin assay buffer. The reaction mix was added to each well prior to testing. Ceruloplasmin performs a 1 electron oxidation of the substrate to a red product. OD was measured in kinetic mode at 560 nm within the first 20 min of the reaction.

For calculation, the standard curve (OD vs. nmol) was plotted, and slope (Ss) was calculated using points that have an OD less than 1. As for the samples, the linear portion of the

curve was used to calculate the slope (Sk). $Sk = (OD_2 - OD_1) / (T_2 - T_1)$, where OD_2 and OD_1 are the absorbance at the end and beginning of the linear portion. Sample ceruloplasmin activity = $Sk / Ss / V * 2$ (mU/mL or U/L), where 2 is the dilution factor.

2.20 Ferrozine-based iron content assay

The ferrozine-based colorimetric assay was used to measure whole-body iron content. 10 *Mco4^{-/-}* wandering larvae were collected for each biological replicate. Larvae were washed in PBS three times to flush out gut content. Samples were homogenized in 125 μ L of lysis buffer (20 mM Tris, 137 mM NaCl, 1% Triton X⁻¹⁰⁰, 1% glycerol) repetitively every 10 min on ice for a total of one hour. Samples were centrifuged at 16,000 rpm for 30 min at 4°C to remove the insoluble material. The supernatant was centrifuged again 16,000 rpm for 5 min at 4°C, and 80 μ L of the final sample was recovered and transferred to fresh tubes. Protein concentrations were determined using the bicinchoninic acid assay (BCA) protein assay. 77 μ L of the protein sample (or the lysis buffer as a negative control) were added with 17 μ L of concentration hydrochloric acid and vortexed gently. The mixture was boiled for 20 min at 90°C. After that, samples were centrifuged at 16,000 rpm for 2 min, and 66 μ L of the supernatant was recovered and transferred to fresh tubes. The samples were centrifuged again at 16,000 rpm for 2 min, and 50 μ L of supernatant was taken and transferred to a 96-well plate. 20 μ L of 75 mM ascorbate was added to each sample, followed by brief vortexing and a quick spin down. Subsequently, 20 μ L of 10 mM ferrozine (3-(2-Pyridyl)-5,6-diphenyl-1,2,4-triazine-*p*, *p'*-disulfonic acid monosodium salt hydrate, sigma, #63451-29-6) was added, followed by adding 40 μ L of 5 M ammonium acetate. Complex formation showed a purple color and was measured by absorbance at 562 nm. The concentration of iron was calculated based on the molar extinction coefficient of the iron-ferrozine complex of 27,900 $M^{-1} cm^{-1}$. The formula is: $[Fe] (pmol/\mu L) = [(OD_{562} \times 94/77 \times 130/50)/27900] \times 10^6$. Three biological replicates were performed, and the difference between controls and experimental groups was statistically assessed by an unpaired Student's t-test.

2.21 Gel extraction of PCR products

The QIAquick Gel Extraction kit (QIAGEN, #28704) was used to extract PCR products from agarose gels. DNA was isolated from the agarose gel by cutting it out under a UV imager

with a scalpel. The gel was then placed in a fresh tube and weighed. To dissolve the gel, a ratio of three volumes of QG buffer was added for every one volume of the gel (approximately 100 mg equating to ~100 μ l). This mixture was incubated at 50°C for 10 min, with vortexing every 2-3 min until the gel completely dissolved. Following this, an equal volume of isopropanol to that of the gel was added to the mixture, vortexed, and then applied to a QIAquick spin column. The spin column was centrifuged for 1 minute at maximal speed, and the flow-through was discarded. 500 μ l of QG buffer was added to the column and centrifuged for another 1 min. The flow-through was discarded afterwards. The DNA was then washed twice by adding 750 μ l of PE buffer to the column, letting it sit for 5 min, and centrifuging for 1 minute at 13,000 rpm. The column was then transferred to a fresh 1.5 mL tube, and the DNA was eluted with 30 μ l of EB buffer by centrifugation at 13,000 rpm for 1 minute. The concentration of the eluted DNA was assessed using a NanoDrop spectrophotometer.

2.22 Schneider 2 cell culturing

This protocol is adopted from "Schneider 2 (S2) Cells User Guide" by Thermo Fisher Scientific. The culture medium used in this study was Schneider's *Drosophila* Medium (Thermo Fisher Scientific, Cat. # 21720024) enriched with 10% heat-inactivated fetal bovine serum (FBS, Thermo Fisher Scientific, Cat. # A4766801). Cell density and viability were routinely assessed using hemocytometer counts and trypan blue staining. Cells viabilities were maintained between 95–99%. Cells were kept in T⁻²⁵ cm² flasks or multi-well plates under 26°C - 28°C. The S2 cells exhibited a doubling time of around 24 hours, with passages done during their logarithmic to mid-logarithmic growth phases. For recovering cell cultures from frozen stocks, cell vials were thawed at 30°C. All vial exteriors and related equipment were sanitized with 70% ethanol prior to complete thawing. The contents were then transferred to a sterile conical tube containing 4 mL of room-temperature complete Schneider's *Drosophila* Medium, followed by centrifugation at 100 rpm for 5–10 min. The supernatant was carefully removed, and the cell pellet was resuspended in 5 mL of fresh medium and transferred to a T-25 cm² flask for incubation at 26°C - 28°C in a non-humidified incubator. The flask was vented to ensure sufficient oxygenation. Cells were allowed to grow until reaching a concentration of 0.6×10^7 – 2.0×10^7 cells/mL over 3–4 days.

Cell passage was conducted before cells reached a density of around 5×10^6 cells/mL. Cell clumps were dispersed first. Cells were diluted and divided into new flasks containing fresh complete Schneider's *Drosophila* Medium. The dilution ratio ranged from 1:2 to 1:5. The cells were then cultured until they reached a density of 0.6×10^6 - 2.0×10^6 cells/mL. Cell passage was done regularly to ensure the culture's health. For preservation of S2 cells, a Freezing Medium (45% conditioned complete Schneider's *Drosophila* Medium, 10% heat-inactivated FBS, 45% fresh complete medium, 10% heat-inactivated FBS, 10% DMSO) was prepared. Cells were removed from the flask when reaching a density of 1×10^7 - 2×10^7 cells/mL. Cells were then centrifuged at 1000 rpm for 2-3 min, washed with 10 mL PBS, re-pelleted again at 1000 rpm for 2-3 min, and finally resuspended in Freezing Medium (45% conditioned complete Schneider's *Drosophila* Medium, 45% fresh complete Schneider's *Drosophila* Medium, 10% DMSO). Aliquots of every 1 mL cell were frozen and kept at -80°C .

2.23 Generation of constructs of S2 cell transfection

The backbone for S2 cell constructs were amplified from the *pPUI10-Evi5-C-3Flag*[120] plasmid containing the *Drosophila* Actin5C (Act5C) promoter and three Flag tags at the C-terminus. Full-length cDNAs of *Mco4*, *HEPH*, and *Mvl* were obtained from the reverse-transcribed cDNA library of *w¹¹¹⁸* whole larvae and amplified by PCR. The backbone and cDNA fragments were combined using Gibson assembly, generating *pPUI10-Mco4-C-3Flag*, *pPUI10-HEPH-C-3Flag*, and *pPUI10-Mvl-C-3Flag*. *pAC5-EGFP-C-4Myc* was used as a negative control. The positive colonies were screened using colony PCR, and the final plasmids were sequenced with Sanger sequencing. The plasmids were extracted using the QIAGEN plasmid Midiprep kit and stored at -20°C .

2.24 S2 cell transfection

This procedure was modified from the "Schneider 2 (S2) Cells User Guide" by Thermo Fisher Scientific, using the calcium phosphate transfection technique. Protein expression analysis was carried out over a period of 2 to 5 days following transfection. The day before transfection, around 3×10^6 S2 cells were transferred into a 35-mm dish containing 3 mL of complete

Schneider's *Drosophila* Medium and incubated at 28°C for 6-16 hours to achieve a cell density of 2×10^6 to 4×10^6 cells/mL.

On the day of transfection, a transfection mix was prepared using Solution A and Solution B. Solution A consisted of 36 μ L of 2 M CaCl₂ and 19 μ g of plasmid DNA. Nuclease-free water was added to reach a final volume of 300 μ L. Solution B was 300 μ L of 2X HEPES-Buffered Saline (50 mM HEPES, 1.5 mM Na₂HPO₄, 280 mM NaCl, pH 7.1). Solution A was gradually added dropwise into Solution B with continuous mixing, resulting in the formation of a fine precipitate after 1-2 min. This transfection mixture was incubated at RT for 30-40 min and then applied dropwise to the S2 cells with continuous mixing. Cells were then incubated at 28°C for 16-24 hours, with potential extension to 36-48 hours. Following incubation, the calcium phosphate solution was removed, and the cells were washed twice with the complete medium and kept at 28°C until needed.

2.25 S2 cell immunostaining and imaging

This method is modified from the Cell Signaling Technology immunostaining guidelines. Cells were grown on coverslips in multi-well plates with complete Schneider medium until use. The medium was removed from wells, and the cells were then fixed using 1X PBS with 4% formaldehyde for 30 min at RT. Following fixation, the cells were washed three times with 1X PBS for 5 min each. After that, 200 μ l of Blocking Buffer (1X PBS, 5% Normal Goat Serum (Abcam, #ab138478), 0.3% Triton X⁻¹⁰⁰) was added and incubated for one hour at RT. The appropriate primary antibody (see Table 2.3) was prepared in the antibody dilution buffer (1X PBS, 1% BSA, 0.3% Triton X⁻¹⁰⁰). After removing the blocking buffer, 200 μ l of the diluted primary antibody was added to the cells and incubated overnight at 4°C with shaking.

On the following day, the cells were washed three times with 1X PBS for 5 min each. A fluorochrome-conjugated secondary antibody (see Table 2.3) was prepared in the same antibody dilution buffer and incubated with the cells for 2 hours at RT in the dark. Following incubation, the cells were washed again with 1X PBS for 5 min each. 1X DAPI (Cell Signaling, #4083) was added to the cells and incubated for 15 min. The cells were then washed with 1X PBS for 5 min each. For microscopy, the coverslip was placed cell-side down on a slide prepped with a drop of

mounting buffer (50% PBS and 50% glycerol). Slides were stored at -20°C protected from light. Imaging was done using a Nikon Eclipse 80i Confocal C2+ microscope and camera.

2.26 Western blot analysis

For the preparation of 1.5 mm-thick SDS-PAGE gels (sodium dodecyl sulfate-polyacrylamide gel electrophoresis), glass plates were assembled with appropriate spacers (1 mm thickness) in a casting frame and positioned on a casting stand. 7 mL of the separating gel mixture (10-12.5%, recipe in Appendix A4) was poured into the space between the plates. To level the surface of the separating gel, 100 µL of isopropanol was added on top. The gel was left to solidify at RT for 30-45 min, and the isopropanol was discarded. Subsequently, 3 mL of the stacking gel (recipe in appendix A4) was added on top of the separating gel, and a comb of either 10-well or 15-well was applied. The gel was allowed to solidify at RT for 30-45 min.

The Mini-PROTEAN Tetra Vertical Electrophoresis Cell (Bio-Rad, Catalog # 1658007FC) was used to run the gels. This cell was filled with 1X running buffer (3 g of Tris base, 14.4 g of glycine, and 1 g of SDS in 1 L of Milli-Q water). After removing the comb, protein samples (boiled and denatured) were loaded into the gel alongside a pre-stained protein ladder (Thermoscientific, #26616). The electrophoresis was conducted over 1.5 hours at 110 volts (V), followed by the transfer of proteins onto a PVDF membrane. This membrane (0.2 µM) was pre-rinsed with 20 mL methanol for 15 s. 70 mL Milli-Q water and 10 mL 10X Tris-glycine (30.3 g of Tris base, 144 g of glycine in 1 L of Milli-Q water) were added to the membrane, making a total of 100 mL of transfer buffer. The membrane was kept in the transfer buffer until use. In the meantime, 100 mL of 10X Tris-glycine, 200 mL of methanol, and 700 mL of Milli-Q water were added to make the 1X transfer buffer. Before protein transfer, the stacking gel was removed. A transfer stack was prepared within a Mini Trans-Blot Cell by the following order: sponge, filter paper, the gel, the PVDF membrane, filter paper and sponge. The stack was placed in the transfer system under 100 V for 1.5 hours. The system was placed under 4°C or in an ice-water mixture with an ice pack.

After membrane transfer, the PVDF membrane was incubated with a blocking solution (1X TBS, 0.1% Tween-20, and 5% (w/v) skim milk powder) for 1 hour at RT to minimize non-

specific binding. After that, the blocking buffer was removed, and the appropriate primary antibody (see Table 2.5) was diluted in the blocking buffer and added to the membrane. The membrane was then incubated overnight at 4°C on a rotating platform. On the following day, the membrane was removed from the primary antibody solution, and washed three times with the wash buffer (1X TBS, 0.5% Tween-20) for 15 min each on a rotator. The secondary antibody (see Table 2.5) was diluted in the blocking buffer and applied to the membrane. The membrane was incubated at RT for at least an hour. After that, the membrane was washed three times in the washing buffer for 15-20 min each.

Signal detection was done using the Amersham ECL Prime Western Blotting Detection Reagent as per the manufacturer's instructions. For each membrane, an ECL reaction mix was made by combining 200 µL of solution A with 200 µL of solution B. The membrane was blotted to remove excess liquid and applied to the ECL mix for 15 s with the protein side contacting the mix. The membrane was sealed in a transparent plastic bag and imaging was done with a ChemiDoc system (Bio-Rad).

2.27 Coomassie blue staining

The SDS-PAGE gel was removed from the glass plates, rinsed in Milli-Q water, and immersed into Coomassie staining solution (1 g of Coomassie R250 dye, 100 mL of glacial acetic acid, 400 mL of methanol, and 500 mL of Milli-Q water) for 1 hour at RT. After staining, the gel was rinsed twice with Milli-Q water. For de-staining, the gel was placed in the de-stain solution (20% methanol, 10% acetic acid). Kimwipes were tied into a knot and positioned around the gel within the de-staining solution to absorb the stain. The gel was incubated overnight at RT on a rocking platform. On the following day, the de-staining procedure continues until the gel reached the desired clarity.

2.28 Generation of *Mco4* knock-in CRISPR line

2.28.1 gRNA plasmids construction

The *Mco4* target region was obtained from FlyBase (<http://flybase.org>). Two guide RNA (gRNA) target sites were identified using the Harvard CRISPR gRNA tool

(<http://www.flyrnai.org/crispr/>). Primers were designed to amplify the gRNA sequences as well as the gRNA scaffold (see Appendix A5 for complete primer sequences) from *pCFD5* (Addgene, #73914). *pCFD5* was treated with the BbsI restriction enzyme (NEB, #R3539S) at 37°C for 1.5 h to prepare the gRNA vector backbone. The amplified gRNA fragments and backbone were annealed using Gibson assembly. The plasmid was prepared using the QIAGEN midi-prep kit, and the concentration was measured by NanoDrop.

2.28.2 Donor plasmids construction

pDsRed-attP (addgene, #51019) was used to prepare the backbone of the donor plasmid. The left and the right homology arms were PCR amplified from *w¹¹¹⁸* genomic DNA and gel-purified. Each homology arms were 1 kb long. Left arm was amplified using primers *Mco4* donor-Left arm-Fwd and *Mco4* donor-Left arm-Rev (see Table 2.5). Right arm was amplified using primers *Mco4* donor-Right arm-Fwd and *Mco4* donor-Right arm-Rev. The donor DNA consists of three sequences: *Mco4*-3Flag, *Mco4*-UTR and the DsRed region. *Mco4*-3Flag includes the end of *Mco4* genomic DNA sequence with a 3xFlag tag inserted before the stop codon. This sequence was amplified from pPU10-*Mco4*-3xflag using the primers *Mco4*-Flag-Fwd and *Mco4*-Flag-Rev. *Mco4*-UTR region is part of the 3'UTR region of genomic *Mco4*, and this fragment was amplified from *w¹¹¹⁸* using the primers *Mco4*-UTR-Fwd and *Mco4*-UTR-Rev. The DsRed sequence was amplified from *pDsRed-attP* using the primers DsRed-attP-Fwd and DsRed-attP-Rev. The DsRed sequence, *Mco4*-UTR fragment and *Mco4*-3Flag fragment were annealed together with assembly PCR to form the complete donor DNA. Finally, the backbone was amplified using primers Backbone-Fwd and Backbone-Rev from *pDsRed-attP*, and the backbone was fused with left homology arm, right homology arm and the donor DNA to construct the complete donor plasmid. The plasmid was prepared using the QIAGEN midi-prep kit, and the concentration was measured by NanoDrop.

2.28.3 Injection and generation of homozygous line

gRNAs and donor plasmids were sequenced using Sanger sequencing. Embryo Injection was done at the GenetiVision Production, where gRNAs and donor plasmids were co-injected into the *nos-Cas9* line. Following injection, positive male transformants carrying the DsRed

marker were crossed with *yw*. The presence of the DsRed marker manifests as red eyes under UV light. In the following generation, the offspring with red-eyes, which was all females due to *Mco4* being located on the X-chromosome, was crossed with *FM7i* males (X-chromosome balancer line). In the following generation, DsRed-expressing males and females were selected and allowed to be inbred. Finally, DsRed males and females that did not display balancer phenotypes (bar-shaped or heart-shaped eyes) were selected and kept together as a homozygous stocks.

2.29 Generation of *UAS-Mco4-V5-Tb* line

pUAS-V5-TurboID-NES (Addgene, #116904) carrying the mini-*white* marker was used to amplify the backbone using primers Backbone-1 and Backbone-2 from Table 2.6. The end products were 4509 bp and 5471 bp respectively, The nuclear export signal sequence (NES) was removed from the backbone. *Mco4* cDNA was amplified using primers *Mco4-FP* and *Mco4-RP*. TurboID sequence with a V5 tag was amplified from *pUAS-V5-TurboID-NES* using the primer TbV5-FP and TbV5-RP (see Table 2.6). The two backbone fragments, *Mco4* cDNA fragment and TurboID-V5 sequences were annealed with the backbone by Gibson assembly to generate *pUAS-Mco4-V5-Tb* (see Appendix A6 for the complete primer sequence). The plasmid was prepared using the QIAGEN midi-prep kit, sequenced with Sanger sequencing, and the concentration was measured by NanoDrop. Embryo Injection was done at the GenetiVision Production, where the plasmids were injected into the *attP40* line. The *attP40* docking site incorporated the transgene into the second chromosome. Mini-*white* expressing flies have red eye phenotype. Following injection, positive male transformants were crossed with *w¹¹¹⁸* females. The red-eyed offspring were selected and crossed with a second chromosome balancer line (*w-; CyO/Ser; Tb/TM6, Hu*). In the next generation, red-eyed progeny with balancer phenotype (*curly* wings) were selected and allowed to be inbred. In the following generation, red-eyed progeny that did not display balancer phenotypes were selected and kept together as the homozygous stock.

Table 2.1 List of *Drosophila* stocks used in this study

Genotype or name	Sources	Description
<i>w¹¹¹⁸</i>	BDSC, Stock #3605	reference line/control
<i>w: tubulin-Gal4/TM3, GFP</i>	BDSC, Stock #5138	ubiquitously expressed driver
<i>Act5C-Gal4</i>	BDSC, # 42713	ubiquitously expressed driver
<i>Fm7a</i>	Dr. Anna Phan's lab	X-chromosome balancer
<i>w; CyO/Sco; TM2/TM6</i>	KKJ lab, Dr. Wen Liu	Balancer for <i>UAS-Mco4</i> line
<i>Mco4 -/-</i> (<i>yw; nos-Cas9/CyO</i>)	KKJ lab, Areeg Elhafiz	<i>Mco4</i> knock-out line, used for survival rate study
<i>UAS-TurboID-V5</i>	KKJ lab, Dr. Wen Liu	Expresses biotin ligase with a V5 tag under <i>UAS-Gal4</i> system, used as a control for TurboID experiment
<i>UAS-Mco4-3xMyc</i> (<i>yw nos-PhiC31; attP40</i>)	KKJ lab, Areeg Elhafiz	Expresses a C-terminal 3xMyc tagged <i>Mco4</i> under <i>UAS-Gal4</i> system, used for localization and overexpression studies
<i>UAS-Mco4-V5-Tb</i> (<i>yw nos-PhiC31; attP40</i>)	Generated in this study	Expresses biotin ligase and <i>Mco4</i> with a C-terminal V5 tag under <i>UAS-Gal4</i> system, used in TurboID experiment
<i>UAS-V5-Tb-Mco4</i>	Generated in this study	Expresses biotin ligase and

<i>(yw nos-PhiC31; attP40)</i>		<i>Mco4</i> with a N-terminal V5 tag under <i>UAS-Gal4</i> system
<i>Mco4-3xFlag</i> <i>(yw; nos-Cas9/CyO)</i>	Generated in this study	A CRISPR knock-in line expressing <i>Mco4</i> with a C-terminal 3xFlag tag, used in localization study
<i>Mco4-3xMyc</i> <i>(yw; nos-Cas9/CyO)</i>	Generated in this study	A CRISPR knock-in line expressing <i>Mco4</i> with a C-terminal 3xMyc tag, used in localization study

Table 2.2 List of plasmids used in this study

Plasmid name	Sources	Purpose
For CRISPR line construction		
<i>pCFD5</i>	Addgene, #73914	CRISPR line construction
<i>pDsRed-attP</i>	Addgene, #51019	CRISPR line construction
<i>pCFD5-Mco4-KI</i>	Generated in this study	Expresses two gRNAs for <i>Mco4</i> CRISPR knock-in line
<i>pDsRed-Mco4-3xflag</i>	Generated in this study	Expresses 3xFlag tagged <i>Mco4</i> donor DNA for CRISPR knock-in line
<i>pDsRed-Mco4-3xMyc</i>	Generated in this study	Expresses 3xMyc tagged <i>Mco4</i> donor DNA for CRISPR knock-in line
For S2 cell transfection		
<i>pPUI10-Evi5-3xFlag</i>	KKJ lab, Dr. Sattar Soltani	Expresses a C-terminal 3xFlag tagged <i>Evi5</i> in S2 cells
<i>pPUI10-Mco4-3xFlag</i>	Generated in this study	Expresses a C-terminal 3xFlag tagged <i>Mco4</i> in S2 cells

<i>pPUI0-HEPH-3xFlag</i>	Generated in this study	Expresses a C-terminal 3xFlag tagged human Hephaestin in S2 cells
<i>pPUI0-Mvl-3xFlag</i>	Generated in this study	Expresses a C-terminal 3xFlag tagged Malvolio in S2 cells
<i>pPUI0-Mco1-3xFlag</i>	Generated in this study	Expresses a C-terminal 3xFlag tagged <i>Mco1</i> in S2 cells
<i>pPUI0-sp-Fet3-3xFlag</i>	Generated in this study	Expresses a C-terminal 3xFlag tagged yeast <i>Fet3</i> with <i>Mco4</i> 's signal peptide in S2 cells
<i>pPUI0-sp-Ftr1-3xFlag</i>	Generated in this study	Expresses a C-terminal 3xFlag tagged yeast <i>Ftr1</i> with <i>Mco4</i> 's signal peptide in S2 cells
For UAS overexpression line construction		
<i>pAc5-EGFP-C-4xMyc</i>	KKJ lab, Areeg Elhafiz	Expresses a C-terminal 4xMyc tagged EGFP, used as a control for S2 cells experiments
<i>pUAS-V5-TurboID-NES</i>	Addgene, #116904	Provides backbone for <i>UAS-TurboID</i> overexpression line construction
<i>pUAS-Mco4-V5-</i>	Generated in this	Expresses V5 tagged biotin ligase at the C-terminus

<i>TurboID</i>	study	of Mco4, used for TurboID experiments
<i>pUAS-V5-TurboID-Mco4</i>	Generated in this study	Expresses V5 tagged biotin ligase at the N-terminus of Mco4

Table 2.3 List of antibodies used in this study

Antibody name	Source	Experiments	Dilution
monoclonal rabbit anti-FLAG	Cell Signaling, #14793S	IF	1:1000
		IP	1:100
		WB	1:1000
monoclonal mouse anti-FLAG	Cell Signaling, #8146S	IF	1:1000
		IP	1:100
		WB	1:1000
monoclonal mouse anti-Myc	Cell Signaling, #2276S	IF	1:1000
		IP	1:100
		WB	1:1000
monoclonal rabbit anti-Myc	Cell Signaling, #2278S	IF	1:1000
		IP	1:100
		WB	1:1000
monoclonal mouse anti-V5	Thermo Fisher Scientific, #R96025	WB	1:10,000
goat anti-mouse IgG H&L Alexa Fluor 488	Abcam, #150113	IF	1:2000

goat anti-rabbit IgG H&L Alexa Fluor 488	Abcam, #150077	IF	1:2000
goat anti-mouse IgG H&L Alexa Fluor 555	Abcam, #150114	IF	1:2000
Streptavidin-HRP	Thermo Fisher Scientific, #S911	WB & TurboID	0.3 μ g/mL
goat anti-mouse IgG H&L HRP	Abcam, #97023	WB	1:10,000
goat anti-rabbit IgG H&L HRP	Abcam, #97051	WB	1:10,000
DAPI	Cell Signaling, #4083	IF	1:500,000
IF: immunofluorescence; IP: immunoprecipitation; WB: western blot.			

Table 2.4 List of qPCR primers

Name	Sequence (5' to 3')	Purpose
<i>rp49</i> FP	TTCCTTGACGTGCCAAAAC	Normalization of qPCR sample
<i>rp49</i> RP	AATGATCTATAACAAAATCCCCTGA	
<i>Mco4</i> FP	CAGCCGATGACCTGCTACTA	Measure <i>Mco4</i> transcript levels
<i>Mco4</i> RP	CAGCCGATGACCTGCTACTA	
FP: Forward Primer; RP: Reverse Primer		

Table 2.5 List of knock-in transgenic line primers

Name	Sequence (5' to 3')	Purpose
pCFD5-Fwd	TTCGATTCCCGGCCGA TGCAGACTGTTCGAGT AGAACCGCGTTTTAGA GCTAGAAATAGC	Construction of pCFD5- <i>Mco4</i> ^{3F} guide RNA plasmid
pCFD5-Rev	CTATTTCTAGCTCTAAA ACTCGTGCACGTTAAC GGCACATGCACCAGCC GGGAATCGAAC	
pCFD5-gRNA-sequencing- Fwd	GCACAATTGTCTAGAA TGCATAC	Sequencing of pCFD5- <i>Mco4</i> ^{3F} guide RNA plasmid
pCFD5-gRNA-sequencing- Rev	ACGTTTTATAACTTATG CCCCTAAG	
3'- <i>Mco4</i> -UTR-Fwd	TGGGGTTCCTGGGTCC CGAA	Generation of the 3'UTR region of genomic <i>Mco4</i>
3'- <i>Mco4</i> -UTR-Rev	ACGAAGTTATCGATGA TTGGAAGTGCATTTC CAA	
<i>Mco4</i> -Flag-Fwd	GTTCTACTCGAACAGT CCCGGCTAC	Generation of the end of genomic <i>Mco4</i> with a 3xFlag tag
<i>Mco4</i> -Flag-Rev	TTCGGGACCCAGGAAC CCCATCAATGTATCTTA TCAT	
<i>Mco4</i> donor-Right arm	CAAGGGCGACACAAAA	Generation of the homology right

Fwd	TTTATGCACGTTAACG GCACA	arm
<i>Mco4</i> donor-Right arm Rev	GCGGCAATGGAAATGG CAAT	
<i>Mco4</i> donor-Left arm Fwd	TCTCTCAGTTGGGGGC GTAGGTCAAGGCCGCC AAGCC	Generation of the homology left arm
<i>Mco4</i> donor-Left arm Rev	CGCAGAATCGTGTACC CGAA	
DsRed-attP-Fwd	CCAATCATCGATAACT TCGTATAATGTATGCT ATACG	Amplifying loxP-dsRed-loxP region
DsRed-attP-Rev	TAAATTTTGTGTCGCCC TTG	
Backbone-Fwd	attgccattccattgccgcAGAA GAGCACTAGTAAAG	Generation of the pDsRed-attP- <i>Mco4</i> ^{3F} backbone
Backbone-Rev	CTACGCCCCCAACTGA GAGA	
Donor plasmid- sequencing1-Fwd	CGTTAAGGGATTTTGG TCAT	Sequencing pDsRed-attP- <i>Mco4</i> ^{3F} whole plasmid
Donor plasmid- sequencing2-Fwd	TGCTTTTCTGTGACTGG TGA	
Donor plasmid- sequencing3-Fwd	GAATATGGCTCATAAC ACCC	

Donor plasmid-sequencing4-Fwd	TTTCGCCCCGGGCTAATT ATG	
Donor plasmid-sequencing5-Fwd	TGCTGGGAATAGCATA TCGT	
Donor plasmid-sequencing6-Fwd	TGTTCCACTGTCACATA TCG	
Donor plasmid-sequencing7-Fwd	GTGAGCAACTGCGGTC TGTG	
Donor plasmid-sequencing8-Fwd	AGTTATCACTCAAATC CCTG	
Donor plasmid-sequencing9-Fwd	AAAAAGTCTGCTAAAT GGCC	
Donor plasmid-sequencing10-Fwd	GCGCAGCTGAACAAGC TAAA	
Donor plasmid-sequencing11-Fwd	GTGAACTTCCCCTCCG ACGG	
Donor plasmid-sequencing12-Fwd	ACTAGTAAAGATCTCC ATGC	
Donor plasmid-sequencing13-Fwd	CCTAGGCCTTCTGCAG CTC	
Donor plasmid-sequencing14-Fwd	GAGACGGACCCCCGAA GAAG	
Donor plasmid-sequencing15-Fwd	AAAGTTGCTAATCGTG GCCC	

Donor plasmid-sequencing16-Fwd	CGTCAGGGGCCTTCTG CTTA	
Donor plasmid-sequencing17-Fwd	CAGAGTTCTTGAAGTG GTGG	
Fwd: Forward Primer; Rev: Reverse Primer		

Table 2.6 List of TurboID transgenic line primers

Name	Sequence (5' to 3')	Purpose
<i>Mco4</i> -FP	ATGAAATTCAATTTGGTGCAGAC	Amplifying <i>Mco4</i> cDNA region
<i>Mco4</i> -RP	GCTACCTCCGCCGCCTGAACCTCCACC TCCGGCCACCGAACTGCACAGACC	
Backbone 1-FP	CGAAGGACGTTGACACATTGGCCACC AGAGTGACCAGC	Amplifying pUAS-TurboID-V5- <i>Mco4</i> backbone
Backbone 1-RP	GTCTGCACCAAATTGAATTTTCATCATG GTGAAGGGGG	
Backbone 2-FP	TAGAAGGGTGGGCGCGCCGACCCAGC TTTCTTGTACAAAGT	
Backbone 2-RP	ATGTGTCAACGTCCTTCGGATATCTAA TATCCTGCG	
TbV5-FP	GCGGCGGAGGTAGCGGCAAGCCCATC CCCAAC	Amplifying TurboID sequence with a V5 tag
TbV5-RP	CGCGCCCACCCTTCTACTTTTCGGCAG ACCGCAGACTGAT	
Sequenci ng-FP1	GCAATAAACAGTAAACACGA	Sequencing pUAS-TurboID-V5- <i>Mco4</i> whole plasmid
Sequenci ng-FP2	GGCAGTTGAAGAAGTGCAG	
Sequenci ng-FP3	GTGTGGAATCAGGCAATTCT	

Sequenci ng-FP4	TGCCCAAGAAAGCTACCC	
Sequenci ng-FP5	CCGGATGGCGATACTTG	
Sequenci ng-FP6	ACTACAAGCGTTATGCTCAT	
Sequenci ng-FP7	CAATCACTCAAAAAACAACAA	
Sequenci ng-FP8	TATCATCGATCTCGAGGCT	
Sequenci ng-FP9	AGAACTCTGAATAGGGAATTG	
Sequenci ng-FP10	GAGCGGCAAGGAGTACAT	
Sequenci ng-FP11	AACATTCTGATCAACGGGC	
Sequenci ng-FP12	AATCTCAATGCCAGCGAC	
FP: Forward Primer; RP: Reverse Primer		

Table 2.7 List of S2 cell primers

Name	Sequence (5' to 3')	Purpose
<i>Mco4</i> -F	ATGAAATTCAATTTGGTGCAGAC	For construction of pPU10- <i>Mco4</i> -cflag
<i>Mco4</i> -R	TCATGGTCTTTGTAGTCGCCGGCCACC GAACTGCACAGACC	
Backbone - <i>Mco4</i> -F	GGCGACTACAAAGACCATGA CGGTGATTATAAAGATCATG	
Backbone - <i>Mco4</i> -R	GTCTGCACCAAATTGAATTTTCATGGCC ATGGTGGCGA	
HEPH-F	ATGACCCAGACTTTGCCCTA	For construction of pPU10- HEPH-cflag
HEPH-R	TCATGGTCTTTGTAGTCGCC CTGTTTGAAAGACAGAA	
HEPH- Backbone -F	GGCGACTACAAAGACCATGA CGGTGATTATAAAGATCATG	
HEPH- Backbone -R	TAGGGCAAAGTCTGGGTCATGGCCATG GTGGCGAATT	
Sequenci ng 1	GACACAAAGCCGCTCCATCA	Sequencing of pPU10- <i>Mco4</i> -cflag and pPU10-HEPH-cflag
Sequenci ng 2	CACTGTCACATATCGCCGCA	
Sequenci	CTCTTGGTGGAGTGGTTTGG	

ng 3		
F: Forward Primer; R: Reverse Primer		

CHAPTER 3 Characterization of *Mco4* expression

3.1 Introduction

The *Mco4* gene is predicted to encode a single transmembrane domain based on SignalP 5.0 software. This notion is supported by previous experiments conducted by Areeg Abd Elhafiz[121], who utilized ubiquitous *Mco4* overexpression to demonstrate its membrane-bound localization in the gut, PG and salivary gland tissues of *Drosophila*. The localization and expression levels of *Mco4* can provide insights into its functional significance, particularly in iron homeostasis[72][73]. For *Mco4* to function as a high-affinity iron importer, I expect a specific expression pattern: first, membrane-bound localization in the gut membrane, facing the gut lumen, and second, increased expression under iron-deprived conditions.

I used a previously constructed *UAS-Mco4-3xMyc* line[121] and validated it by observing *Mco4*'s localization in the gut, PG and salivary gland. In this chapter, I will further validate *Mco4* localization by examining its expression using S2 cells and an overexpression sample. For the overexpression study, I chose to examine the fat body from whole body *Mco4* overexpression samples. In S2 cells, I used a new *Mco4-C-3xFlag* vector to assess its subcellular localization. These transfected S2 cells will also be used in another experiment (Ferroxidase Activity Assay) detailed in Chapter 5. Verifying *Mco4*'s membrane-bound expression in S2 cells is therefore crucial for this subsequent experiment.

To further investigate the localization of endogenously produced *Mco4*, I constructed a knock-in line with a 3xFlag tag inserted at the C-terminus of *Mco4* (Figure 3.3). The line also carries the DsRed selectable marker. A homozygous line was established, and gut, BRGC, fat body tissues were dissected and examined for *Mco4* localization using anti-Flag antibodies (detailed method in Chapter 2.6). All *Mco4* constructs used in this study have their epitope tag attached in the C-terminus of it. The reason being the N-terminus contains a signal peptide, which has a predicted cleavage site between the 22nd and 23rd amino acid, as predicted by SignalP 5.0. Signal peptides guide proteins to the endoplasmic reticulum, where they undergo post-translational modifications. The proteins are then incorporated into the cell's plasma membrane. At this stage, a signal peptidase cleaves the signal peptide at a cleavage site.

RT-qPCR was also performed to measure *Mco4* expression levels under high and low dietary iron levels in BRGC, gut and fat body tissues. Immunolocalization may be unsuitable to detect lowly expressed genes and is not the best way to quantify expression changes. The idea was that RT-qPCR would allow me to determine whether *Mco4* expression was indeed affected by iron availability and how strongly *Mco4* was induced by iron deprivation.

3.2 Results

3.2.1 Validation of *Mco4* localization using S2 cells

To further validate the subcellular localization of Mco4, I used *Drosophila* Schneider 2 cells as a model system due to their simplicity and high DNA uptake efficiency upon transfection. I generated the construct *pAc5-Mco4-3xFlag*, driven by the *Drosophila* Actin5C promoter and included the full-length *Mco4* cDNA sequence fused with sequences encoding a 3xFlag tag at the C-terminus. This construct was transfected to S2 cells. I then used the mouse anti-Flag antibodies to detect the Mco4 in transfected S2 cells, coupled with Goat anti-mouse as secondary antibodies for immunolocalization (detailed method in Chapter 2.25). This strategy showed that Mco4 localized to the plasma membrane, consistent with earlier results (Figure 3.1).

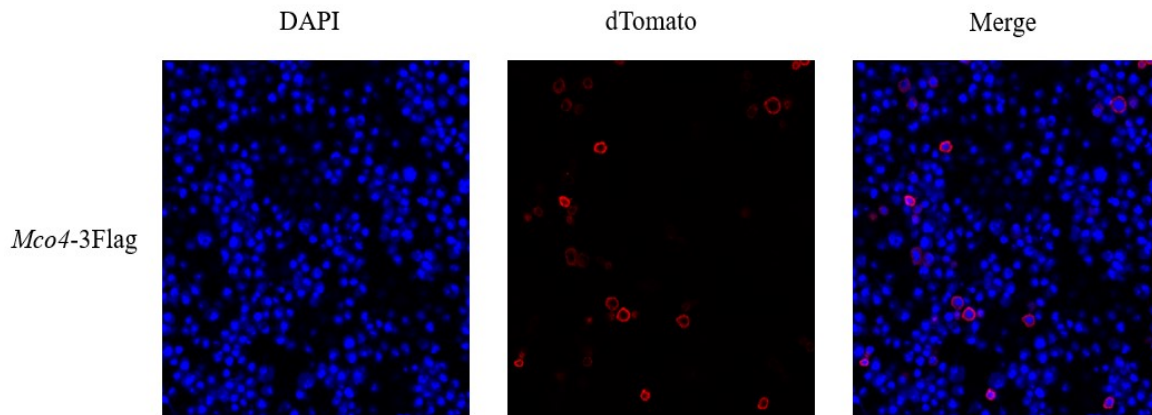


Figure 3.1 Immunofluorescence analysis of Mco4 localization in S2 cells transfected with *Act5-Mco4-3xFlag* construct

The construct is driven by the *Drosophila* Actin5C promoter and includes the full-length *Mco4* cDNA fused with three FLAG tags at the C-terminus. S2 cells were transiently transfected with

the *Ac5-Mco4-3xFlag* construct. Cells were stained with anti-FLAG antibody and DAPI. Images were obtained with confocal microscopy under 40X. The red signals indicate the membrane localization of Mco4, and DAPI/blue signal is used to visualize the nuclear.

3.2.2 Analysis of *Mco4* localization in a transgenic line

To validate the localization of Mco4 in vivo, I crossed *UAS-Mco4-3Myc* flies with the *actin5C-Gal4* driver to achieve strong ubiquitous expression of *Mco4*. The *UAS-Mco4-3Myc* construct was designed to include three Myc epitope tags at the C-terminus of Mco4. The fat body, PG and gut tissues were dissected from the resulting larvae and analyzed using fluorescence microscopy to determine the subcellular localization of Mco4. The fluorescence microscopy analysis revealed that Mco4 also exhibited a membrane-bound localization in all of the three tissues (Figure 3.2). I primarily focused on taking pictures of the fat body, because Mco4 localization in this tissue had not been examined before.

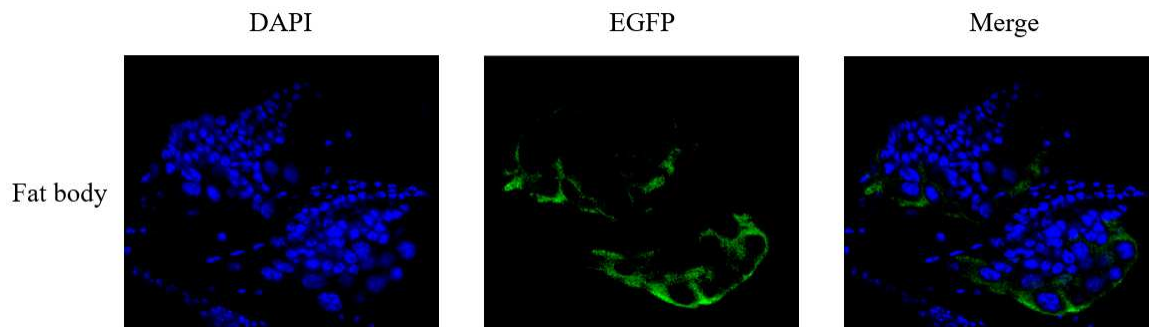


Figure 3.2 Subcellular localization of Mco4 in fat body tissue

UAS-Mco4-3Myc was crossed with a ubiquitously expressed Gal4 driver to generate *actin5C>UAS-Mco4-3Myc* animals. Fat body tissue was dissected from L3. Samples were incubated with anti-Myc antibody and DAPI. Images were obtained with confocal microscopy under 40X. The green signals indicate the subcellular localization of Mco4, and DAPI/blue signal is used to visualize the nuclear.

3.2.3 Generation of *Mco4* CRISPR/Cas9 knock-in line

Since I suspected that *Mco4* expression pattern changed in response to iron deprivation, overexpression studies alone are insufficient to conclude on its natural expression patterns. Moreover, overexpression of proteins from a transgene might not replicate the precise spatial and temporal expression patterns of the gene and cause non-specific negative effect[75][76]. To investigate the natural expression pattern of *Mco4*, I generated a CRISPR/Cas9 knock-in line where a 3xFlag tag was placed at the C-terminus of *Mco4*. This approach allowed for precise tagging of the *Mco4* protein, facilitating its detection without altering its endogenous expression levels.

The CRISPR/Cas9 technique uses guide RNAs (gRNAs) to direct the Cas9 nuclease to a specific genomic locus, introducing a double-strand break adjacent to a protospacer motif (PAM) sequence. Homology-directed repair (HDR) is triggered in the presence of a repair template, which is provided in the form of injected donor DNA, resulting in a replacement of the endogenous DNA with the corresponding DNA in the repair template (Figure 3.3) [77]. For the *Mco4* knock-in construct, the gRNA vector was obtained from pCFD5 and included two gRNAs that introduced cuts on each side of the end of the *Mco4* transcription unit: one in Exon 4 before the stop codon, and the other in the untranslated region downstream of *Mco4*.

The donor plasmid, serving as the repair template, contained right and left homology arms, along with a 3xFlag tag sequence and a transformation marker, 3xP3-DsRed. The dsRed marker in the donor plasmid allows for easy identification of successful insertions, as DsRed expression, in the presence of UV light, results in red fluorescence in the eyes, central lobes of the brain (CNS), hindgut, and anal plates of larvae throughout all three larval stages. The 3xP3 promoter consists of three tandem repeats of the Pax-6 paired box 3 (P3) sequence, which is derived from the promoter region of the Pax-6 gene. The Pax-6 gene is crucial for eye and neural development in insects[78]. In this study, the donor plasmid is created from pHD-DsRed-attp, and DsRed was placed between the homology arms. Each arm was 100 bp long and represented the exact same sequence as the wild type. The donor DNA contains the end of *Mco4* sequence attached with the 3xFlag tag (Figure 3.3).

The donor plasmid and gRNA vector were co-injected during embryo injection. Upon receiving the injected embryos, I crossed the resulting flies with an X-chromosome balancer stock, *FM7a*, to establish a stable line. Over successive generations, I screened for homozygous individuals carrying the knock-in construct to ensure stable and uniform expression of the tagged protein.

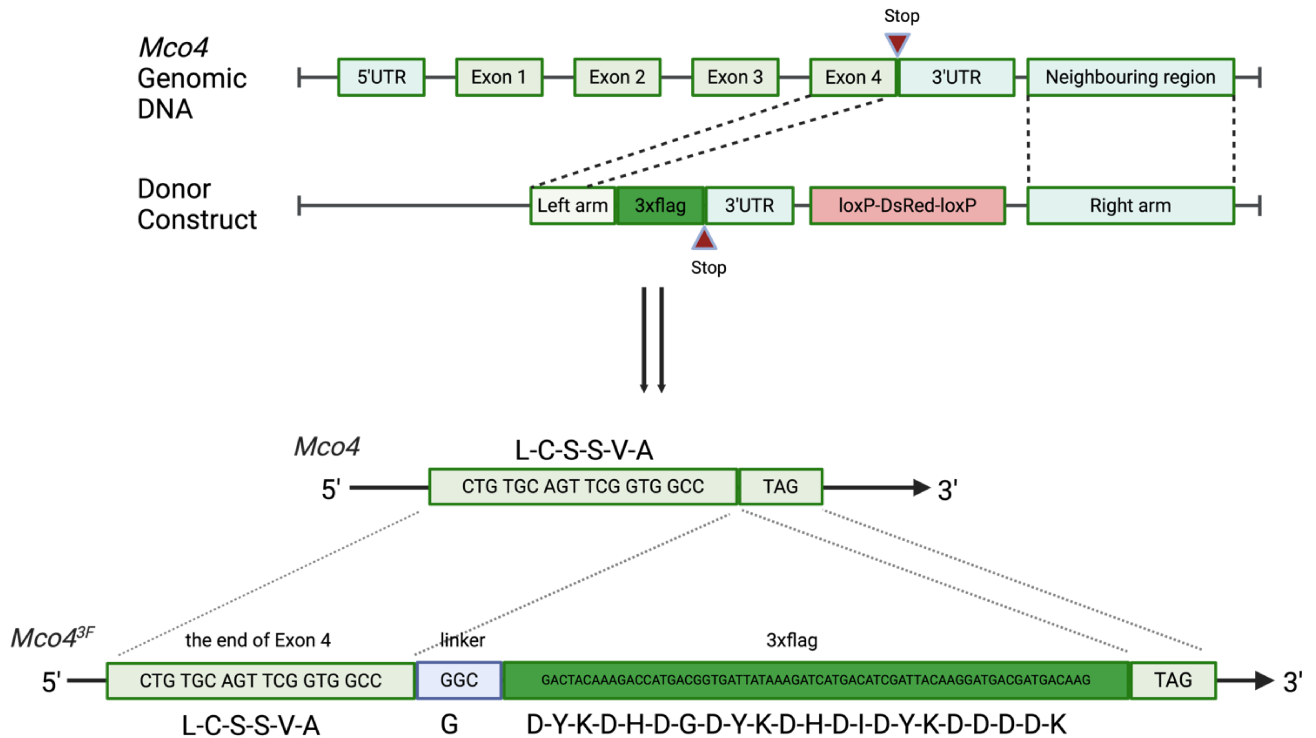


Figure 3.3 *Mco4* knock-in line (*Mco4*^{3F}) generated by CRISPR/Cas9

The *Mco4* gene region was replaced by a tagged version with a 3xFlag tag at the C-terminus before the stop codon. The donor plasmid contains a DsRed marker under the 3xP3 promoter. It also contains the donor DNA, which has the *Mco4* sequence with the 3xFlag tag. Two homology arms are included in the donor vector as the repair template. Two gRNAs introduced cuts on each side of the end of *Mco4*: one in Exon 4 before the stop codon, and the other in the

untranslated region downstream of *Mco4*. The donor vector was co-injected with the gRNA vector. The positive transformants were crossed with an X-chromosome balancer to establish a homozygous *Mco4* knock-in stock. In the homozygous knock-in stock, both *Mco4* alleles are replaced by *Mco4*^{3F}.

3.2.4 *Mco4* is strongly expressed in the proventriculus regardless of dietary iron concentrations

Using this knock-in line, I performed immunofluorescence analysis on gut, BRGC, fat body and salivary gland tissues. I found out that regardless of whether the flies were fed iron-enriched or iron-depleted food, the only fluorescence signal detected was in the proventriculus (PV). Specifically, *Mco4* expression formed a distinct torus-like structure in this tissue with most signals coming from the outermost layer of the PV. Additionally, under iron depletion conditions induced by BPS, the *Mco4* signal remained relatively stable in the PV, and the signal was not seen in any other tissues (Figure 3.4). As for the rest of the gut and PG, there were discontinuous and weak signals, which were similar to the background noise and cannot be confidently identified as a real signal.

Mco4 expression in the PV came as a surprising finding, since there has not been any direct link between PV and iron and it contradicts my initial prediction that *Mco4* is expressed in the gut. The PV is a specialized structure located at the junction of the foregut and midgut in *Drosophila*. There is some controversy regarding the classification of the PV. Some studies suggest that it is the beginning of the midgut, while others argue that it is part of the foregut. It functions as a valve regulating the passage of food into the rest of the gut and is involved in the production of the type II peritrophic matrix, which serves as a barrier against pathogens and abrasive particles[79]. The PV contains specific cells that produce this protective layer, ensuring gut integrity and preventing infections. Most studies done with the PV focused on its role in peritrophic matrix formation, and whether or not it is involved in absorption or digestion remains unclear.

One recent paper classified the types of cells in the PV using single-cell RNA-seq and divided the whole PV into different layers based on the cell types[79]. Compared to their result,

the torus-like expression pattern of *Mco4* I observed in the PV corresponds to the PV5.5 cell cluster, which is a thin layer located in the outer side of the PV. This study also identified *Mco4*, along with CG7567 and CG5162, as major marker genes specific to the PV5.5 cell type[79]. There are more than 10 genes also shown to be expressed in this layer, although not specific, and one of them is *Mco1*. Their study served as a confirmation of *Mco4*'s endogenous location. However, neither CG7567 nor CG5162 showed iron-dependent regulation in our previous RNA-Seq data, and the genes identified from PV5.5, except for *Mco1* and *Mco4*, are not involved in iron regulation.

There are several possibilities by which *Mco4* expression in the PV could be linked to iron. Based on the genes that were identified in different layers[79], the PV is suspected to function in dietary sensing, possibly via hormonal signaling. In fact, most animals' foregut (or sometimes the start of midgut) has neural communication with the brain as a way to report nutritional and immune status[79]. The PV's connection to the ring gland via neurons also raises the possibility of a regulatory role for *Mco4* in communicating nutritional status, in particular iron levels in the diet, to the ring gland. This communication could result in systemic hormonal signals that help regulate iron homeostasis throughout the organism. In this context, *Mco4* might function as an iron sensor, contributing to the regulation of systemic iron levels by influencing the activity of the ring gland and other iron-regulating mechanisms.

Regardless, there is no evidence on PV's role in nutrient uptake from diet. The stable expression of *Mco4* in the PV, even under varying dietary iron levels, suggests a fundamental role that is independent of dietary iron levels. This expression suggests that the *Mco4* is not functioning as an iron importer in the PV and most likely influence iron metabolism through a different mechanism.

Although immunofluorescence is a powerful technique for visualizing the localization and distribution of proteins in cells and tissues, the sensitivity of immunofluorescence is constrained by several factors, including the specificity and affinity of the primary antibodies, making it less sensitive to lowly expressed targets. Consequently, while *Mco4* was robustly detected in the PV, its presence in other tissues may require other techniques. As mentioned in Chapter 1.5.2, we detected *Mco4* upregulation in the ring gland in response to both iron

deprivation and disruption of AGBE and Evi5 function via RNAi. Since I was not able to observe the presence of Mco4 protein with anti-Flag antibodies, it was possible that immunolocalization, at least with the antibodies I used, lacks the sensitivity to detect Mco4 at endogenous levels.

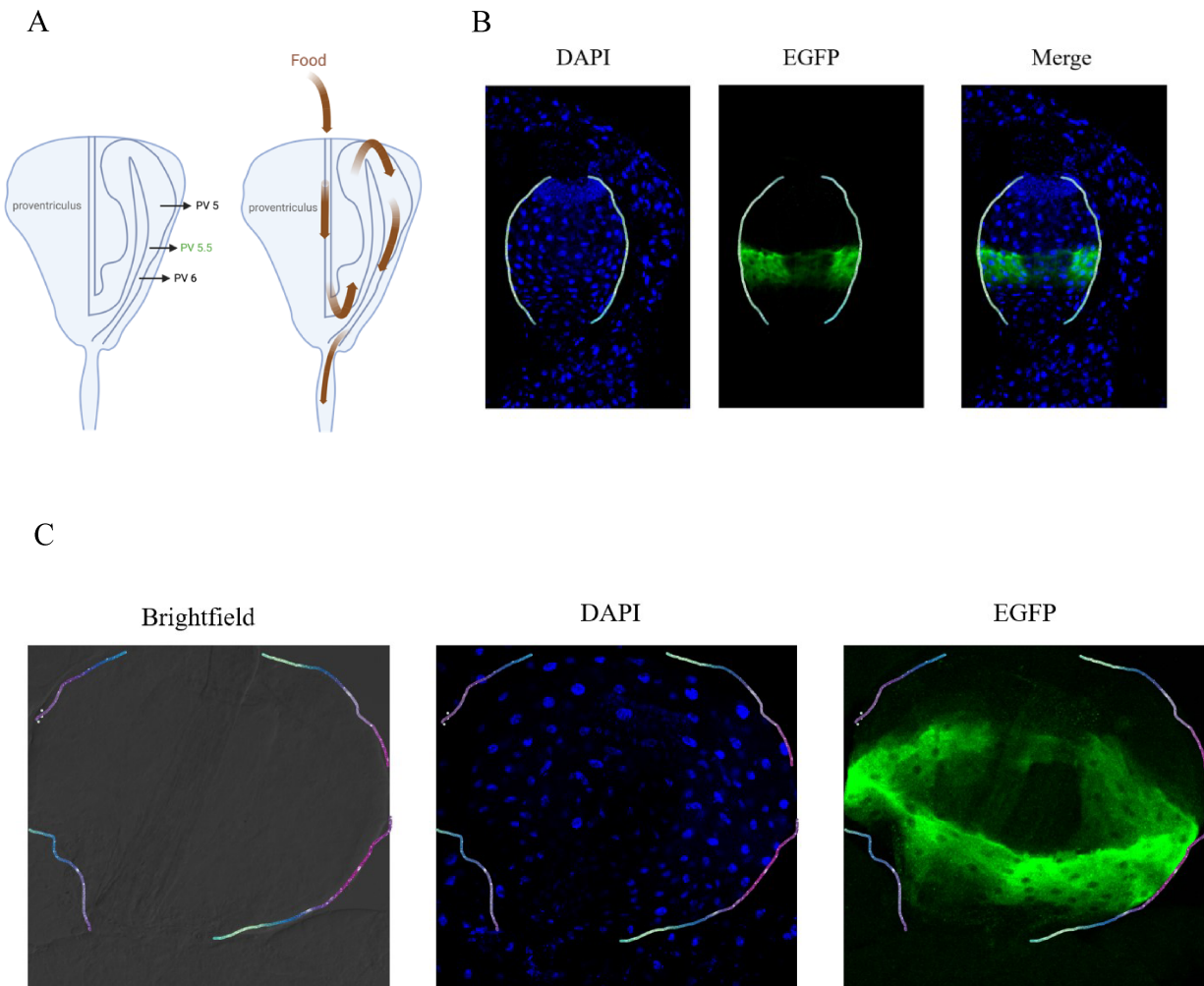


Figure 3.4 *Mco4* is strongly expressed in the PV

Proventriculi were dissected from of *Mco4*-3xFlag L3. Samples were incubated with anti-Flag antibody (Cell Signaling, #8146S) and DAPI. (A) Schematic of PV layers classified by cell types. PV 5.5 is a thin layer between PV5 and PV6. It is located on the outer wall of PV. Food enters through the central esophagus tube and move down through PV1 to PV6 before entering

the rest of the midgut. (B) Proventriculus images obtained with confocal microscopy under 20X. (C) Proventriculus images obtained with confocal microscopy under 40X. The green signals indicate the localization of *Mco4*, and DAPI/blue signal is used to visualize the nuclear. The circled area represents the shape of the proventriculus. The green signal was not seen in other tissues.

3.2.5 *Mco4* is strongly upregulated in the gut under iron-deprived conditions

To further investigate the endogenous expression pattern of *Mco4* and its link to iron, I performed RT-qPCR to quantify *Mco4* expression levels under BPS and Nutri-fly food. This method provided a more sensitive and quantitative assessment compared to immunofluorescence, particularly for detecting mRNA levels of lowly expressed genes. Previous RT-qPCR studies have indicated that *Mco4* is upregulated in response to iron deprivation in the whole larvae, but in what tissues such upregulation occurs remains unknown. Since the antibody stains showed strong and stable *Mco4* expression in the PV independent of dietary iron levels, it was possible that *Mco4* was induced in other tissues only when iron was scarce.

To assess whether *Mco4* was expressed in the gut outside the PV region, I performed RT-qPCR using samples representing the PV, the gut without the PV (gut w/o PV) and carcass (whole body w/o gut) obtained from larvae raised on Nutri-fly with or without 200 μ M BPS. The rationale of using 200 μ M as a concentration for BPS was that it was non-lethal but quite a bit stronger than 120 μ m, allowing me to induce significant iron deprivation in the first generation. The RT-qPCR results revealed that *Mco4* expression increased around 48-fold in the gut w/o PV samples and 9-fold in the carcass under iron-deprived conditions (Figure 3.5). The expression level in the proventriculus remained stable and increased by 1.1-fold in BPS food. Together, this showed that *Mco4* in the PV did not respond to iron deprivation, whereas *Mco4* in the remaining gut and the carcass was significantly upregulated. While RT-qPCR is mainly used to express relative changes in expression, one can also assess the absolute levels by analyzing the number of cycles it takes to cross the cycle threshold (CT value), which is the number of cycles it takes for PCR products to generate more fluorescence than the background level. Under normal conditions, *Mco4* expression in the gut was extremely low (CT \sim 37), and it increases under BPS conditions (CT \sim 31), although still not comparable to its expression in the PV (CT \sim 23). The fact

that iron-triggered upregulation of *Mco4* is only seen outside of PV further supports the idea that *Mco4* has different functions in the PV compared to the rest of the gut.

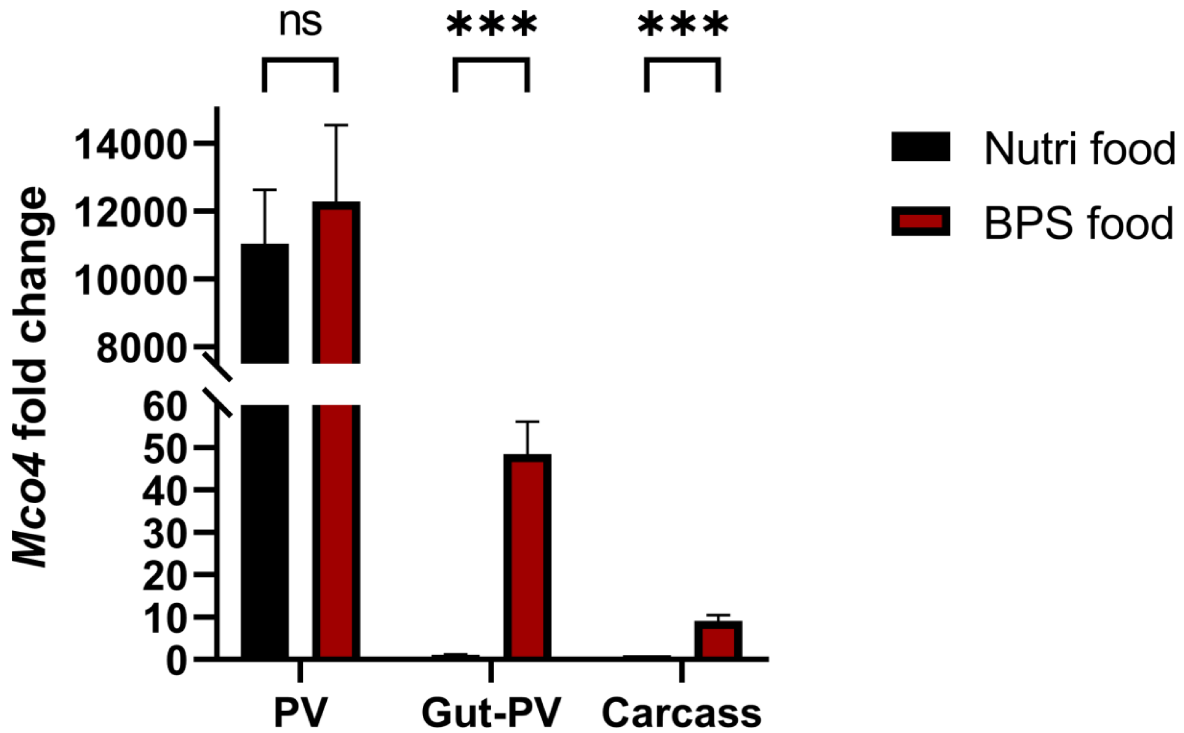


Figure 3.5 *Mco4* upregulation in different tissues in response to dietary iron deprivation

Quantitative RT-qPCR was used to analyze *Mco4* expression in three tissues: PV, gut without PV (gut - PV) and carcass (whole body - gut). 20 flies were raised on either Nutri-fly food or Nutrifly food supplemented with 200 μ M BPS. Iron deprivation resulted in an increase in the gut-PV and the carcass. Larval genotypes are *w¹¹¹⁸*. Data was normalized to *rp49* expression. Fold changes are relative to Nutrifly food carcass samples. Data are from three biological replicates. Means and the 95% confidence intervals are shown. Differences in expression were calculated using the $\Delta\Delta$ Ct method (***p* < 0.001, ns=no significance). PV: Proventriculus.

3.3 Discussion and future directions

3.3.1 *Mco4* have separate functions in the PV and gut

The expression pattern of *Mco4* is suggestive of different roles depending on iron availability. Under iron replete conditions, *Mco4* is predominantly expressed in the proventriculus (PV). This role may involve iron sensing and communication with the ring gland. The PV's stable expression of *Mco4*, regardless of dietary iron levels, indicates a constitutive function independent of iron import and potentially in signaling nutritional status. When iron is deprived, *Mco4* expression significantly increased in the rest of the gut potentially to increase iron uptake from the diet. This upregulation aligns with the hypothesis that *Mco4* functions as a component of a high-affinity iron importer, facilitating the absorption of ferric iron under conditions of scarcity. Additionally, *Mco4* expression increases in the carcass, which presumably originates from the prothoracic gland but likely includes other tissues as well, as the prothoracic gland represents only a very small component of the carcass sample, which cannot account for the entirety of the observed upregulation. The distinct expression patterns of *Mco4* in the PV and the rest of the gut suggest separate functions in these regions.

3.3.2 *Mco4* as an indicator of dietary iron deprivation in flies

Mco4's upregulation in response to iron deprivation, both genetically and through dietary manipulation, positions it as a possible marker gene for iron starvations. This consistent response across different conditions suggests that *Mco4* expression levels could be used as a biomarker for monitoring iron status in *Drosophila*.

3.3.3 PV-specific and gut-specific *Mco4* knockdown

To delineate the distinct functions of *Mco4* in the PV and the remainder of the gut, future research can focus on the tissue-specific RNA interference (RNAi) to knock down *Mco4* expression in these two tissues separately. The PV5.5-specific drivers established in previous studies provide a valuable tool for targeting this layer in the PV[79]. I would recommend using the PV5.5 specific driver and a gut driver to knock down *Mco4* expression in these two tissues

separately and raise the flies on 200 μ M BPS food. Flies should be observed for iron related phenotype, such as reduced survival in the first generation and less iron content in their body. These are the phenotypes observed in *Mco4* null mutants, which will be further discussed in Chapter 4. If *Mco4* knockdown in the PV only does not lead to iron deficiency symptoms, then it's further supporting an iron-independent role in the PV. From there researcher should screen for other potential phenotypes such as changes in gut morphology, digestive efficiency, or stress responses. Instead, if knocking down *Mco4* in the gut (excluding the PV) results in iron deficiency symptoms under BPS conditions, it would support that *Mco4* in gut tissues is essential for high-affinity iron uptake.

3.3.4 Investigating the PV's role in dietary sensing

The PV in *Drosophila* is an essential structure of the foregut and located anterior to the midgut. This organ's equivalent in other animals can be found in many forms, adapted to their specific dietary and physiological needs[81]. In birds, the proventriculus is a glandular stomach that secretes digestive enzymes before the food passes into the gizzard, which mechanically breaks down the food for easier digestion[82], since birds lack teeth to chew/grind food. In mammals, a similar regulatory function is performed by the pyloric sphincter, which controls the passage of partially digested food from the stomach to the duodenum[80].

In vertebrates, such as chickens, the proventriculus works alongside the gizzard to ensure efficient digestion. The proventriculus secretes acid and digestive enzymes to initiate protein breakdown, while the gizzard uses muscular contractions and grit, often in conjunction with ingested stones or grit, to grind the food, aiding in mechanical digestion[84]. This dual-function system ensures thorough processing of ingested food, much like the combined regulatory and digestive roles of the *Drosophila* foregut and midgut[81]. Although the *Drosophila* PV is mostly characterized for the role in the synthesis of the peritrophic matrix that acts as a gut barrier, its potential involvement in digestion or sensory function is a topic for future studies. It is especially interesting to note that similar ring-like expression patterns are often found in sensory systems, such as the gustatory receptors in the taste buds and the mechanoreceptors in the cochlea, which are organized in circle structures to optimize their sensory functions[85]. Specifically, ring structures allow for a dense packing of sensory receptors within a limited space, maximizing the

number of sensory cells that can detect stimuli. The circular arrangement also provides a large surface area for the receptors, allowing the system to detect stimuli coming from any angle. This is particularly important for functions like taste, where the gustatory receptors need to detect chemicals from food contacting different parts of the tongue[85]. Since the PV is the first site where food enters the digestive system, it's possible that it senses nutritional information and communicate with the brain.

3.3.5 Investigating *Mco4* expression in the gut membrane using high resolution IF

One crucial aspect that remains to be investigated is the specific localization of *Mco4* within the enterocyte membrane. If *Mco4* functions as an iron importer, it is expected to be expressed on the apical side of enterocyte cells, facing the gut lumen. The apical membrane of enterocytes is characterized by the presence of microvilli, which form a brush border that increases the surface area for nutrient absorption[81]. This brush border can be visualized using high-resolution immunofluorescence techniques[86]. In the current study, I was not able to detect *Mco4* protein outside the PV. This lack of detection is likely due to the inherently low expression levels of *Mco4*, combined with high background noise that obscures the real signal. To overcome these limitations, future research should focus on using more advanced immunofluorescence techniques such as paraffin-embedded tissue sections and tyramide signal amplification (TSA)[87]. The use of paraffin-embedded tissue sections allows for cross-sectional imaging of the gut. This method can provide clearer and more detailed views of the tissue architecture and enable the precise localization of *Mco4* on the apical or basolateral sides of enterocytes. TSA amplifies the immunofluorescence signals using a tyramide substrate that is labelled with a reporter molecule, such as a fluorescent dye. The HRP enzyme from the secondary antibody catalyzes the conversion of the tyramide substrate into a highly reactive intermediate, which binds to tyrosine residues on proteins that are in close proximity to the enzyme-labeled secondary antibody. This results in a dense deposition of the labeled tyramide around the site of the target antigen and thus, an amplified signal[122][123]. If high resolution IF still fails to detect *Mco4* signal, then researcher could consider the possibility that *Mco4* is subject to post-transcriptional regulation that leads to inefficient translation or rapid degradation. In that case, further study can focus on using ribosome profiling, which detects ribosome positions on mRNAs, to determine if *Mco4* mRNA is being actively translated and to what extent[124].

CHAPTER 4 Characterization of *Mco4* null mutant phenotype

4.1 Introduction

4.1.1 *Mco4*^{-/-} flies shows no phenotypes under a normal iron diet

To analyze *Mco4*'s potential function in iron metabolism, it is crucial to examine the phenotypic effects of *Mco4* knockout in *Drosophila*. The *Mco4* null mutation (*Mco4*^{-/-}) was generated with CRISPR/Cas9, where the *Mco4* genomic region was removed and replaced with a DsRed marker[121]. Initial survival tests conducted with the *Mco4*^{-/-} line under standard Nutri-Fly food conditions revealed no obvious phenotypes. Specifically, the *Mco4*^{-/-} flies did not exhibit any morphological differences or reduced survival rates compared to controls, nor did they exhibit decreased body iron content. Additionally, these flies were tested for survival under mild iron-depletion conditions using 100 μM BPS in their food. The *Mco4*^{-/-} flies showed no noticeable phenotypic differences compared to control flies under these conditions as well.

However, it is important to consider that *Drosophila* have stored iron reserves and can inherit iron from their parents. Previous studies in my lab have shown that it takes five generations of iron depletion for the *w¹¹¹⁸* to achieve a 50% decrease in overall survival (Soltani et al., manuscript submitted) using 100 μM BPS food. This suggests that a one either needs a longer-term generational study using mild iron deprivation via BPS or higher levels of BPS for single-generation studies in order to examine the impact of the *Mco4* null mutation on iron absorption. I observed *Mco4*^{-/-} flies over several generations using 100 μM and 160 μM BPS, and I hope to assess the cumulative effects of iron depletion and determine if *Mco4* plays a critical role in maintaining iron homeostasis under prolonged iron-deficient conditions.

4.1.2 Dietary iron deprivation is achieved by adding BPS to Nutri-fly food

Iron chelators are molecules that bind to iron ions, forming a complex that can be excreted from the body or rendered inactive. Some commonly used iron chelators are desferrioxamine (DFO), 1,10-Phenanthroline (OP), deferiprone and BPS[128]. DFO has high affinity for Fe³⁺, but it also binds to Cu²⁺, which can lead to unintended side effects[128]. OP is highly toxic to cells and would affect flies' survival if put into diet. Deferiprone is another Fe³⁺ iron chelator and also has shown toxicity[128]. As mentioned in Chapter 1.5.1, BPS is a highly specific and effective chelator for ferrous iron and has been used in my lab to make iron-

deprived diet. Its chelation mechanism involves the formation of a stable complex with Fe^{2+} , preventing it from participating in biological reactions such as being unavailable to ferrous iron importers. BPS binds to Fe^{2+} in a 3:1 ratio, meaning three BPS molecules bind to one ferrous iron ion[128]. To achieve an iron-depleted diet using BPS, the compound is added to Nutri-fly food (Figure 4.2). The concentration of BPS needs to be carefully controlled to ensure it effectively chelates available ferrous iron without causing toxicity or unintended side effects. Higher concentrations of BPS result in severe iron deprivation. At 500 μM , the chelation capacity is so high that it leads to acute iron deficiency, causing lethality within the same generation. This concentration effectively sequesters all available Fe^{2+} , preventing essential biological functions and leading to rapid organismal death. To address this concern, I carried out two separate survival studies using *Mco4^{-/-}* flies raised on different concentrations of BPS food and observed their survival across generations.

4.2 Results

4.2.1 Validation of *Mco4*^{-/-} line

The *Mco4*^{-/-} null mutant was generated via CRISPR-Cas9 and a repair template[121]. The presence of DsRed in the progeny indicated successful integration of the donor DNA and validation that this had occurred at the *Mco4* locus was carried out using RT-qPCR with *w*¹¹¹⁸ as the control and *rp49* as the reference/housekeeping gene. I used L3 whole body larvae as a source for the samples. This step is to ensure that the deletion of *Mco4* is complete. The result revealed that *Mco4* expression was reduced close to 0 in this null mutant line (Figure 4.1).

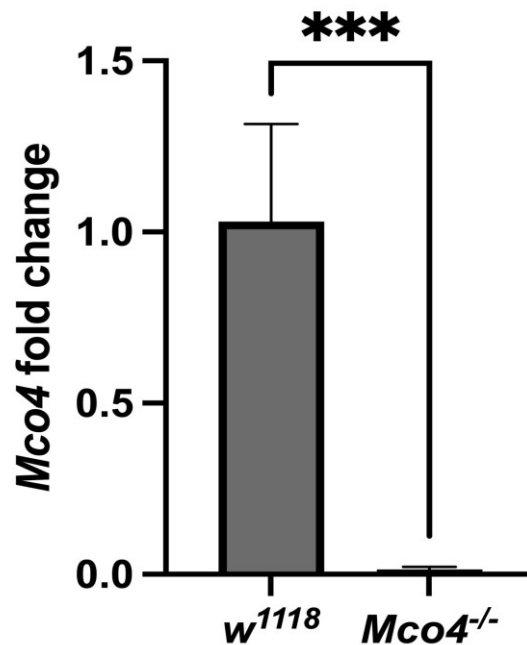


Figure 4.1 The validation of *Mco4* null mutants with RT-qPCR

10 L3 larvae of each genotype were raised on Nutri-fly food. *w*¹¹¹⁸ served as the control. Data was normalized to *rp49* expression. Data are from three biological repeats. Means and 95% confidence intervals are shown. Differences in expression were calculated using the $\Delta\Delta$ Ct method (***)p<0.001).

4.2.2 *Mco4*^{-/-} flies displayed reduced survival under multi-generational iron-deprivation

In this study, I investigated the effects of iron depletion on *Mco4*^{-/-} flies using a BPS concentration of 100 μ M, resulting in mild iron deprivation. The *w¹¹¹⁸* flies served as the control group. Throughout the first four generations (G1-G4), there were no significant differences in survival between the control and *Mco4*^{-/-} flies, regardless of dietary iron levels. Both groups exhibited comparable survival rates, indicating that the initial exposure to BPS did not immediately impact the *Mco4*^{-/-} flies.

However, a notable change occurred starting from the fifth generation (G5). The survival rate of *Mco4*^{-/-} flies began to decline significantly compared to the control group (t-test, $p < 0.0001$). This trend continued, with survival rates dropping further in the sixth generation (G6). By the seventh generation (G7), all *Mco4*^{-/-} flies died at the larval stage, while the control flies exhibited normal survival and development. These findings collectively indicate a progressive and severe impact of iron depletion on *Mco4*^{-/-} flies, beginning at G5 and culminating in complete lethality by G7 under 100 μ M BPS treatment (Figure 4.2). In comparison, through the seven generations the control flies remain a survival rate that is above 70%.

In a second experiment, I increased the BPS concentration to 160 μ M, a moderate level, to determine if the same survival trend observed at 100 μ M would persist. In the following experiment, I included an iron-supplemented diet using ferric ammonium citrate (FAC), which provides a readily bioavailable source of ferrous iron to the food. FAC supplements the diet with ferrous iron and dissociates in the digestive tract, releasing ferrous ions that can be readily absorbed and utilized by the organism. By adding FAC I wanted to see if the decreased survival trend would still persist under a high iron diet.

Starting from the first generation (G1), there was a significant decrease in the survival of *Mco4*^{-/-} flies compared to the control group (t-test, $p < 0.0001$). This reduced survival rate was evident in the first generation and continued to decline gradually over the next two generations (G2 and G3) (Figure 4.3). Interestingly, flies reared on FAC-supplemented food also showed a slightly decreased survival ($p < 0.5$), but the difference is not significant in Nutri-fly food group. The data is showing that *Mco4*^{-/-} knockout increased lethality under iron-deprived conditions, starting from the first generation when exposed to moderate BPS levels. The absence of this

lethality in iron-replete conditions suggests that the observed phenotype is specifically due to iron deprivation. However, regardless of the food types, there seems to be a consistent trend that *Mco4^{-/-}* flies do not survive as well as the wild type.

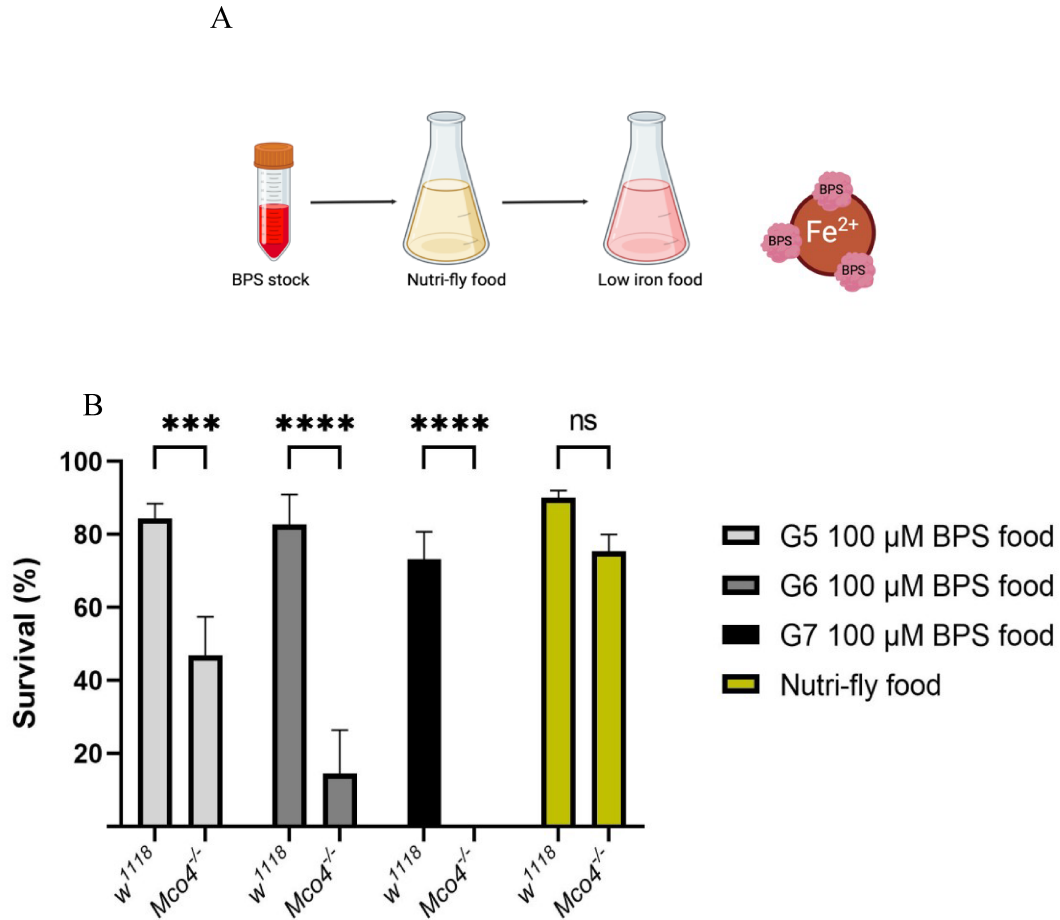


Figure 4.2 *Mco4^{-/-}* showed gradually decreased survival over generations on an iron deprived diet

(A) Iron deprived diet was made by adding BPS to Nutri-fly food. BPS chelates ferrous iron from the diet, forming a complex that has a light pink color. The end concentration is 100 μM BPS. BPS binds to ferrous iron in a 3:1 ratio. (B) *Mco4^{-/-}* survival on BPS food over seven generations. Fifty embryos were collected per one replicate and placed on Nutri-fly food or BPS food. The number of adult flies was counted to calculate the overall survival. Mean and SD are

shown. (***) $p < 0.0001$, ns=no significance). BPS: Bathophenanthroline disulfonic acid; G: Generation.

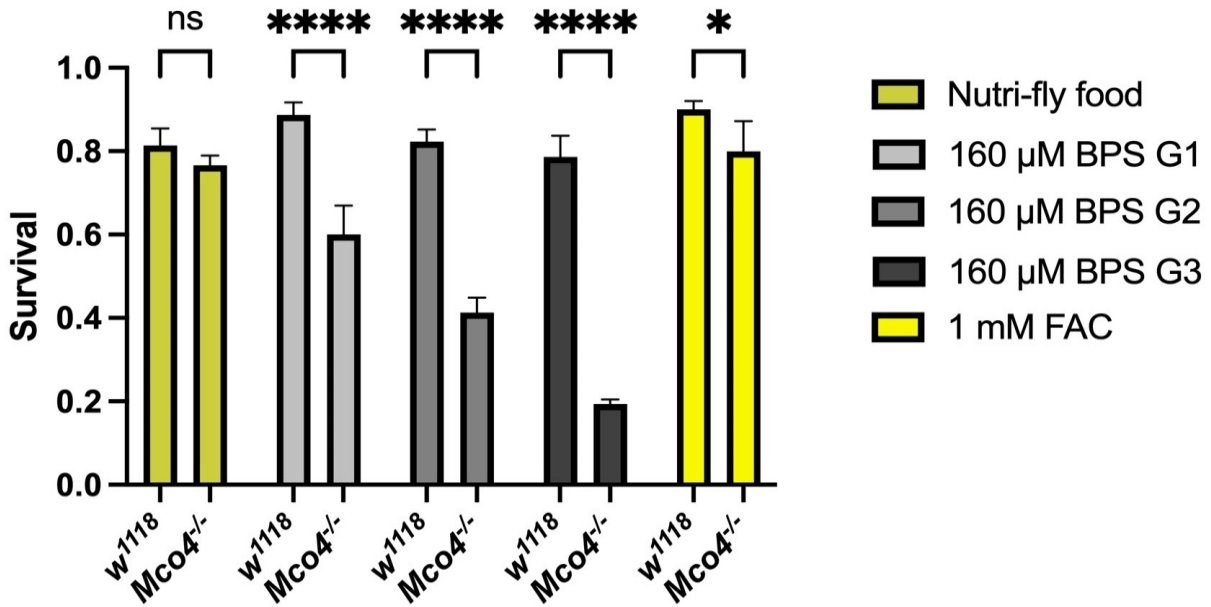


Figure 4.3 *Mco4^{-/-}* showed gradually decreased survival over generations on an iron deprived diet using a higher concentration of BPS.

The iron-deprived diet was made by adding BPS to Nutri-fly food to a final concentration 160 μM. Fifty embryos were collected for each replicate and placed on Nutri-fly food or BPS food. The number of adult flies was counted to calculate the overall survival. Mean and SD are shown. (* $p < 0.01$, *** $p < 0.0001$, ns = not significant). BPS: Bathophenanthroline disulfonic acid; FAC: Ferric ammonium citrate; G(n): Generation (number).

4.2.3 *Mco4*^{-/-} flies displayed reduced iron content

Following the survival experiments, Dr. Sattar Soltani from our lab conducted two separate studies using the *Mco4*^{-/-} lines. The first experiment involved quantifying the amount of metals, including copper and iron, in *Mco4*^{-/-} and *w*¹¹¹⁸ flies reared on either BPS-supplemented food or standard Nutri-Fly food. This analysis was performed using Inductively Coupled Plasma Mass Spectrometry (ICP-MS).

ICP-MS is a highly sensitive and precise technique that works nebulizing the (typically liquid) sample to produce an aerosol, which is then directed into a hot, ionized gas, which atomizes and ionizes the metals in the sample. The ionized sample is then analyzed by a mass spectrometer to detect and measure the metal ions, and quantification occurs by using standards to generate calibration curves[89]. This method is particularly effective for quantifying trace elements, such as iron, due to its ability to detect extremely low concentrations. This sensitivity is essential for accurately assessing iron levels in small biological samples like *Drosophila* tissues[90][91].

The results revealed that *Mco4*^{-/-} (aka *Mco4*^{KO}) mutants had comparable iron levels to the control (*w*¹¹¹⁸) when reared on Nutri-fly food. However, when reared on BPS-supplemented medium, *Mco4*^{KO} mutants exhibited approximately 60% lower iron levels compared to controls. In contrast, *w*¹¹¹⁸ flies did not show significant variation in iron levels under either food condition (Figure 4.4).

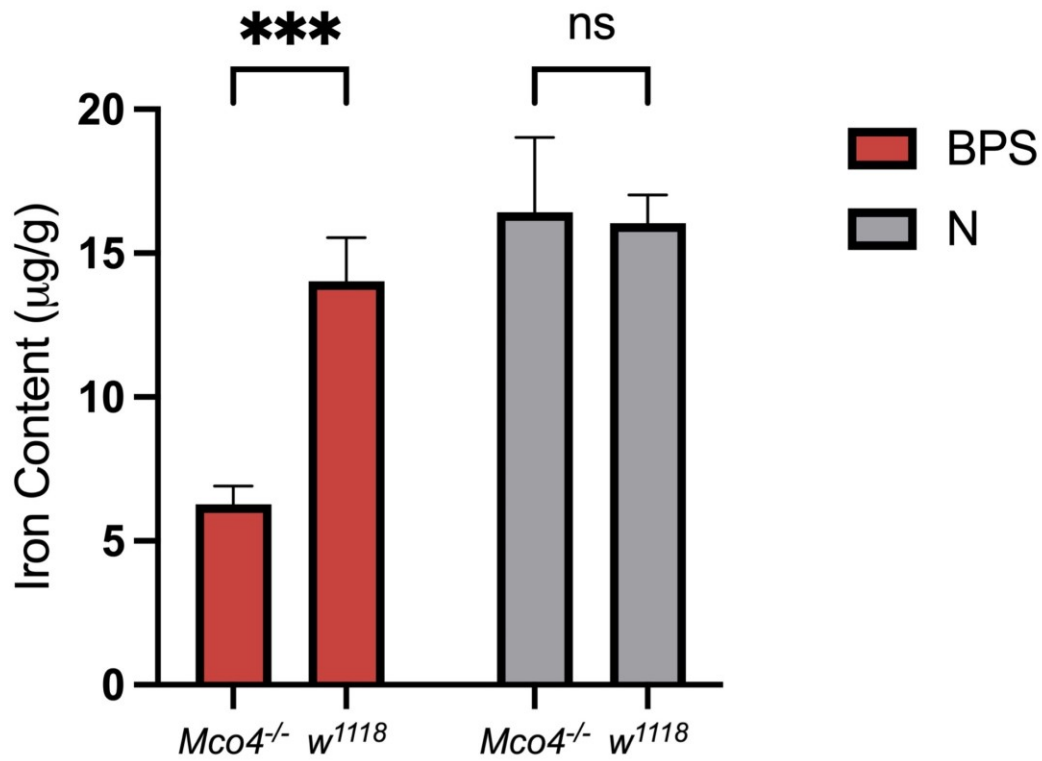


Figure 4.4 *Mco4^{-/-}* flies showed less iron content when reared on BPS-supplemented food.

10-15 larvae were collected for each of the three replicates. Larvae were washed, frozen and weighed before being sent to ICP-MS. Iron content was normalized to total sample weight (g).

BPS concentration used is 120 µM. (***) $p < 0.0001$, ns=no significance). BPS:

Bathophenanthroline disulfonic acid; N: Nutri-fly food. Data was collected by Dr. Sattar Soltani.

4.2.4 *Mco4* knockout combined with *AGBE*-RNAi resulted in more severe iron deficiency phenotype

The second experiment Dr. Soltani conducted was to test the effect of the *Mco4* null mutation in a *PG>AGBE*-RNAi background. Specifically, animals with RNAi targeting *AGBE* transcripts in the prothoracic gland (i.e., *PG>AGBE*-RNAi) exhibit impaired cellular iron homeostasis, causing a stall in heme biosynthesis and red autofluorescence. Importantly, supplementing the fly media with iron completely rescues the red autofluorescence in *PG>AGBE*-RNAi ring glands, however, as shown below, we have now demonstrated that the rescue via dietary iron supplementation requires *Mco4* function.

When *PG>AGBE*-RNAi is carried out in a homozygous *Mco4*^{KO} background, the resulting phenotype is more severe than *PG>AGBE*-RNAi alone, exhibiting increased autofluorescence and further enlarged ring glands, indicative of more severe iron deficiency. In contrast, disruption of *Mco4* alone does not result in these phenotypic changes. Moreover, the iron complement did not rescue the red ring gland phenotype in this mutant, as these animals still show strong red autofluorescence.

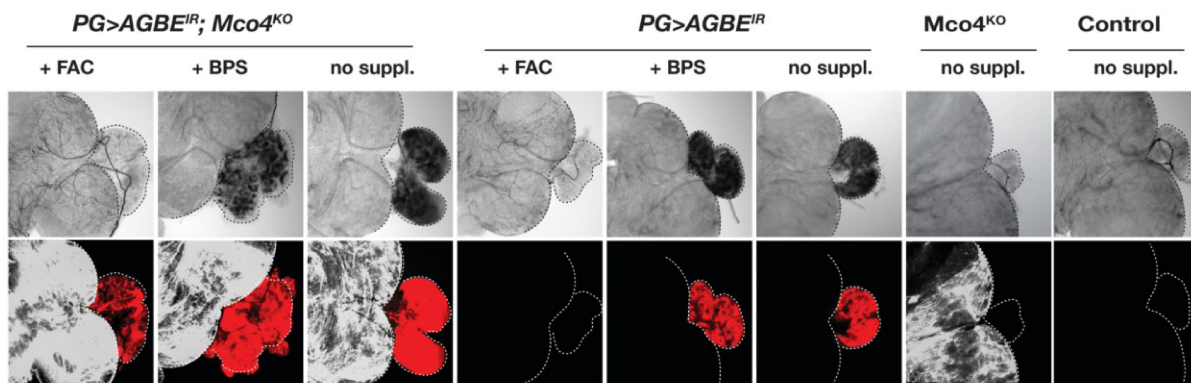


Figure 4.5 *Mco4*^{KO} in *PG>AGBE*-RNAi background results in more severe iron deficiency phenotype in the PG.

The *Mco4*^{KO} null allele was crossed into the *PG>AGBE*-RNAi background. L3 larval brain-ring gland complexes were dissected. The autofluorescence comes from the accumulation of heme precursors due to insufficient levels of mitochondrial iron. BPS concentration used was 120 μ M. FAC concentration was 1mM. Pictures were taken with confocal microscopy under 40X. BPS:

Bathophenanthroline disulfonic acid; FAC: Ferric ammonium citrate. Data was collected by Dr. Sattar Soltani.

4.3 Discussion and future directions

4.3.1 Mco4 imports iron under iron-deprived conditions

Mco4 is specifically upregulated under iron-deprived conditions, and the phenotype associated with *Mco4* knockout is only observed when flies are fed BPS-supplemented food. These observations strongly suggest that *Mco4* is activated primarily when iron levels are low and is not required under normal dietary iron levels. This finding suggests *Mco4* as a crucial component of the high-affinity iron import system in flies when dietary iron is low.

As mentioned in Chapter 1.8, some nongraminaceous plants have both high and low-affinity iron import systems. Our findings suggest that *Drosophila* may have a similar dual system for iron uptake. Under normal conditions, the non-divalent metal transporter Mvl facilitates the uptake of ferrous iron (Fe^{2+}) along with other metals from the gut. However, when BPS is added to the diet, it chelates ferrous iron (the degree of chelation is a function of BPS concentration), reducing its availability for Mvl-mediated transport. I have shown that *Mco4* is strongly upregulated in the gut in response to iron depletion, suggesting it facilitates iron import as part of a secondary, high-affinity iron import mechanism. The gradual decrease in survival of *Mco4*^{-/-} flies on moderately iron-depleted media supports the role of *Mco4* in dietary iron absorption in the gut. This suggests that Mco4 is a critical backup system when the primary ferrous iron uptake via Mvl is insufficient. Additionally, Mco4 likely plays a role in peripheral tissues, such as the PG, which also exhibit iron-related phenotypes under these conditions.

4.3.2 Upregulation of Mco4 as a compensatory mechanism to import iron into the PG

My qPCR results from Chapter 4 demonstrated that *Mco4* is significantly upregulated in the carcass when flies are fed BPS-supplemented food. The prothoracic gland (PG), a tissue with a high demand for iron, appears is – at least in part – responsible for this upregulation. When iron availability is compromised—either through dietary deprivation or genetic disruption—the PG

likely sends signals to activate *Mco4* expression in order to enhance iron uptake and meet its metabolic needs. This indicates that *Mco4* acts outside the gut, suggesting it acts as a backup iron uptake system for peripheral tissues as well. If *Mco4* functions in the same manner as in the gut, then this would suggest that the hemolymph harbours circulating iron in the form of “non-transferrin bound iron” (NTBI). While NTBI is well established in human blood, there are no studies that examined its existence in flies.

4.3.3 Examine *Mco4* and *Mvl* double knockout mutant phenotypes

Single knockout studies reveal that *Mvl* knockout (*Mvl*^{-/-}) flies are viable, which is consistent with the idea that *Mco4* acts as a backup ferric iron importer[92]. Similarly, *Mco4* knockout (*Mco4*^{-/-}) flies are viable on standard Nutri-Fly food because *Mvl* is sufficient to facilitate ferrous iron uptake. To further elucidate the interplay between these two iron import systems, future research should focus on creating and analyzing *Mco4* and *Mvl* double knockout mutants. The hypothesis is that without both *Mvl* and *Mco4*, flies would lose all ways to import ferrous and ferric iron from the diet, leading to more severe phenotypes. It is possible that heme may act as a source for iron, and one could test whether supplementation with hemin (commercially available heme bound to ferric iron) rescues these double mutants.

CHAPTER 5 Characterization of Mco4 function

5.1 Introduction

5.1.1 Mco4 is a potential ferroxidase and may require a partner to function

The MCOs are a diverse family of enzymes include ferroxidases, which is crucial for a ferric iron import system. For example, Mco1, while exhibiting some ferroxidase activity, functions as a potent ascorbate oxidase[60]. Conversely, Mco3 is known for its significant ferroxidase activity. Additionally, all three human multicopper oxidases, ceruloplasmin, hephaestin, and zyklopen, possess ferroxidase activity.

One well-studied member of this family is Fet3, the yeast ortholog of Mco4 and is known for its ferroxidase activity. Fet3 requires a partner protein, Ftr1, which possesses six transmembrane domains and is responsible for transporting oxidized ferric iron across the membrane[70][71]. The high degree of conservation between the sequences of *Mco4* in *Drosophila* and Fet3 in yeast suggests that Mco4 might share similar functional properties, including the necessity for a partner protein to facilitate iron transport.

Therefore, it is crucial to investigate whether Mco4 exhibits ferroxidase activity. To address this question, I conducted a series of experiments using *Drosophila* S2 cells transfected with Mco4. As a control, human hephaestin, a known Mco ferroxidase, was also transfected into S2 cells. Fresh cell lysates from these transfected cells were then subjected to a ferroxidase activity assay to determine the presence and extent of ferroxidase activity in Mco4. In addition to assessing ferroxidase activity, it is important to identify potential interacting partners of Mco4, since it is plausible that Mco4 may require a partner protein to function effectively, similar to the Fet3-Ftr1 system in yeast.

5.1.2 The effect of *Mco4* overexpression on iron homeostasis

While overexpression is generally not the ideal approach to study a protein's function due to the potential for non-physiological effects and artifacts, it can still provide valuable insights under certain conditions. Overexpression can sometimes lead to observable phenotypic changes that offer clues about the protein's role. In the case of *Mco4*, I suspect that it requires a partner protein to import iron. If this is true, overexpressing *Mco4* alone may not fully reveal its function

if the necessary interactor is not or present in sufficient quantities. Ubiquitous overexpression of a transgene can also lead to unintended effects, as the protein may be expressed in tissues where it is not normally present, potentially altering its function.

Despite these limitations, I overexpressed *Mco4* (*Actin>Mco4-3xMyc*) to examine whether this would result in any detectable phenotypic changes that could provide insights into its function. Specifically, I investigated whether larvae overexpressing *Mco4* had higher iron levels than controls, which I measured with a ferrozine-based iron content assay. Additionally, Dr. Sattar Soltani from my lab tested the resistance of these larvae to low iron food conditions to see if overexpression of *Mco4* conferred any advantage in highly iron-depleted environments with BPS food. To further complete his results, I did a supplementary test on the toxicity of high BPS food. I supplemented the food used in this study with different concentrations of FAC, testing if any enough iron supplement would rescue the lethality from high BPS.

5.2 Results

5.2.1 *Mco4* has ferroxidase activity

S2 cells were transfected with vectors expressing either *Mco4* or HEPH under the control of the Ac5 promoter. An EGFP-containing vector was used as a control. HEPH, a known human ferroxidase, served as a positive control to validate the experimental setup (Figure 5.1 A). Post-transfection, cell lysates were prepared and subjected to Western blot analysis to confirm the expression of *Mco4* and HEPH. The WB results demonstrated successful expression of both *Mco4* and HEPH in the transfected S2 cells, as evidenced by the presence of distinct bands corresponding to the expected molecular weights of these proteins (Figure 5.1 B).

New fresh lysates were collected to evaluate their ferroxidase activity using a human ceruloplasmin activity kit. The assay results revealed that HEPH exhibited a ferroxidase activity of approximately 60 mU/g, while *Mco4* showed a similar activity level of around 55 mU/g. Both *Mco4* and HEPH activities were significantly higher than those of the EGFP control vector or the buffer, with statistical significance ($P < 0.00001$) (Figure 5.1 C). These findings indicate that *Mco4* possesses substantial ferroxidase activity, comparable to that of human hephaestin.

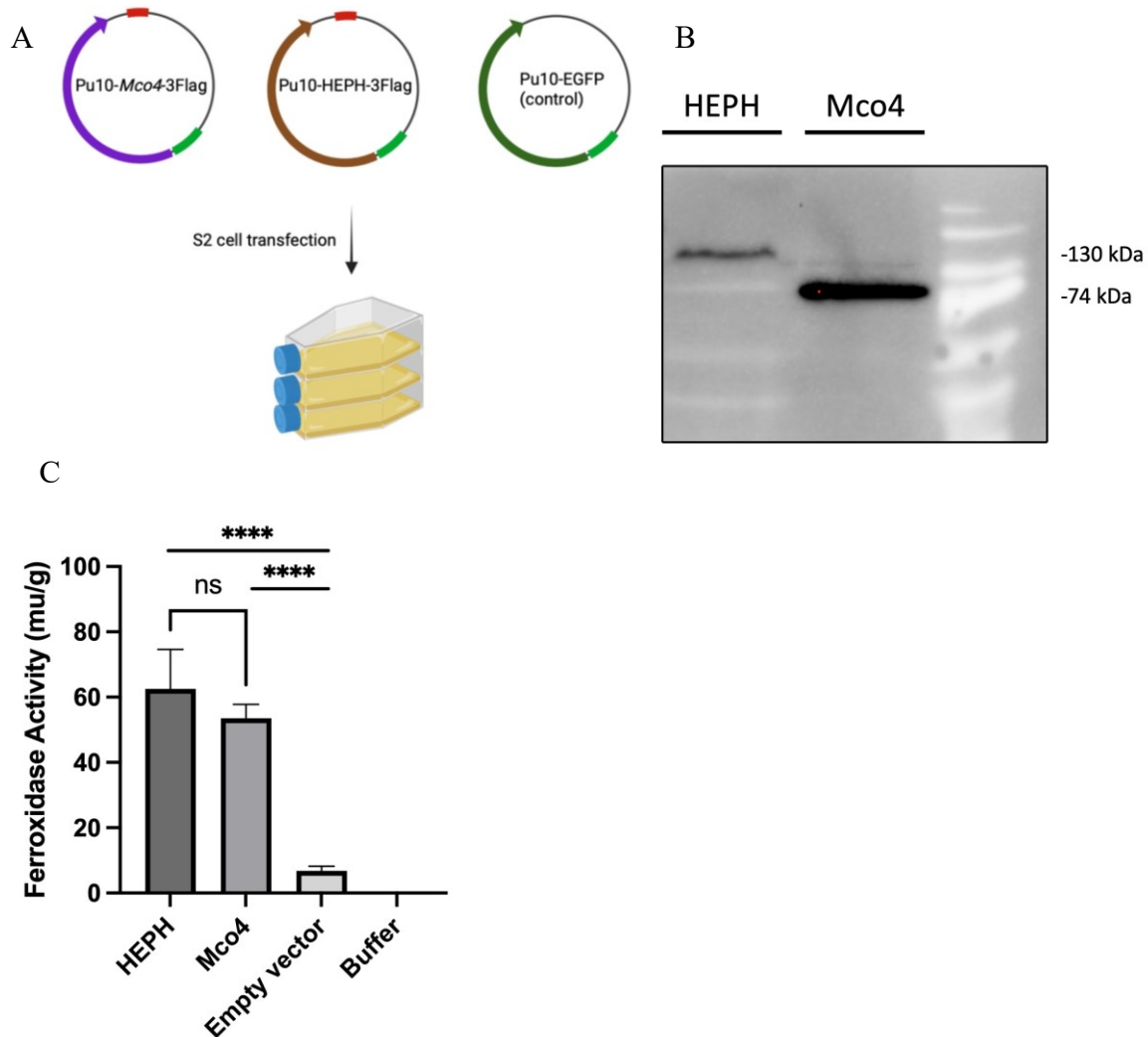


Figure 5.1 Ferroxidase activity assay of Mco4 and HEPH.

(A) S2 cells transfected with *Mco4*, HEPH, or empty vectors. *Mco4* and HEPH were expressed under the Act5C promoter with a 3xFlag tag at the C-terminus. (B) To confirm expression following transfection, S2 lysates post transfection were tested using Western blot analysis. *Mco4* with the tag is estimated to be 74 kDa, and HEPH with the tag is around 133 kDa. (C) Ferroxidase assay using S2 cell lysates. Lysates were removed of chloride and mixed with Oxidizer from Ceruloplasmin Assay Kit. OD was monitored for the duration (15 min) of the reaction. Slope = OD/mmol of oxidized substrate. Ferroxidase activity = $S_k/S_s/V * 2$ (mU/mL). S_k = kinetic slope of the sample in the first 15 mins of the curve. S_s = slope of the standard

curve. 2 = Dilution factor. n=3, means and SD are shown. Differences in areas were assessed by performing unpaired t-test. ns = no significance; ****p<0.0001.

5.2.2 *Mco4* overexpression increased iron content

To investigate whether the overexpression of *Mco4* could enhance iron import in larvae, my lab conducted a series of overexpression experiments. Specifically, I assessed the total iron content in whole larvae upon *Mco4* overexpression. Here I utilized a ferrozine-based iron content assay to quantitatively measure the iron levels. Ubiquitous expression of *Mco4* was achieved using the *actin>UAS-Mco4* transgenic line, while the control group was represented by the *actin>w¹¹¹⁸* samples. Additionally, the lysis buffer used was included in all assays as the negative control. The results indicated that the overexpression of *Mco4* led to a moderate increase in total iron content in the larvae (n=3, p<0.05) (Figure 5.2).

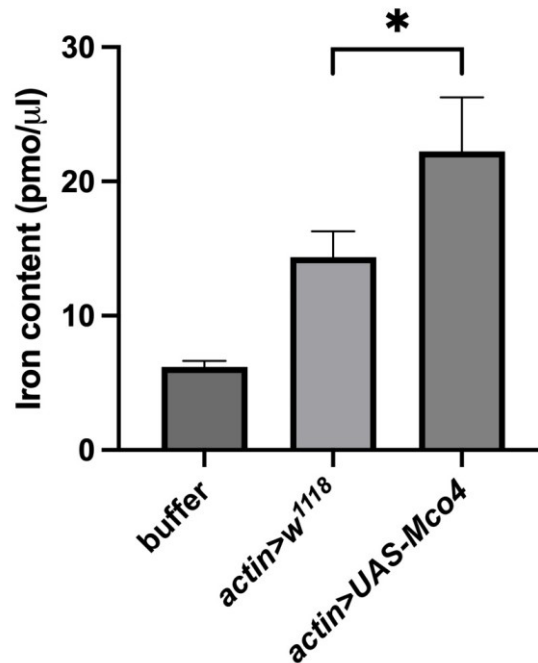


Figure 5.2 *Mco4* whole body overexpression increased iron content in larvae.

Iron content assayed by Ferrozine. 20 *actin>UAS-Mco4* or control larvae were lysed with 1% NP-40 buffer. Iron content was calculated based on the iron-Ferrozine complex of 27,900 M⁻¹

cm-1. [Fe] (pmol/ μ L) = [(OD562 x 94/77 x 130/50)/27900] x 10^6 . Differences were assessed by unpaired Student's t-test. Means and SD are shown. * $p < 0.05$, $n = 3$.

5.2.3 *Mco4* overexpression increased resistance to iron deficiency

In previous experiments, Dr. Soltani established that it took five generations for w^{1118} flies to exhibit a 50% decrease in survival when exposed to 160 μ M BPS. Dr. Soltani later extended this work by exposing w^{1118} flies to a significantly higher concentration of 500 μ M BPS, which resulted in 100% lethality, preventing the flies from reaching the pupation stage.

In contrast, when *Mco4* was overexpressed in the whole body (using the *tub>UAS-Mco4* construct) and these flies were exposed to the same high concentration of BPS, approximately 50% of the flies managed to pupate and survive. This finding suggests that overexpressing *Mco4* in a high BPS environment can mitigate the lethal effects observed in w^{1118} flies. This is a remarkable result, as it shows that extra copies of *Mco4* enzymes allow survival on extreme iron depleted media, which I interpret as strong support for the idea that *Mco4* is part of a high-affinity iron uptake system.

Historically, our lab has avoided using such high concentrations of BPS due to concerns about non-specific effects on the flies. To assess the toxicity and specificity of BPS, I performed control experiments by raising w^{1118} flies on high BPS food supplemented with ferrous ammonium citrate (FAC), a ferrous iron supplement. The rationale behind this approach was that if high BPS concentrations kill the flies primarily through iron deprivation, then supplementing the food with FAC should rescue the flies[96]. Conversely, if iron supplementation cannot rescue BPS treatment, it will indicate that BPS exerts its lethal effects via an iron-independent mechanism[97]. BPS functions by forming a complex with iron, where three BPS molecules bind to one ferrous iron[98][99]. Therefore, theoretically, one molecule of FAC should counter the effects of three molecules of BPS. I tested this hypothesis by adding varying concentrations of FAC to the BPS-containing food and examining the overall survival of w^{1118} flies. When 500 μ M FAC was added to 500 μ M BPS food, w^{1118} survival was bounced back to around 80%, clearly demonstrating that BPS causes lethality via iron depletion and not non-specific effects.

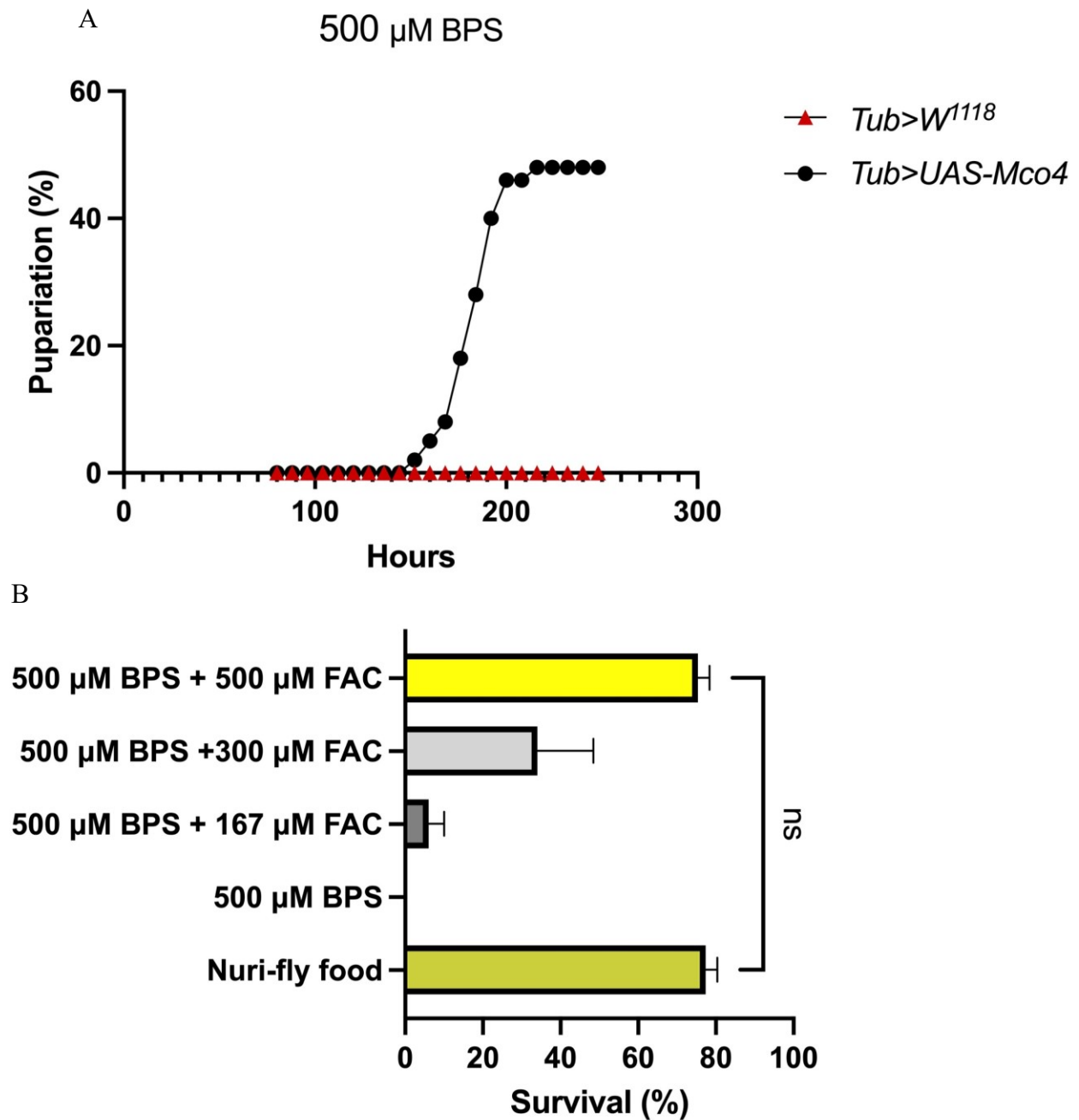


Figure 5.3 *Mco4* overexpression increased resistance to iron deficiency.

(A) The effect of high concentration of BPS on flies' survival. 50 embryos were collected for each replicate. Three replicates were conducted for each genotype. *tub>w¹¹¹⁸* or *tub>UAS-Mco4* were raised on 500 μ M BPS food, and the number of pupariation was counted. *tub>UAS-Mco4*

had a survival of 50%. (B) The effect of FAC on w^{1118} survival under 500 μ M BPS food. 50 embryos were collected for each replicate and raised on different combinations of BPS and FAC concentrations. Supplementing 500 μ M can rescue w^{1118} survival back to around 80%. $n=3$. Means and SD are shown. Differences were assessed using unpaired t-test. ns = no significance.

5.2.4 TurboID as a tool to investigate protein-to-protein interactions

To identify protein interactions involving Mco4, I used the TurboID-based proximity labeling technique. TurboID is a method that offers several advantages over traditional crosslinking coupled with co-immunoprecipitation (co-IP)[93]. TurboID works by fusing a bacterial biotin ligase enzyme (typically biotin ligase encoded by *BirA* from *Escherichia coli*), to the protein of interest—in this case, Mco4. When expressed in cells, the TurboID enzyme catalyzes the biotinylation of proteins (predominantly lysine residues) that come into close proximity to Mco4. This biotinylation occurs in live cells and under physiological conditions, allowing for the capture of transient and weak interactions that might be missed by co-IP[93].

Once biotinylated, the interacting proteins can be isolated using streptavidin beads, which have a high affinity for biotin. This selective isolation ensures that even low-abundance interactors can be effectively captured and enriched[94]. The enriched proteins are then analyzed using mass spectrometry to identify the biotinylated interaction partners of Mco4 (Figure 5.1).

The advantage of TurboID over traditional co-IP lies in its ability to capture interactions in their native cellular context without the need for cell lysis and harsh washing conditions, which can disrupt fragile protein-protein interactions[95]. Additionally, TurboID can label proteins within a defined spatial proximity to Mco4, providing a more comprehensive and accurate interaction network. This technique is particularly useful for studying proteins with dynamic interactions and for identifying novel interactors that may play critical roles in Mco4's function and regulation.

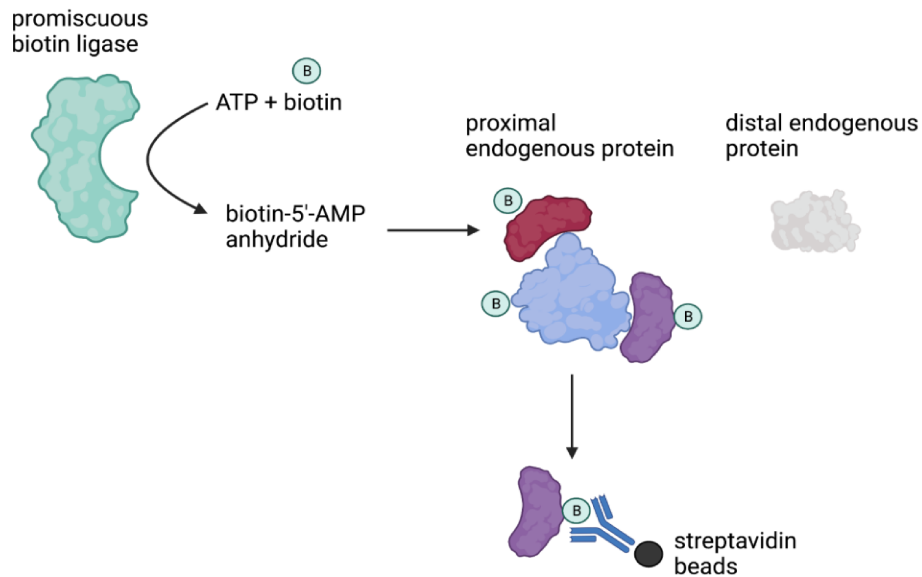


Figure 5.4 The TurboID technique.

TurboID works by fusing a biotin ligase enzyme to the protein of interest. The TurboID enzyme catalyzes the biotinylation of nearby proteins that are physically close to the target proteins. The biotinylated proteins can be captured and pulled down by streptavidin beads, which can then be analyzed by mass spectroscopy.

5.2.5 Construction and validation of TurboID-*Mco4* lines

To investigate the interactors of *Mco4* using the TurboID technique, I constructed a *UAS-Mco4-V5-TurboID* line, where the V5 tag is positioned between the biotin ligase and the *Mco4* cDNA (Figure 5.5 A). As a control, I used a line expressing only TurboID and V5 under the UAS promoter, which was already available in the lab. The TurboID line and the control line were maintained as homozygous stocks. For this experiment, they were crossed with *Actin-Gal4* for ubiquitous overexpression on either Nutri-Fly food or 200 μ M BPS food.

For the Nutri-Fly food group, the larvae were allowed to grow to the early L3 stage. At this point, half of the larvae were transferred to food supplemented with 100 μ M biotin for an additional 24 hours. This step was taken because the extent of protein biotinylation with the larvae's endogenous biotin was uncertain, and adding biotin to the food was expected to enhance biotinylation. However, we subsequently found that excessive biotin negatively impacted the survival of larvae with transgenic expression of biotin ligase. For the BPS food group, the flies exhibited mild underdevelopment due to iron deprivation and were severely affected by additional biotin supplementation, to the extent that I could not collect any larvae. Therefore, for the BPS group, I decided not to add additional biotin to the food.

To verify the expression of fusion proteins and the activity of the TurboID ligase, Western blotting was performed using anti-V5 antibody and streptavidin-HRP, respectively. Even with endogenous biotin alone, a significant number of protein bands were detected. The addition of biotin to the food resulted in the detection of more protein bands. The *TurboID-V5-Mco4* fusion protein is estimated to be around 111 kDa, while TurboID-V5 alone is around 39 kDa. For the BPS group, fewer bands were observed due to the absence of additional biotin, but the fusion protein bands were still detectable (Figure 5.5 B).

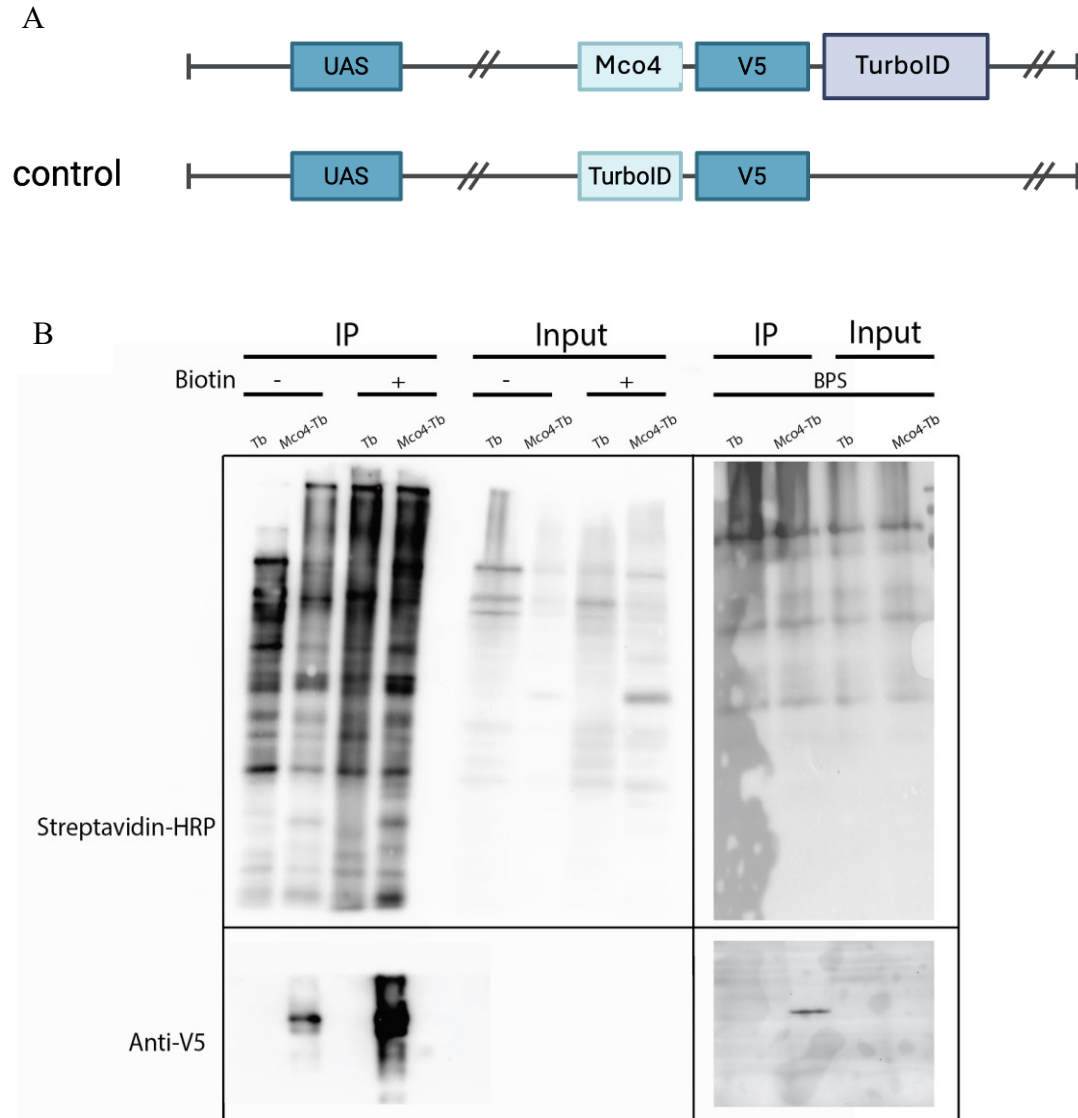


Figure 5.5 Construction and verification of *UAS-Mco4-V5-TurboID*.

(A) The TurboID constructs. The V5 tag and biotin ligase were placed at the C-terminus of Mco4 under the control of the *UAS-Gal4* system. The control is the biotin ligase with V5 tag alone. (B) *UAS-Mco4-V5-TurboID* and *UAS-TurboID-V5* were crossed with *actin-Gal4*. Western blot analysis of TurboID lines crossed and raised on Nutri-fly or 200 μ M BPS food. For the Nutri-fly group, half of the samples were transferred to biotin-containing food (100 μ M biotin) for 24 hours before the lysates were collected. The input and elution (IP) were incubated with either the streptavidin-HRP beads or the anti-V5 antibody. The incubated protein samples were

collected for protein detection. The *Mco4*-V5-TurboID fusion protein is estimated to be around 111 kDa, while TurboID-V5 alone is around 39 kDa. Tb: TurboID.

5.2.6 *Mco4* interacts with iron-related proteins

All candidate proteins pulled down by streptavidin beads were subjected to MALDI-TOF mass spectrometry analysis. For each experimental condition, three biological replicates were analyzed, providing three distinct interaction profiles. A candidate protein was considered a positive interactor if it appeared in at least two out of the three replicates. If a protein was detected in only one replicate, it was considered a false positive and excluded from further analysis. This filtering process allowed us to construct final interaction maps for each genotype under each condition.

In the Nutri-Fly food group, 157 proteins were identified in the TurboID samples, and 125 proteins were identified in the controls (TurboID without *Mco4*). Of these, 85 proteins were found in both the TurboID samples and the controls, indicating that these proteins are likely not specific to *Mco4* but rather to the biotin ligase itself. By subtracting these 85 non-specific interactors from the 157 total candidates, I identified 72 proteins that specifically interacted with *Mco4* when larvae were reared on Nutri-Fly medium. A similar filtering process was applied to the BPS-fed cohort. In total, 145 proteins were identified in the TurboID samples, and 136 proteins were identified in the controls. There were 65 overlapping proteins, representing non-specific interactors. By subtracting these 65 non-specific interactors from the 145 total candidates, I identified 80 proteins that specifically interact with *Mco4* under the BPS food condition.

Comparing the interaction lists from both conditions, I found 16 proteins that overlapped between the Nutri-Fly and BPS food groups ($p < 0.00001$). These 16 proteins are likely highly enriched for true interactors of *Mco4* and represent the most significant focus of our analysis. Subtracting these 16 overlapping proteins, I identified 56 proteins that interact with *Mco4* primarily under the Nutri-Fly food condition and 64 proteins that interact with *Mco4* only when BPS is present (Figure 5.6).

Among the 16 proteins identified as interactors of Mco4 under both Nutri-Fly and BPS food conditions (Table 5.1), both the Ferritin heavy chain (*Fer1HCH*) and the Ferritin light chain (*Fer2LCH*) were present. Moreover, the *Fer2HCH* interaction was found in all the TurboID replicates, whereas the *Fer2LCH* was in 2 out of the 3 replicates. These chains form the 24-subunit fly ferritin complex. The Ferritin heavy chain (*Fer1HCH*) is predicted to possess ferroxidase activity, which is crucial for the conversion of ferrous iron (Fe^{2+}) to ferric iron (Fe^{3+})[100]. The Ferritin light chain (*Fer2LCH*), on the other hand, plays a role in stabilizing the iron core within the ferritin complex[102]. The presence of both chains in the interactor list strongly supports Mco4's role in iron homeostasis.

Other candidates included CG1371, which is expressed in the endomembrane system in head, heart and midgut. Its human orthologs are NOMO1, NOMO2 and NOMO3, which are involved in carbohydrate binding or aiding the insertion of membrane protein[103].

Grp170 is another interactor, it is involved in cellular response to hypoxia and located in extracellular space[104]. Hypoxia is actually closely linked to iron metabolism due to iron's role in hemoglobin for oxygen transport and its involvement in mitochondrial function. As such, iron deprivation and hypoxia have similar outcomes (no iron => no oxygen transport). While the link between hypoxia and iron is firmly established in vertebrates, it has not been formally demonstrated in *Drosophila*. In any case, under hypoxic conditions, hypoxia-inducible factors (HIFs) are activated, regulating genes involved in iron uptake, storage, and red blood cell production[107][105]. Additionally, iron regulatory proteins adjust iron homeostasis to meet increased oxygen demands[106]. Proper iron regulation is also crucial for minimizing oxidative stress, as unregulated iron can catalyze the formation of reactive oxygen species (ROS)[107]. From this list there was another protein, Prx2, found in relation to protection against oxidative. Prx2 is a thiol-specific peroxidase that catalyzes the reduction of hydrogen peroxide and organic hydroperoxides to water and alcohols, and it detoxifies superoxides and acts as a sensor of hydrogen peroxide-mediated signaling events[108].

The next notable candidate is CG13321, which is expressed in the PV and the entirety of the midgut. This is similar to the expression pattern of *Mco4*. Its function and localization are unknown, making this gene a top candidate for future analysis.

Other interesting proteins found in the list are CG8036, which is expressed in the brain and midgut, functioning in thiamine pyrophosphate binding activity[111], CG5474, which is a signal sequence receptor found in the endomembrane, as well as ERp44, which is predicted to enable protein disulfide isomerase activity and also locates in the endomembrane system[112].

From the list of 16 candidate proteins, none stood out as a clear or obvious transmembrane transporter. Given that *Mco4*'s role as an iron importer is primarily significant under iron-deprived conditions, I shifted my focus to the 64 proteins that specifically interact with *Mco4* in the presence of BPS.

The 64 interacting proteins identified in this study span a diverse range of functional categories, including ribosomal proteins, metabolic enzymes, structural proteins, and signaling molecules (Table 5.2). Gene ontology analysis reveals that these proteins are predominantly involved in the structural constituent of the ribosome (14 proteins), oxidoreductase activity (7 proteins), and RNA binding (9 proteins), among other functions. A significant number of ribosomal proteins were identified, including RpS7, RpS8, RpL7A, RpL11, and RpS15Aa. These proteins are essential components of the ribosome, playing crucial roles in protein synthesis. Such interactions may suggest a potential role in regulating translation, possibly in response to iron availability.

Around 10 metabolic enzymes also interact with *Mco4*. For example, Glutamate Dehydrogenase (*Gdh*) is involved in the oxidative deamination of glutamate to alpha-ketoglutarate and ammonia[113]. *Gdh* plays a critical role in amino acid catabolism and the tricarboxylic acid (TCA) cycle, linking it to cellular energy production[114]. Isocitrate Dehydrogenase 3b (*Idh3b*) is a key enzyme in the TCA cycle, important for energy production and metabolic regulation[115]. Phosphogluconate Dehydrogenase (*Pgd*) participates in the pentose phosphate pathway, crucial for generating NADPH and ribose-5-phosphate[116]. Glycogen Phosphorylase (*GlyP*) catalyzes the breakdown of glycogen to glucose-1-phosphate, vital for maintaining blood sugar levels and energy supply[116].

Proteins involved in stress response and antioxidant defense were also identified. Thioredoxin Peroxidase 2 (*Jafrac2*) is an antioxidant enzyme that reduces hydrogen peroxide, protecting cells from oxidative damage and maintaining redox balance[118]. Glycoprotein 93

(Gp93) is involved in protein folding and stress responses within the endoplasmic reticulum[119]. Given Mco4's potentially different roles in the PV vs. the gut, it is unclear whether any of these interactors are a required transmembrane transporter that works with Mco4. Judging from this list alone, *Mco4* appears to be integral in coordinating cellular responses to iron availability and managing iron-induced oxidative stress

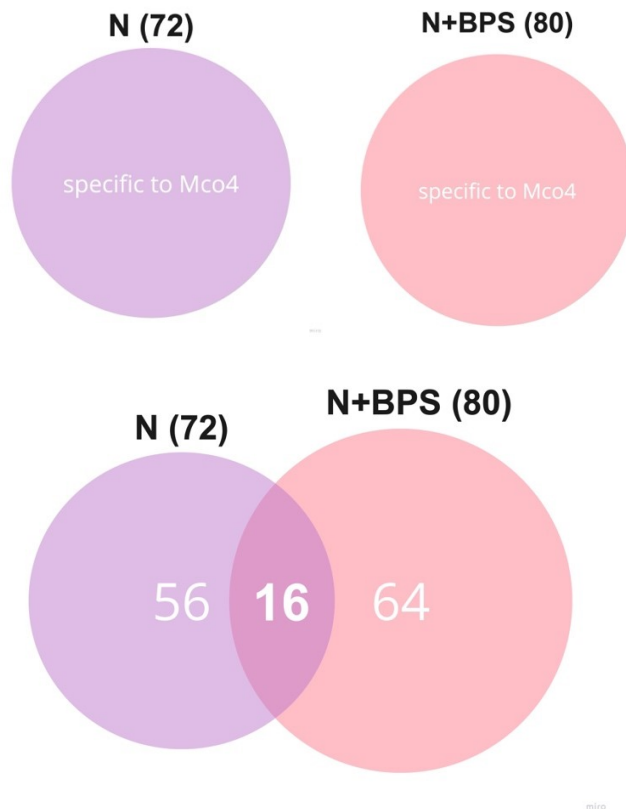


Figure 5.6 Overlaps of Mco4 interacting proteins.

All candidate proteins pulled down by streptavidin beads underwent mass spectrometry analysis across three biological replicates for each experimental condition. A protein was deemed a positive interactor if it appeared in at least two of the three replicates; otherwise, it was excluded as a false positive. In the N group, 157 proteins were identified in the TurboID samples, with 125 proteins in the controls. Among these, 85 proteins were common to both, indicating non-specific interaction with the biotin ligase. Subtracting these 85 proteins, I identified 72 specific interactors with Mco4 in the N condition. Similarly, in the N+BPS condition, 145 proteins were

identified in the TurboID samples and 136 in the controls, with 65 overlapping proteins. After removing these non-specific interactors, 80 specific Mco4 interactors were identified in N+BPS. Comparing both conditions, 16 proteins overlapped between Nutri-Fly and BPS food groups ($p < 0.00001$), representing likely true interactors of Mco4. Excluding these 16 proteins, I identified 56 proteins interacting with Mco4 primarily in the Nutri-Fly condition and 64 proteins interacting specifically in the N+BPS group. N: Nutri fly food; N+BPS: BPS food.

Table 5.1 16 interacting candidates of Mco4 on both Nutri-fly food and BPS food

Protein Name	Key Role	Does the abundance score increase with BPS added?
CG1371	carbohydrate binding or aiding the insertion of membrane protein	yes
Fer1HCH	ferritin heavy chain, crucial for the conversion of ferrous iron to ferric iron	no
Grp170	cellular response to hypoxia and located in extracellular space	yes
Lsp2	a store of amino acids for synthesis of adult proteins	unknown
Vha68-2	a component of the V1 subunit of the vacuolar ATPase	yes
CG13321	is expressed in the PV and all of the midgut, function unknown	yes
CG8036	thiamine pyrophosphate binding activity,	unknown
Prx2	thiol-specific peroxidase that catalyzes the reduction of hydrogen peroxide and organic hydroperoxides to water and alcohols	yes
Mccc2	Predicted to be involved in fatty acid metabolic process.	no
Fer2LCH	stabilizing the iron core within the ferritin complex	yes
Cyp12a4	carboxyltransferase subunit of the 3-methylcrotonyl-CoA carboxylase,	unknown
Got2	encodes an L- aspartate:2-oxoglutarate aminotransferase involved in glutamate biosynthesis	unknown
SsRbeta	signal sequence receptor found in the endomembrane	no
Mco4	(the target protein)	no
Had1	involved in fatty acid metabolic process.	no

ERp44	enable protein disulfide isomerase activity and also locates in the endomembrane system	yes
--------------	---	-----

Table 5.2 64 interacting candidates of Mco4 identified only on BPS food

Protein Name	Key Involvement
ScsbetaA	tricarboxylic acid cycle
Gp210	nuclear pore organization
CG42336	function unknown
lectin-22C	calcium-dependent cell-cell adhesion via plasma membrane cell adhesion molecules
CG45076	function unknown
mfas	sexual reproduction
Fbp1	Function unknown
Pgd	pentose-phosphate shunt, oxidative branch
Rack1	positive regulation of protein phosphorylation
RpL10	translation
Ccp84Ag	chitin-based cuticle development
alphaTub84B	microtubule-based process
alphaTub84D	spermatogenesis
Lcp3	larval chitin-based cuticle development
Sgs5	pupal adhesion
Col4a1	oviduct morphogenesis
Act87E	DNA repair-dependent chromatin remodeling
Lsp1beta	a store of amino acids for synthesis of adult proteins.
RpS2	highly conserved component of the 40S ribosome
RpL13	cytoplasmic translation
eIF2alpha	translational initiation
RpL11	cytoplasmic translation

RpL7A	cytoplasmic translation
RpS15Aa	cytoplasmic translation
Gdh	NADH oxidation
RpS3A	cytoplasmic translation
eIF4A	translational initiation
RpS3	positive regulation of apoptotic signaling pathway
RpS11	translation
eIF2gamma	formation of translation preinitiation complex
betaTub56D	microtubule cytoskeleton organization
ACC	response to sucrose
D2hgdh	organic acid metabolic process
sea	mitochondrial citrate transmembrane transport
CG17896	valine metabolic process
fon	hemolymph coagulation
RpS8	larval lymph gland hemopoiesis
CG44250	function unknown
Reg-2	function unknown
Ldh	lactate metabolic process
RpL8	cytoplasmic translation
VhaSFD	dsRNA transport
Prx4	response to oxidative stress
Mccc1	conversion of 3-methylcrotonyl-CoA to 3-methylglutaconyl-CoA
RpS7	ribosomal small subunit biogenesis
Gp93	heat shock protein Hsp90 family member that is involved in midgut development.
RpL27	A structural constituent of ribosome.
Sil1	SRP-dependent co-translational protein targeting to membrane
Idh3b	salivary gland cell autophagic cell death
CG4830	enable long-chain fatty acid-CoA ligase activity
Ak3	nucleobase-containing compound metabolic process

CG8507	regulation of receptor-mediated endocytosis
Tig	cell-substrate adhesion
Acsf2	fatty acid metabolic process
vkg	somatic muscle development
Creld	mitochondrion organization
Mfe2	fatty acid beta-oxidation using acyl-CoA oxidase
Tudor-SN	mRNA catabolic process
Mtpbeta	fatty acid beta-oxidation
RpL5	ribosomal large subunit assembly
Glyp	regulation of glycogen catabolic process
Tps1	trehalose biosynthetic process
CG5254	mitochondrial alpha-ketoglutarate transmembrane transport
trol	regulation of neuroblast proliferation
sesB	cellular response to oxidative stress

5.2 Discussion and future directions

5.2.1 Mco4 interaction necessity and independence

The necessity of a partner protein for Mco4 function has been a topic of significant interest, primarily due to its yeast counterpart, Fet3, which requires the transmembrane partner Ftr1 to transport ferrous iron into cells. Given the structural and functional similarities between Fet3 and Mco4, I initially hypothesized that Mco4 might also need a partner similar to Ftr1. However, the results from the overexpression tests suggest a more complex scenario. The overexpression tests showed that increasing Mco4 levels alone led to a rise in iron content within the larvae. One possibility is that Mco4 can function independently without a specific partner protein to facilitate iron transport. This would imply that Mco4 alone is sufficient to enhance iron uptake or storage. Another hypothesis is that if Mco4 does require a partner, this partner might be naturally more abundant than Mco4. Consequently, even under normal conditions, the partner may not be a limiting factor for iron transport, in which case the overexpression of Mco4 alone suffices to increase iron content. The TurboID results did not reveal any obvious candidate proteins that might function in a similar fashion to Ftr1. This suggests that if Mco4 does require an interaction partner, I need additional tests to identify such a protein. Together these findings highlight that Mco4's function might be more versatile and less dependent on a single interaction partner than previously assumed.

5.2.2 The possible regulatory role between Mco4 and ferritin

Given that Fer1HCH has ferroxidase activity, the interaction with Mco4 may be essential for the proper functioning of this enzyme. Mco4 might modulate or complement the ferroxidase activity of Fer1HCH, thus influencing the conversion of Fe^{2+} to Fe^{3+} and the subsequent storage of iron in its ferric form within the ferritin complex. Mco4 may act as a regulatory protein, ensuring that ferritin's iron storage capacity is synchronized with cellular iron levels. This regulation could involve Mco4 modulating the expression or activity of ferritin subunits. The physical interaction between Mco4 and ferritin subunits might facilitate the assembly or disassembly of the ferritin complex, thus playing a direct role in iron sequestration and release.

5.2.3 Tissue-specific interactions of Mco4

The expression patterns of *Mco4* under BPS conditions showed that it is primarily expressed in the PV and only lowly expressed in the gut. This differential expression suggests that *Mco4* may serve distinct functions in different tissues. Moreover, the above TurboID studies only used whole-body samples, where non-specific targets can interfere the real interaction signal, and low-expressed proteins may not be detectable. A more focused approach is required. Future studies should aim to perform TurboID analysis on specific tissues separately, such as the gut and the proventriculus.

5.3 Conclusion and outlook

In this study, I have shown that *Mco4* potentially functions as a high affinity iron importer in *Drosophila*. Under normal dietary iron level, the gene is primarily expressed in the PV. When iron is scarce, *Mco4* is upregulated in the rest of the gut, oxidizing ferrous iron to ferric iron on the gut membrane. Whether this process requires another transmembrane partner remains further study. *Mco4* null mutants have less iron content in their body and cannot survive on a mild BPS food. *Mco4* overexpression leads to increased iron content and can rescue lethality caused by dietary iron depletion. The possible high-affinity iron import system involving *Mco4* is significant as it represents the first such system described in animals.

References:

- [1] Andrews, N. C., & Schmidt, P. J. (2020). *Iron homeostasis*. Annual Review of Physiology, 69, 69-85. doi:10.1146/annurev.physiol.69.031905.164337
- [2] Ganz, T. (2019). *Systemic iron homeostasis*. Physiological Reviews, 93(4), 1721-1741. doi:10.1152/physrev.00008.2013
- [3] Rouault, T. A. (2015). *Iron-sulfur clusters: novel biochemical targets of iron regulatory proteins*. Biochimica et Biophysica Acta (BBA) - Molecular Cell Research, 1823(9), 1451-1458. doi:10.1016/j.bbamcr.2012.05.007
- [4] Torti, F. M., & Torti, S. V. (2013). *Iron and oxidative stress: new avenues for bioenergetic intervention*. Current Opinion in Pharmacology, 13(3), 329-333. doi:10.1016/j.coph.2013.03.009
- [5] Ward, R. J., Zucca, F. A., Duyn, J. H., Crichton, R. R., & Zecca, L. (2014). *The role of iron in brain ageing and neurodegenerative disorders*. The Lancet Neurology, 13(10), 1045-1060. doi:10.1016/S1474-4422(14)70117-6
- [6] McLean, E., Cogswell, M., Egli, I., Wojdyla, D., & de Benoist, B. (2009). *Worldwide prevalence of anemia, WHO Vitamin and Mineral Nutrition Information System, 1993-2005*. Public Health Nutrition, 12(4), 444-454. doi:10.1017/S1368980008002401
- [7] Pietrangelo, A. (2010). *Hereditary hemochromatosis: pathogenesis, diagnosis, and treatment*. Gastroenterology, 139(2), 393-408. doi:10.1053/j.gastro.2010.06.013
- [8] Ganz, T., & Nemeth, E. (2015). *Iron homeostasis in host defence and inflammation*. Nature Reviews Immunology, 15(8), 500-510. doi:10.1038/nri3863
- [9] Calap-Quintana, P., Gonzalez-Fernandez, J., Sebastiá-Ortega, N., Llorens, J. V., & Moltó, M. D. (2017). *Drosophila melanogaster models of metal-related human diseases and metal toxicity*. International Journal of Molecular Sciences, 18(7), 1456. doi:10.3390/ijms18071456
- [10] Llorens, J. V., Alvarez, L., Soriano, S., Roselló, S., Calap-Quintana, P., & Moltó, M. D. (2005). *The role of iron in the pathogenesis of Friedreich's ataxia: insights from studies in human tissues and Drosophila*. Frontiers in Neuroscience, 9, 265. doi:10.3389/fnins.2015.00265
- [11] Mandilaras, K., & Missirlis, F. (2012). *Genes for iron metabolism influence circadian rhythms in Drosophila melanogaster*. Metallomics, 4(8), 928-936. doi:10.1039/c2mt20094c
- [12] Yamanaka, N., Rewitz, K. F., & O'Connor, M. B. (2013). *Ecdysone control of developmental transitions: lessons from Drosophila research*. Annual Review of Entomology, 58, 497-516. doi:10.1146/annurev-ento-120811-153608
- [13] Ghosh, S., Singh, A., Mandal, S., & Mandal, L. (2015). *Active hematopoietic hubs in Drosophila adults generate hemocytes and contribute to immune response*. Developmental Cell, 33(4), 478-488. doi:10.1016/j.devcel.2015.04.014
- [14] Krishnan, N., Davis, A. J., & Giedroc, D. P. (2009). *Regulation of heme biosynthesis in bacteria: heme and heme-containing sensor proteins*. Chemical Reviews, 109(10), 4644-4681. doi:10.1021/cr900166p

- [15] Ponka, P. (1999). *Cell biology of heme*. American Journal of the Medical Sciences, 318(4), 241-256. doi:10.1016/s0002-9629(15)40621-0
- [16] Beale, S. I., & Castelfranco, P. A. (1974). *The biosynthesis of delta-aminolevulinic acid in higher plants*. Journal of Biological Chemistry, 249(7), 2371-2378.
- [17] Jordan, P. M. (1991). *Biosynthesis of tetrapyrroles*. In H. Dailey (Ed.), *Biosynthesis of heme and chlorophylls*. McGraw-Hill.
- [18] Blanche, F., Debussche, L., Thibaut, D., & Cameron, B. (1991). *Biosynthesis of vitamin B12: structure and mechanism of action of S-adenosyl-L-methionine: uroporphyrinogen III methyltransferase*. Journal of Bacteriology, 173(14), 4572-4582. doi:10.1128/jb.173.14.4572-4582.1991
- [19] Sassa, S. (2006). *Modern diagnosis and management of the porphyrias*. British Journal of Haematology, 135(3), 281-292. doi:10.1111/j.1365-2141.2006.06289.x
- [20] Ajioka, R. S., Phillips, J. D., & Kushner, J. P. (2006). *Biosynthesis of heme in mammals*. *Biochimica et Biophysica Acta (BBA) - Molecular Cell Research*, 1763(7), 723-736. doi:10.1016/j.bbamcr.2006.05.006
- [21] Puy, H., Gouya, L., & Deybach, J. C. (2010). *Porphyrias*. The Lancet, 375(9718), 924-937. doi:10.1016/S0140-6736(09)61925-5
- [22] Elder, G. H. (1990). *Porphyria: pathophysiology, diagnosis and treatment*. *Clinics in Dermatology*, 8(4), 54-64. doi:10.1016/0738-081X(90)90055-Q
- [23] Anderson, K. E., & Bloomer, J. R. (2001). *Somatic porphyrias: acute intermittent porphyria, variegate porphyria, hereditary coproporphyria, and porphyria cutanea tarda*. In C. R. Scriver, A. L. Beaudet, W. S. Sly, & D. Valle (Eds.), *The metabolic and molecular bases of inherited disease*
- [24] Andrews, N. C. (1999). *Disorders of iron metabolism*. New England Journal of Medicine, 341(26), 1986-1995. doi:10.1056/NEJM199912233412607
- [25] Donovan, A., Brownlie, A., Zhou, Y., Shepard, J., Pratt, S. J., Moynihan, J., ... & Paw, B. H. (2005). *Positional cloning of zebrafish ferroportin1 identifies a conserved vertebrate iron exporter*. Nature, 403(6771), 776-781. doi:10.1038/35001596
- [26] Gilbert, L. I. (2004). *Halloween genes encode P450 enzymes that mediate steroid hormone biosynthesis in Drosophila melanogaster*. Molecular and Cellular Endocrinology, 215(1-2), 1-10. doi:10.1016/j.mce.2003.11.018
- [27] Gkouvatzos, K., Papanikolaou, G., & Pantopoulos, K. (2012). *Regulation of iron transport and the role of transferrin*. Biochimica et Biophysica Acta (BBA) - General Subjects, 1820(3), 188-202. doi:10.1016/j.bbagen.2011.10.013
- [28] Hentze, M. W., Muckenthaler, M. U., & Andrews, N. C. (2010). *Balancing acts: molecular control of mammalian iron metabolism*. Cell, 117(3), 285-297. doi:10.1016/j.cell.2004.04.018
- [29] Muckenthaler, M. U., Rivella, S., Hentze, M. W., & Galy, B. (2017). *A red carpet for iron metabolism*. Cell, 168(3), 344-361. doi:10.1016/j.cell.2016.12.034

- [30] Niwa, R., Matsuda, T., Yoshiyama, T., Namiki, T., Mitsuda, H., & Kataoka, H. (2004). *CYP306A1, a cytochrome P450 enzyme, is essential for ecdysteroid biosynthesis in the prothoracic glands of Bombyx and Drosophila*. *Journal of Biological Chemistry*, 279(34), 35942-35949. doi:10.1074/jbc.M404514200
- [31] Rewitz, K. F., Rybczynski, R., Warren, J. T., & Gilbert, L. I. (2006). *The Halloween genes code for cytochrome P450 enzymes mediating synthesis of the insect moulting hormone*. *Biochemical Society Transactions*, 34(6), 1256-1260. doi:10.1042/BST0341256
- [32] Sharp, P. A., & Srail, S. K. (2007). *Molecular mechanisms involved in intestinal iron absorption*. *World Journal of Gastroenterology*, 13(35), 4716-4724. doi:10.3748/wjg.v13.i35.4716
- [33] Theil, E. C. (2004). *Iron, ferritin, and nutrition*. *Annual Review of Nutrition*, 24, 327-343. doi:10.1146/annurev.nutr.24.012003.132212
- [34] Thummel, C. S. (2001). *Molecular mechanisms of developmental timing in C. elegans and Drosophila*. *Developmental Cell*, 1(4), 453-465. doi:10.1016/S1534-5807(01)00053-4
- [35] Vulpe, C. D., Kuo, Y. M., Murphy, T. L., Cowley, L., Askwith, C., Libina, N., ... & Anderson, G. J. (1999). *Hephaestin, a ceruloplasmin homologue implicated in intestinal iron transport, is defective in the sla mouse*. *Nature Genetics*, 21(2), 195-199. doi:10.1038/5979
- [36] Yamanaka, N., Rewitz, K. F., & O'Connor, M. B. (2013). *Ecdysone control of developmental transitions: lessons from Drosophila research*. *Annual Review of Entomology*, 58, 497-516. doi:10.1146/annurev-ento-120811-153608
- [37] Hentze, M. W., Muckenthaler, M. U., & Andrews, N. C. (2010). *Balancing acts: molecular control of mammalian iron metabolism*. *Cell*, 117(3), 285-297. doi:10.1016/j.cell.2004.04.018
- [38] Rouault, T. A. (2006). *The role of iron regulatory proteins in mammalian iron homeostasis and disease*. *Nature Chemical Biology*, 2(8), 406-414. doi:10.1038/nchembio807
- [39] Salahudeen, A. A., Thompson, J. W., Ruiz, J. C., Ma, H. W., Kinch, L. N., Li, Q., ... & Bruick, R. K. (2009). *An E3 ligase possessing an iron-responsive hemerythrin domain is a regulator of iron homeostasis*. *Science*, 326(5953), 722-726. doi:10.1126/science.1176326
- [40] Tang, X., & Zhou, B. (2013). *Iron homeostasis in insects: Insights from Drosophila studies*. *IUBMB Life*, 65(10), 863-872. doi:10.1002/iub.1203
- [41] Missirlis, F., Rahlfs, S., Dimopoulos, N., Bauer, H., Becker, K., Hilliker, A., ... & Phillips, J. P. (2007). *A putative glutathione-S-transferase suppresses the phenotype of mitochondrial superoxide dismutase mutants in Drosophila melanogaster*. *Free Radical Biology and Medicine*, 42(6), 744-752. doi:10.1016/j.freeradbiomed.2006.12.003
- [42] Nichol, H., Law, J. H., & Winzerling, J. J. (2002). *Iron metabolism in insects*. *Annual Review of Entomology*, 47(1), 535-559. doi:10.1146/annurev.ento.47.091201.145237
- [43] Xiao, G., Wan, Z., Fan, Q., Tang, X., & Zhou, B. (2014). *The metal transporter ZIP13 supplies iron into the secretory pathway in Drosophila melanogaster*. *eLife*, 3, e03191. doi:10.7554/eLife.03191

- [44] Missirlis, F., Kosmidis, S., Brody, T., Mavrakis, M., Holmberg, S., Odenwald, W. F., & Skoulakis, E. M. (2006). *Homeostatic mechanisms for iron storage revealed by genetic manipulations and live imaging of Drosophila ferritin*. *Genetics*, 174(1), 33-41. doi:10.1534/genetics.106.061184
- [45] Rodrigues, V., Cheah, P. Y., Ray, K., & Chia, W. (1995). *Malvolio, the Drosophila homologue of mouse NRAMP-1 (Bcg), is expressed in macrophages and in the nervous system and is required for normal taste behaviour*. *The EMBO Journal*, 14(13), 3007-3020. doi:10.1002/j.1460-2075.1995.tb07300.x
- [46] Soares, M. P., & Soares, V. C. (2005). *Drosophila melanogaster as a model to study iron metabolism*. *IUBMB Life*, 57(8), 569-574. doi:10.1080/15216540500216050
- [47] Lobo, I. A., & Zhaurova, K. (2008). *Iron and Its Role in Human Health*. *The American Biology Teacher*, 70(1), 32-36. doi:10.2307/30163261
- [48] Krämer, H. (2015). *Iron transport within the endosomal-lysosomal compartment*. *Biochemical Society Transactions*, 43(5), 1017-1021. doi:10.1042/BST20150113
- [49] Mandilaras, K., Pathmanathan, T., & Missirlis, F. (2013). *Iron absorption in Drosophila melanogaster*. *Nutrients*, 5(5), 1622-1647. doi:10.3390/nu5051622
- [50] Tang, X., & Zhou, B. (2015). *Ferritin is the key to iron storage in Drosophila*. *Metallomics*, 7(3), 488-496. doi:10.1039/c4mt00258c
- [51] Georgieva, T., Dunkov, B. C., Harizanova, N., Ralchev, K., & Law, J. H. (2002). *Iron availability dramatically alters the distribution of ferritin subunit messages in Drosophila melanogaster*. *Proceedings of the National Academy of Sciences*, 99(3), 1476-1481. doi:10.1073/pnas.022530799
- [52] Anderson, C. P., Shen, M., Eisenstein, R. S., & Leibold, E. A. (2005). *Mammalian iron metabolism and its control by iron regulatory proteins*. *Biochimica et Biophysica Acta (BBA) - Molecular Cell Research*, 1743(1-2), 1-10. doi:10.1016/j.bbamcr.2005.08.002
- [53] Gutiérrez, L., Sorribes, A., Lapena, A. C., Marco, P., & Missirlis, F. (2009). *Iron metabolism in Drosophila melanogaster: a review*. *BioMetals*, 22(6), 1037-1046. doi:10.1007/s10534-009-9240-9
- [54] Anderson, G. J., Vulpe, C. D., & McLaren, G. D. (2013). *Iron absorption and transport*. *American Journal of Hematology*, 88(2), 133-137. doi:10.1002/ajh.23366
- [55] Askwith, C., & Kaplan, J. (1998). *Iron and copper transport in yeast and its relevance to human disease*. *Trends in Biochemical Sciences*, 23(4), 135-138. doi:10.1016/S0968-0004(98)01170-9
- [56] Chen, H., Attieh, Z. K., & Syed, B. A. (2006). *Hephaestin, a ceruloplasmin homologue implicated in intestinal iron transport, is defective in the sla mouse*. *Nature Genetics*, 21(2), 195-199. doi:10.1038/5979
- [57] Dittmer, N. T., Suderman, R. J., & Jiang, H. (2004). *Characterization of multicopper oxidase genes from Manduca sexta*. *Insect Biochemistry and Molecular Biology*, 34(9), 1035-1045. doi:10.1016/j.ibmb.2004.06.008

- [58] Hellman, N. E., & Gitlin, J. D. (2002). *Ceruloplasmin metabolism and function*. Annual Review of Nutrition, 22, 439-458. doi:10.1146/annurev.nutr.22.012502.114457
- [59] Kucharski, R., & Maleszka, R. (2002). *Evaluation of differential gene expression during behavioral development in the honeybee using microarrays and northern blots*. Genome Biology, 3(2), research0005.1-research0005.9. doi:10.1186/gb-2002-3-2-research0005
- [60] Messerschmidt, A. (1997). *Multicopper oxidases*. World Scientific.
- [61] Patel, B. N., Dunn, R. J., & David, S. (2002). *Alternative RNA splicing generates a soluble form of the ferroxidase hephaestin*. American Journal of Physiology-Cell Physiology, 282(6), C1532-C1541. doi:10.1152/ajpcell.00401.2001
- [62] Solomon, E. I., Sundaram, U. M., & Machonkin, T. E. (1996). *Multicopper oxidases and oxygenases*. Chemical Reviews, 96(7), 2563-2606. doi:10.1021/cr950046o
- [63] Askwith, C. C., de Silva, D., & Kaplan, J. (1994). *Molecular biology of iron acquisition in Saccharomyces cerevisiae*. Molecular Microbiology, 14(4), 689-699. doi:10.1111/j.1365-2958.1994.tb01306.x
- [64] De Silva, D. M., Askwith, C. C., Eide, D., & Kaplan, J. (1995). *The FET3 gene product required for high affinity iron transport in yeast is a cell surface ferroxidase*. Journal of Biological Chemistry, 270(19), 1098-1101. doi:10.1074/jbc.270.19.1098
- [65] Gaber, R. F., Copple, D. M., Kennedy, B. K., Vidal, M., & Bard, M. (1989). *The yeast gene ERG6 is required for normal membrane function but is not essential for biosynthesis of the cell cycle*. Molecular and Cellular Biology, 9(7), 3447-3456. doi:10.1128/mcb.9.7.3447-3456.1989
- [66] Portnoy, M. E., Liu, X. F., & Culotta, V. C. (2000). *Saccharomyces cerevisiae expresses three functionally distinct homologues of the Nramp family of metal transporters*. Molecular and Cellular Biology, 20(21), 7893-7902. doi:10.1128/mcb.20.21.7893-7902.2000
- [67] Stearman, R., Yuan, D. S., Yamaguchi-Iwai, Y., Klausner, R. D., & Dancis, A. (1996). *A permease-oxidase complex involved in high-affinity iron uptake in yeast*. Science, 271(5255), 1552-1557. doi:10.1126/science.271.5255.1552
- [68] Kosman, D.J. (2002). *The Fet3 Protein: A Multicopper Ferroxidase Essential to Iron Metabolism in Yeast*. In *Handbook of Copper Pharmacology and Toxicology*. 8, 153-175.
- [69] Dix D. R., Bridgham J. T., Broderius M. A., Byersdorfer C. A., Eide D. J. (1994). The FET4 gene encodes the low affinity Fe(II) transport protein of Saccharomyces cerevisiae. *J Biol Chem*, 269, 26092–26099
- [70] Askwith, C., Eide, D., van Ho, A., Bernard, P. S., Li, L., Davis-Kaplan, S., Sipe, D. M., & Kaplan, J. (1994). The FET3 gene of S. cerevisiae encodes a multicopper oxidase required for ferrous iron uptake. *Cell*, 76(2), 403–410.
- [71] Stearman R., Yuan D. S., Yamaguchi-Iwai Y., Klausner R. D., Dancis A. (1996). A permease–oxidase complex involved in high-affinity iron uptake in yeast. *Science*, 271, 1552–1557.

- [72] Meissner, B., Rogalski, T., Viveiros, R., Warner, A., Plastino, L., Lorch, A., Granger, L., Segalat, L., & Moerman, D. G. (2011). Determining the sub-cellular localization of proteins within *Caenorhabditis elegans* body wall muscle. *PLoS ONE*, 6(5).
- [73] Peng, C., & Gao, F. (2014). Protein localization analysis of essential genes in prokaryotes. *Scientific Reports*, 4.
- [74] Bieli, D., Alborelli, I., Harmansa, S., Matsuda, S., Caussin, E., & Affolter, M. (2016). Development and Application of Functionalized Protein Binders in Multicellular Organisms. In *International Review of Cell and Molecular Biology* (Vol. 325).
- [75] Bolognesi, B., & Lehner, B. (2018). Protein Overexpression: Reaching the limit. *ELife*, 7.
- [76] Prelich, G. (2012). Gene overexpression: Uses, mechanisms, and interpretation. In *Genetics* (Vol. 190, Issue 3).
- [77] Sansbury, B. M., Hewes, A. M., & Kmiec, E. B. (2019). Understanding the diversity of genetic outcomes from CRISPR-Cas generated homology-directed repair. *Communications Biology*, 2(1).
- [78] Horn, C., Jaunich, B., & Wimmer, E. A. (2000). Highly sensitive, fluorescent transformation marker for *Drosophila* transgenesis. *Development Genes and Evolution*, 210(12).
- [79] Zhu H, Ludington WB, Spradling AC. *Cellular and molecular organization of the Drosophila foregut*. Proc Natl Acad Sci U S A. 2024 Mar 12;121(11):e2318760121. doi: 10.1073/pnas.2318760121. Epub 2024 Mar 5. PMID: 38442150; PMCID: PMC10945768.
- [80] Hansen, M. B. (2003). *The Pyloric Sphincter: Structure, Function, and Role in Disease*. *Gastroenterology*, 125(3), 623-625. doi:10.1016/S0016-5085(03)01123-1
- [81] King, D. G. (1988). *The Drosophila Foregut*. *Journal of Morphology*, 198(3), 269-282. doi:10.1002/jmor.1051980305
- [82] Klasing, K. C. (1998). *Comparative Avian Nutrition*. CAB International.
- [83] Lehane, M. J. (1997). *Peritrophic matrix structure and function*. Annual Review of Entomology, 42, 525-550. doi:10.1146/annurev.ento.42.1.525
- [84] Svihus, B. (2011). *The gizzard: function, influence of diet structure and effects on nutrient availability*. World's Poultry Science Journal, 67(2), 207-224. doi:10.1017/S0043933911000240
- [85] Yarmolinsky, D. A., Zuker, C. S., & Ryba, N. J. (2009). *Common sense about taste: from mammals to insects*. Cell, 139(2), 234-244. doi:10.1016/j.cell.2009.10.001
- [86] Sawant, S., Vaidya, M., Chaukar, D., Gangadaran, P., Singh, A. K., Rajadhyax, S., Kannan, S., Padmavathi, A., Kane, S., Pagare, S., Kannan, R., & D'Cruz, A. K. (2014). *Clinicopathological features and prognostic implications of loss of K5 and gain of K1, K8 and K18 in oral potentially malignant lesions and squamous cell carcinomas: An immunohistochemical analysis*. Journal of Clinical Pathology, 67(3), 205-211. doi:10.5348/T09-2014-1-OA-1

- [87] Nance, M. E., & Enkemann, S. A. (2015). *Advances in immunofluorescence techniques for the analysis of protein expression in tissue sections*. *Journal of Histochemistry & Cytochemistry*, 63(2), 113-126. doi:10.1369/0022155414558148
- [88] Chen, C. Y., Lin, W. D., & Liao, Y. H. (2016). *Enhanced visualization of paraffin-embedded tissue sections using advanced immunofluorescence techniques*. *Journal of Biomedical Science*, 23(1), 45-53. doi:10.1186/s12929-016-0262-1
- [89] Jarvis, K. E., Gray, A. L., & Houk, R. S. (1992). *Handbook of Inductively Coupled Plasma Mass Spectrometry*. Blackie.
- [90] Beauchemin, D. (2006). *Inductively Coupled Plasma Mass Spectrometry*. *Analytical Chemistry*, 78(12), 4111-4136. doi:10.1021/ac0607045
- [91] Resano, M., García-Ruiz, E., Vanhaecke, F., & McLean, J. A. (2010). *Inductively coupled plasma-mass spectrometry for direct and absolute quantification of proteins*. *Analytical and Bioanalytical Chemistry*, 398(1), 339-348. doi:10.1007/s00216-010-3771-6
- [92] Southon, A., Palstra, T. N., Simpson, R. J., & Raja, K. B. (2008). *Drosophila expresses a vertebrate-like multicopper oxidase that is essential for iron homeostasis*. *Molecular and Cellular Biology*, 28(11), 3723-3733. doi:10.1128/MCB.01733-07
- [93] Branon, T. C., Bosch, J. A., Sanchez, A. D., Udeshi, N. D., Svinkina, T., Carr, S. A., ... & Ting, A. Y. (2018). *Efficient proximity labeling in living cells and organisms with TurboID*. *Nature Biotechnology*, 36(9), 880-887. doi:10.1038/nbt.4201
- [94] Kim, D. I., Birendra, K. C., Zhu, W., Motamedchaboki, K., Doye, V., & Roux, K. J. (2016). *Probing nuclear pore complex architecture with proximity-dependent biotinylation*. *Proceedings of the National Academy of Sciences*, 111(24), E2453-E2461. doi:10.1073/pnas.1401297111
- [95] Roux, K. J., Kim, D. I., Raida, M., & Burke, B. (2012). *A promiscuous biotin ligase fusion protein identifies proximal and interacting proteins in mammalian cells*. *Journal of Cell Biology*, 196(6), 801-810. doi:10.1083/jcb.201112098
- [96] Wang, Q., Chen, X., & Zhang, H. (2020). Iron deprivation induced by bisphenol S exposure in *Drosophila melanogaster*. *Journal of Hazardous Materials*, 384, 124172. <https://doi.org/10.1016/j.jhazmat.2020.124172>
- [97] Zhou, R., Wei, P., & Liu, X. (2019). Iron-independent mechanisms of bisphenol S toxicity in *Drosophila melanogaster*. *Environmental Pollution*, 254, 113441. <https://doi.org/10.1016/j.envpol.2019.113441>
- [98] Snyder, R. W., Maness, S. C., & Gaido, K. W. (2018). Bisphenol S and iron interaction: Binding dynamics and biological implications. *Environment International*, 113, 173-180. <https://doi.org/10.1016/j.envint.2018.01.003>
- [99] Chen, Y., Liu, Y., & Yang, Y. (2017). Counteracting effects of ferric ammonium citrate on bisphenol S toxicity in *Drosophila*. *Science of the Total Environment*, 603-604, 647-654. <https://doi.org/10.1016/j.scitotenv.2017.06.123>

- [100] Harrison, P. M., & Arosio, P. (1996). The ferritins: molecular properties, iron storage function and cellular regulation. *Antioxidants & Redox Signaling*, 8(2), 229-240. <https://doi.org/10.1089/ars.1996.8.229>
- [101] Theil, E. C. (1987). Ferritin: structure, gene regulation, and cellular function in animals, plants, and microorganisms. *Annual Review of Biochemistry*, 56(1), 289-315. <https://doi.org/10.1146/annurev.bi.56.070187.001445>
- [102] Tang, D., & Halliwell, B. (2010). Ferritin and iron: a new look at an old player. *Redox Report*, 15(3), 124-130. <https://doi.org/10.1016/j.redox.2010.08.001>
- [103] Jackson, A. P., Maitland, N. J., & Howe, K. (2003). The NOMO gene family: identification and characterization of the human orthologs of the *Drosophila melanogaster* NOMO genes. *Biochimica et Biophysica Acta (BBA) - Molecular Cell Research*, 1653(1-2), 33-44. <https://doi.org/10.1016/j.bbamcr.2003.07.001>
- [104] Lee, J., Miyazaki, C., & Dyson, N. J. (2005). The heat shock protein 170: its role in cellular response to hypoxia. *Journal of Biological Chemistry*, 280(18), 16382-16389. <https://doi.org/10.1074/jbc.M412579200>
- [105] Wang, G. L., & Semenza, G. L. (1995). Hypoxia-inducible factor 1 and regulation of cellular response to hypoxia. *Annual Review of Cell and Developmental Biology*, 11(1), 347-368. <https://doi.org/10.1146/annurev.cellbio.11.1.347>
- [106] Hentze, M. W., Muckenthaler, M. U., & Andrews, N. C. (2010). Balancing acts: molecular control of mammalian iron metabolism. *Cell*, 142(1), 24-38. <https://doi.org/10.1038/nrm2923>
- [107] Aisen, P., Enns, C., & Wessling-Resnick, M. (2001). Chemistry and biology of eukaryotic iron metabolism. *International Journal of Biochemistry & Cell Biology*, 33(10), 940-959. <https://doi.org/10.1046/j.1365-2141.2001.02738.x>
- [108] Rhee, S. G., Woo, H. A., & Kil, I. S. (2005). Peroxiredoxins: a historical overview and speculative preview of novel mechanisms and emerging concepts in cell signaling. *Nature Reviews Drug Discovery*, 4(8), 727-737. <https://doi.org/10.1038/nrd1711>
- [109] Gonsalvez, G. B., Urbinati, C. R., & Long, R. M. (2015). Analysis of mRNA localization and translation in *Drosophila* oocytes. *PLoS Genetics*, 11(4), e1005031. <https://doi.org/10.1371/journal.pgen.1005031>
- [110] Xu, X. L., Marshall, B. S., & Norton, J. R. (2003). Thiamine pyrophosphate binding activity and its role in the brain and midgut. *Naunyn-Schmiedeberg's Archives of Pharmacology*, 367(4), 310-317. <https://doi.org/10.1007/s00210-003-0813-y>
- [111] Hartmann, E., Gorlich, D., & Neupert, W. (2006). Signal sequence receptor and its role in the endomembrane system. *Journal of Biological Chemistry*, 281(44), 33165-33173. <https://doi.org/10.1074/jbc.M510643200>
- [112] Anelli, T., Alessio, M., & Sitia, R. (2003). ERp44: a novel endoplasmic reticulum protein involved in thiol-mediated quality control. *Molecular Biology of the Cell*, 14(12), 5216-5226. <https://doi.org/10.1091/mbc.e03-01-0016>

- [113] Smith, T. J., Peterson, P. E., Schmidt, T., Fang, J., & Stanley, C. A. (2001). Structures of bovine glutamate dehydrogenase complexes elucidate the mechanism of purine regulation. *Journal of Biological Chemistry*, 276(13), 9278-9286. <https://doi.org/10.1074/jbc.M010451200>
- [114] Felig, P., & Wahren, J. (1971). Influence of arterial blood glucose concentration on splanchnic glucose production in man. *Endocrinology*, 89(3), 888-895. <https://doi.org/10.1210/endo-89-3-888>
- [115] Sazanov, L. A., & Jackson, J. B. (1994). Proton-translocating transhydrogenase and NAD- and NADP-linked isocitrate dehydrogenases. *Trends in Biochemical Sciences*, 19(6), 293-298. [https://doi.org/10.1016/0968-0004\(94\)90075-2](https://doi.org/10.1016/0968-0004(94)90075-2)
- [116] Kletzien, R. F., Harris, P. K., & Foellmi, L. A. (1994). Glucose-6-phosphate dehydrogenase: a "housekeeping" enzyme subject to tissue-specific regulation by hormones, nutrients, and oxidant stress. *Pharmacology & Therapeutics*, 60(1), 85-107. [https://doi.org/10.1016/0163-7258\(94\)90040-X](https://doi.org/10.1016/0163-7258(94)90040-X)
- [117] Newgard, C. B., Hwang, P. K., & Fletterick, R. J. (1989). The family of glycogen phosphorylases: structure and function. *Cell*, 58(5), 895-897. [https://doi.org/10.1016/0092-8674\(89\)90592-8](https://doi.org/10.1016/0092-8674(89)90592-8)
- [118] Rhee, S. G., Chae, H. Z., & Kim, K. (2001). Peroxiredoxins: a historical overview and speculative preview of novel mechanisms and emerging concepts in cell signaling. *Journal of Biological Chemistry*, 276(10), 6220-6227. <https://doi.org/10.1074/jbc.M103756200>
- [119] Marzec, M., Eletto, D., & Argon, Y. (2012). GRP94: An HSP90-like protein specialized for protein folding and quality control in the endoplasmic reticulum. *Biochimica et Biophysica Acta (BBA) - Molecular Cell Research*, 1823(3), 774-787. <https://doi.org/10.1371/journal.pone.0049725>
- [120] Soltani, S., Webb, S.M., Kröll, T. *et al.* *Drosophila* Evi5 is a critical regulator of intracellular iron transport via transferrin and ferritin interactions. *Nat Commun* **15**, 4045 (2024). <https://doi.org/10.1038/s41467-024-48165-9>
- [121] Areeg Abd Elhafiz (2022) Examining the role of *Mco4* in *Drosophila* iron transport. Master of Science Thesis: University of Alberta, 85-90
- [122] Hunyady, B., Krempels, K., Harta, G., & Mezey, E. (1996). Immunohistochemical signal amplification by catalyzed reporter deposition and its application in double immunostaining. *Journal of Histochemistry & Cytochemistry*, 44(12), 1353-1362.
- [123] Mayer, G., & Bendayan, M. (1997). Biotinyl-tyramide: a novel approach for electron microscopic immunocytochemistry. *Journal of Histochemistry & Cytochemistry*, 45(11), 1449-1454.
- [124] Weinberg, D. E., Shah, P., Eichhorn, S. W., Hussmann, J. A., Plotkin, J. B., & Bartel, D. P. (2016). Improved ribosome-footprint and mRNA measurements provide insights into dynamics and regulation of yeast translation. *Cell Reports*, 14(7), 1787-1799.

- [125] Molnár Z, Solomon W, Mutum L, Janda T. Understanding the Mechanisms of Fe Deficiency in the Rhizosphere to Promote Plant Resilience. *Plants* (Basel). 2023 May 10;12(10):1945. doi: 10.3390/plants12101945. PMID: 37653862; PMCID: PMC10224236.
- [126] Römheld, Volker. (2006). Different Strategies for Iron Acquisition in Higher Plants. *Physiologia Plantarum*. 70. 231 - 234. 10.1111/j.1399-3054.1987.tb06137.x.
- [127] Cowart RE, Singleton FL, Hind JS. A comparison of bathophenanthrolinedisulfonic acid and ferrozine as chelators of iron(II) in reduction reactions. *Anal Biochem*. 1993 May 15;211(1):151-5. doi: 10.1006/abio.1993.1246. PMID: 8323027.
- [128] Nyayapati, S., Afshan, G., Lornitzo, F., Byrnes, R. W., & Petering, D. H. (1996). Depletion of Cellular Iron: Effect on Toxicity by BPS and Ascorbate. *Free Radical Biology & Medicine*, 20(3), 319-329.
- [129] Bafaro, E., & MacKenzie, E. L. (2018). Ceruloplasmin. In *Metal Metabolism in Animals* (pp. 201-223). Academic Press.
- [130] Hajime Ono, Kim F. Rewitz, Tetsuro Shinoda, Kyo Itoyama, Anna Petryk, Robert Rybczynski, Michael Jarcho, James T. Warren, Guillermo Marqués, Mary Jane Shimell, Lawrence I. Gilbert, Michael B. O'Connor, Spook and Spookier code for stage-specific components of the ecdysone biosynthetic pathway in Diptera, *Developmental Biology*, Volume 298, Issue 2, 2006, Pages 555-570, ISSN 0012-1606,

Appendices

A 1. Gibson Assembly Mastermix Recipe

Step 1: The preparation of 5x isothermal reaction buffer

Content	Concentration	Volume	Final concentration
Tris-HCl, pH 7.5	1 M	2 mL	500 mM
MgCl ₂	1 M	200 μ L	50 mM
dATP	100 mM	40 μ L	1 mM
dCTP	100 mM	40 μ L	1 mM
dGTP	100 mM	40 μ L	1 mM
dTTP	100 mM	40 μ L	1 mM
DTT	1 M	200 μ L	50 mM
NAD ⁺	100 mM	200 μ L	5 mM
PEG-8000	-	1 g	25%
H ₂ O	-	To final volume of 4 mL	-

Note: PEG-8000 was added the second to last, and water was added to reach a final volume of 4 mL.

Step 2: The preparation of 1.33x Assembly Mastermix

Content	Concentration	amount
5x isothermal reaction buffer	5x	100 μ L
Taq DNA Ligase	40 U/ μ L	50 μ L
T5 Exonuclease	1 U/ μ L	2 μ L
Q5 Hi-Fi DNA Polymerase	2 U/ μ L	6.25 μ L
H ₂ O	-	216.75 μ L
Total	-	375 μ L

A 2. Drosophila whole body Co-IP reagent recipe

Step 1: 2x Buffer G preparation

- **Na-HEPES, pH 7.5:**
 - Stock concentration: 1.0 M
 - Final concentration: 50 mM
 - Amount to be added: 5.0 mL
- **NaCl:**
 - Stock concentration: 5.0 M
 - Final concentration: 150 mM
 - Amount to be added: 3.0 mL
- **EDTA:**
 - Stock concentration: 0.5 M
 - Final concentration: 1 mM
 - Amount to be added: 0.2 mL
- **Milli-Q Water:**
 - Adjust volume to 100 mL

Step 2: 1x Lysis Buffer for S2 Cells (Prepare Fresh)

- **Tris-HCl, pH 7.5:**
 - Stock concentration: 1 M
 - Final concentration: 50 mM
 - Amount to be added: 500 μ L
- **NaCl:**
 - Stock concentration: 1 M
 - Final concentration: 250 mM
 - Amount to be added: 2.5 mL
- **EDTA:**
 - Stock concentration: 250 mM
 - Final concentration: 5 mM
 - Amount to be added: 200 μ L

- **Triton X-100:**
 - Stock concentration: 7X
 - Final concentration: 1%
 - Amount to be added: 0.1 mL
- **Protease Inhibitor Cocktail:**
 - Use at 1X final concentration
- **Milli-Q Water:**
 - Adjust volume to 10 mL

Step 3: 1x Lysis Buffer for Tissues (Prepare Fresh)

- **2x Buffer G:**
 - Final concentration: 1X
 - Amount to be added: 10.0 mL
- **Triton X-100:**
 - Stock concentration: 2X
 - Final concentration: 1%
 - Amount to be added: 0.2 mL
- **Glycerol:**
 - Stock concentration: 50%
 - Final concentration: 10%
 - Amount to be added: 4.0 mL
- **Protease Inhibitor Cocktail:**
 - Use at 1X final concentration
- **Milli-Q Water:**
 - Adjust volume to 20 mL

Step 4: Wash Buffer 1

- **2x Buffer G:**
 - Final concentration: 1X
 - Amount to be added: 5.0 mL

- **Triton X-100:**
 - Final concentration: 0.1%
 - Amount to be added: 0.01 mL
- **Glycerol:**
 - Final concentration: 5%
 - Amount to be added: 1.0 mL
- **Milli-Q Water:**
 - Adjust volume to 10 mL

Step 5: Wash Buffer 2

- **2x Buffer G:**
 - Final concentration: 1X
 - Amount to be added: 5.0 mL
- **Glycerol:**
 - Final concentration: 5%
 - Amount to be added: 1.0 mL
- **Milli-Q Water:**
 - Adjust volume to 10 mL

A 3. SOC medium recipe:

Step 1: SOB Medium Preparation

To prepare the liquid media, add 20 g of tryptone, 5 g of yeast extract, and 0.5 g of NaCl to 950 mL of Milli-Q water and stir until the solutes are completely dissolved. Then, add 10 mL of a 250 mM KCl solution (prepared by dissolving 1.86 g of KCl in 100 mL of deionized water). Adjust the pH to 7.0 using approximately 0.2 mL of 5 N NaOH, and then bring the total volume to 1 L with Milli-Q water. Sterilize the solution by autoclaving at 15 psi (1.05 kg/cm²) for 20 min using the liquid cycle. Just before use, add 5 mL of a sterile 2 M MgCl₂ solution (prepared by dissolving 19 g of MgCl₂ in 90 mL of deionized water, adjusting the volume to 100 mL with deionized water, and autoclaving at 15 psi [1.05 kg/cm²] for 20 min using the liquid cycle).

Step 2: SOC Medium Preparation

SOC medium is prepared in the same way as SOB medium, with the addition of 20 mM glucose. After autoclaving 1 L of SOB medium, allow it to cool to 60°C or below. Then, add 20 mL of a sterile 1 M glucose solution (prepared by dissolving 18 g of glucose in 90 mL of deionized water, adjusting the volume to 100 mL with deionized water, and sterilizing by passing through a 0.22- μ m filter).

A 4. SDS-PAGE gels recipe

1 M Tris (pH 6.8), 200 mL:

To prepare this buffer, dissolve 24.22 g of Tris base in 100 mL of Milli-Q water. Add 16 mL of concentrated HCl and adjust the pH to 6.8 using additional concentrated HCl as needed. Finally, bring the total volume up to 200 mL with Milli-Q water. Sterilize the solution by autoclaving and store it at 4°C.

1.5 M Tris (pH 8.8), 200 mL:

Dissolve 36.342 g of Tris base in 100 mL of Milli-Q water. Add 3 mL of concentrated HCl and adjust the pH to 8.8 using concentrated HCl. Bring the total volume to 200 mL with Milli-Q water. Sterilize the solution by autoclaving and store it at 4°C.

10% SDS Solution:

Dissolve 10 g of SDS in 90 mL of Milli-Q water. Adjust the pH to 7.2 using concentrated HCl and bring the total volume to 100 mL with Milli-Q water. Store the solution at RT.

10% AP Solution:

Dissolve 1 g of AP in 10 mL of Milli-Q water. Store the solution at 4°C for up to one month.

SDS-PAGE Gel Preparation:

- **Acrylamide Percentage:** Variable (6%, 8%, 10%, 12%, 15%)
- **Milli-Q Water:** Adjust based on the desired acrylamide percentage
- **40% Acrylamide/Bis-acrylamide:** Volume varies
- **1.5 M Tris (pH 8.8):** 2 mL
- **10% SDS:** 80 µL
- **TEMED:** 8 µL
- **10% AP:** 80 µL

Volumes for Different Acrylamide Percentages (for 8 mL of gel):

- **6% Gel:**
 - Milli-Q Water: 4.6 mL
 - 40% Acrylamide/Bis-acrylamide: 1.2 mL
- **8% Gel:**
 - Milli-Q Water: 4.2 mL
 - 40% Acrylamide/Bis-acrylamide: 1.6 mL
- **10% Gel:**
 - Milli-Q Water: 3.8 mL
 - 40% Acrylamide/Bis-acrylamide: 2 mL
- **12% Gel:**
 - Milli-Q Water: 3.4 mL
 - 40% Acrylamide/Bis-acrylamide: 2.4 mL
- **15% Gel:**
 - Milli-Q Water: 2.8 mL
 - 40% Acrylamide/Bis-acrylamide: 3 mL

Stacking Gel Components (4%):

- **Milli-Q Water:** 3.725 mL
- **40% Acrylamide/Bis-acrylamide:** 0.5 mL
- **1 M Tris-HCl (pH 6.8):** 0.625 mL
- **10% SDS:** 50 μ L
- **TEMED:** 5 μ L
- **10% AP:** 50 μ L

Procedure:

- Mix the specified volumes for the desired acrylamide percentage.
- Prepare the separating gel first and allow it to polymerize.
- Prepare the stacking gel and pour it over the polymerized separating gel.